DEGRADATION OF GLYPHOSATE BY MN-OXIDES: MECHANISMS, PATHWAYS, AND SOURCE TRACKING

by

Hui Li

A dissertation submitted to the Faculty of the University of Delaware in partial fulfillment of the requirements for the degree of Doctor of Philosophy in Plant and Soil Sciences

Summer 2018

DEGRADATION OF GLYPHOSATE BY MN-OXIDES: MECHANISMS, PATHWAYS, AND SOURCE TRACKING

by

Hui Li

Approved: _____
Erik Ervin, Ph.D.
Chair of the Department of Plant and Soil Sciences

Approved: _____
Mark Rieger, Ph.D.
Dean of the College of Agriculture and Natural Resources

Approved: _____
Douglas J. Doren, Ph.D.
Interim Vice Provost for Graduate and Professional Education

I certify that I have read this dissertation and that in my opinion it meets the academic and professional standard required by the University as a dissertation for the degree of Doctor of Philosophy.

Signed: _____

Deb Jaisi, Ph.D.
Professor in charge of dissertation

I certify that I have read this dissertation and that in my opinion it meets the academic and professional standard required by the University as a dissertation for the degree of Doctor of Philosophy.

Signed: _____

Adam Wallace, Ph.D.
Member of dissertation committee

I certify that I have read this dissertation and that in my opinion it meets the academic and professional standard required by the University as a dissertation for the degree of Doctor of Philosophy.

Signed: _____

Angelia L. Seyfferth, Ph.D.
Member of dissertation committee

I certify that I have read this dissertation and that in my opinion it meets the academic and professional standard required by the University as a dissertation for the degree of Doctor of Philosophy.

Signed: _____

Donald Sparks, Ph.D.
Member of dissertation committee

I certify that I have read this dissertation and that in my opinion it meets the academic and professional standard required by the University as a dissertation for the degree of Doctor of Philosophy.

Signed: _____

Jeffry Fuhrmann, Ph.D.
Member of dissertation committee

ACKNOWLEDGMENTS

Ever since I first set foot in the United States, I have looked forward to today, the day to finally write this acknowledgment as the epilogue of my dissertation. Pursuing my doctoral degree at UD has been an unforgettable experience that I will treasure for my entire life. For the past five years, I learnt a series of beneficial lessons, skills, and expertise that shaped me into who I am today. I would like to express my gratitude to the people who have supported, helped and deeply touched me during this period and who I will remember forever. Without them, neither this research nor the dissertation would be as meaningful and would not come to this shape.

I would like to express my deepest gratitude to my advisor Dr. Deb Jaisi, for offering the opportunity to pursue my Ph.D. in his great research group and for all his efforts and kind help during my study. He has always been such a good example for us and continuously conveys a spirit of devotion and diligence in research. Without his guidance and persistent help, this research would never be possible. I would like to express my gratitude to my committee members, Dr. Donald Sparks, Dr. Jeffry Fuhrmann, Dr. Angelia Seyfferth, and Dr. Adam Wallace for their insightful advice and enlightening discussions that significantly improved the quality of my projects. Special thanks to Dr. Adam Wallace who spent a great deal of time and effort on DFT modeling on this project and led me to be familiar with this new research area.

I would also like to express my deepest appreciation to my beloved parents, Mr. Li Yunhai and Mrs. Zheng Aicong. It is hard to really find a word to sufficiently convey my gratitude, for giving me life, for the sacrifice they have made, for the care

they have given, for their wise counsel and a sympathetic ear. They are always there for me, just for me. No matter what, they will always have my respect, my gratitude, and most sincerely my love. For the countless times I may say, thank you so much, Mom and Dad, for being my excellent, wonderful, amazing, gorgeous, fabulous, fantastic, perfect parents!

I would like to thank the splendid group members in the Environmental Biogeochemistry Laboratory (EBL): Lisa Stout, Sunendra Joshi, Jiangqi Wu, Qiang Li, Mingjing Sun, Kristi Bear, Yuge Bai, Jiying Li, Gulcin Tosun, Fatemeh Izaditame, and Hezhong Yuan for your encouragement, support, and assistance. Special thanks to Lisa for picking me up from JFK airport the day when I first arrived the U.S. and for kind help on proofreading my manuscripts and teaching me experimental skills. Special thanks to Jiangqi Wu and Yan Yang for being such great friends and accompanied me through the difficult time and shared lots of happy memories.

In addition, a note of thanks to the staff of the Department of Plant and Soil Sciences for their help: Sue Biddle, Kathleen Turner, Cindy Rechsteiner, and Linda Brannen. Also, thank you to Dr. Gerald Poirier from Advanced Materials Characterization Lab and Dr. Steve Bai from NMR facilities and COBRE NMR CORE Center.

I feel so lucky to have you all in this most important achievement in my life. Thank you all!

TABLE OF CONTENTS

LIST OF TABLES

LIST OF FIGURES

ABSTRACT

Glyphosate is a milestone product developed and introduced into the herbicidal industry by John Franz in the 1970s. It has been widely and heavily applied (e.g., ~280 million pounds in the U.S. in 2015) in agriculture and horticulture and drifted residues are found frequently in soils and other environments. Since the carcinogenicity of glyphosate has undergone intense debate and regulatory agencies have not yet reached consensus, studies on the fate of unreacted glyphosate in the environment are not only necessary but also urgent.

Manganese oxides are of particular importance in abiotic degradation of glyphosate and some of its intermediate degradation products. In this dissertation research, birnessite, δ-MnO_2, and ferrihydrite coated with δ-MnO_2 were used to investigate degradation kinetics, preference in degradation pathways, and to identify source signature of glyphosate and its two products: aminomethylphosphonic acid (AMPA) and orthophosphate. Advanced instrumentation such as phosphate oxygen isotope ratios were used to determine the isotope signatures of parent and daughter products. Similarly, nuclear magnetic resonance (NMR) spectroscopy and high-performance liquid chromatography (HPLC) were utilized to identify and quantify degradation products, and density functional theory (DFT) calculations were used to investigate the bond critical point (BCP) properties of the C–N bond in glyphosate and Mn(IV)-complexed glyphosate.

The oxygen isotope ratios ($\delta^{18}O_P$) of orthophosphate derived from glyphosate clearly demonstrated that the one external oxygen atom in each released

orthophosphate was derived from ambient water, not from dissolved oxygen or minerals, with the other three oxygen atoms inherited from glyphosate. Orthophosphate derived from all commercial glyphosate studied had unusually light $\delta^{18}O_P$ values (3.91–9.30 ‰ VSMOW), which are distinct from many other sources of orthophosphates (varying between 16–24 ‰) known so far. These results provided a new and unsurpassed tool to track glyphosate and its degradation products in the environment by using naturally abundant isotopes in these compounds. Furthermore, this proxy allows distinguishing glyphosate-generated orthophosphate from other organophosphorus compounds in the environment.

The abiotic degradation of glyphosate catalyzed by birnessite under aerobic and neutral pH conditions largely followed the glycine pathway generating glycine, formaldehyde, and orthophosphate. The other minor pathway was the AMPA pathway, forming AMPA and glyoxylic acid that ultimately degraded to form CO_2, H_2O, NH_3, and orthophosphate. Sarcosine, the commonly recognized precursor to glycine, was not detected in any of the experiments performed despite its reasonably longer half-life (~13.6 h) than the sampling intervals. Preferential cleavage of the phosphonate adjacent C–N bond to form glycine directly was also supported by the BCP analysis, which revealed that this C–N bond was disproportionately affected by the interaction of glyphosate with Mn(IV). Overall, these results provide supportive evidence that glyphosate primarily degrades at the C–N bond position favoring the direct formation of glycine, which is less toxic than the major product of the other (AMPA) pathway.

In natural soils, Mn-oxides frequently coexist with Fe-oxides with a relative molar ratio around 0.01. Therefore, Fe_2O_3/δ-MnO_2 core-shell minerals with various

Mn/Fe molar ratios are ideal candidates to test glyphosate degradation. The Mn/Fe ratio of 0.01, close to natural abundance, served as an important boundary because below this ratio glyphosate degradation was essentially absent. Present results highlighted the synergistic effects of the two oxides that are commonly present in soils on degradation and sorption of glyphosate and thus reducing the negative impacts of glyphosate in the environment.

In summary, Mn-oxides with high Mn oxidation states (close to 4) are capable of efficient degradation of glyphosate with a short half-life. The C–N bond is preferentially cleaved to generate glycine and orthophosphate as major products. Stable isotope ratios of orthophosphate derived from glyphosate provide a reliable method to source track glyphosate. Furthermore, the preferential glycine pathway of degradation is more environmentally friendly because of the less toxic products than the AMPA pathway. These results provide useful insights to potential routes to attenuate negative effects of glyphosate in the environment.

Chapter 1

INTRODUCTION AND RESEARCH OBJECTIVES

1.1 Occurrence of Glyphosate in The Environment

1.1.1 Glyphosate: A Potent Herbicide

Glyphosate (N-phosphonomethyl glycine) is a phosphonate herbicide that was synthesized and first introduced into the industry by John E. Franz in the 1970s (Franz et al., 1997). It is the active ingredient of many commercial herbicide products, for example Roundup, Accord, and Rodeo. While Monsanto products dominate the herbicide market, glyphosate is manufactured and marketed worldwide by other companies including Bayer, Dow AgroSciences, DuPont, Cenex/Land O'Lakes, Helena, Platte, Riverside/Terra and Zeneca, with different trade names. Glyphosate is a broad-spectrum, post-emergence, nonselective herbicide and has been widely applied on perennials, woody plants, and grasses in farmlands and urban areas, especially after the commercialization of genetically engineered glyphosate-resistant crops (Franz et al., 1997; Monsanto, 1996). Solid glyphosate is white with a crystalline structure and a high water solubility (1.157 wt%), and low vapor pressure at room temperature (Franz et al., 1997; Sprankle et al., 1975).

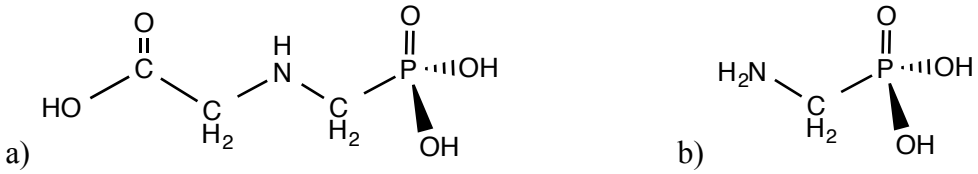

Figure 1.1. The molecular structure of glyphosate (a), and AMPA (b).

Glyphosate is a secondary amine and is comprised of three ionizable functional groups—the amine, carboxyl and phosphonate groups (Figure 1.1a) and four pK_a values: <2, 2.6, 5.6 and 10.6 (Sprankle et al., 1975). These functional groups contribute to multi-charge property—positively charged on the amine group at highly acidic pH and negatively charged on the carboxylic and phosphonate groups at neutral or alkaline pH conditions (Caceres-Jensen et al., 2009; Sprankle et al., 1975). Therefore, under common soil pH conditions, glyphosate primarily exists as net negatively charged ions, and thus undergoes effective sorption onto positively charged mineral surfaces, e.g., goethite and ferrihydrite. The C–P bond in the glyphosate structure as well as in its major metabolite aminomethylphosphonic acid (AMPA) (Figure 1.1b) is very stable and resistant to chemical hydrolysis, thermal decomposition, and photolysis (Freedman and Doak, 1957), thus enabling their long term persistence and frequent occurrence in various environments.

1.1.2 Functioning Mechanism of Glyphosate

Sorption of glyphosate onto a plant is the prerequisite step for its herbicidal action. Once sorbed onto foliage or soft stalk tissues of plants, glyphosate rapidly translocates throughout the plant body via meristematic tissues, thus inhibits plant growth and eventually kills the intact plant in days (Monsanto, 1996). Therefore, glyphosate is only effective on live plants and is applied as a post-emergence

herbicide, rather than pre-emergence. The foliar sorption of glyphosate is influenced by ambient conditions such as pH, types and content of cation, salt species, competing ions, and mineral components (Bailey et al., 2002; Gimsing and Borggaard, 2007). For example, divalent and trivalent metal cations, especially Cu^{2+}, Mn^{2+}, Al^{3+} and Fe^{3+}, can form stable complexations with glyphosate through chelation and inhibit its efficacy as herbicide (Barrett and McBride, 2005; Bernards et al., 2005). Fe minerals (e.g., goethite and ferrihydrite) can efficiently sorb and immobilize glyphosate and limit its uptake by plants (Gimsing and Borggaard, 2007).

The primary functional mechanism of glyphosate is through the inhibition of the shikimate pathway—present in plants and some microorganisms—a requisite for the synthesis of aromatic amino acids. These amino acids are required for fundamental biosynthesis of proteins and other secondary metabolites; for example, growth promoters, growth inhibitors, and phenolic and lignic acids (Herrmann and Weaver, 1999; Steinrticken and Amrhein, 1980). Glyphosate exclusively targets 5-enolpyruvylshikimate-3-phosphate synthase (EPSPS) in the shikimate pathway, preventing the production of chorismate—required to biosynthesize vital aromatic amino acids in plants—and resulting in the accumulation of shikimic acid in plant tissues (Amrhein et al., 1980; Steinrticken and Amrhein, 1980). The genetically engineered glyphosate-resistant crops contain genes that encode glyphosate insensitive EPSPS, and therefore are not affected by glyphosate treatment. The shikimate pathway is not present in animals or human beings (Bentley and Haslam, 1990; De Roos et al., 2004; Steinrticken and Amrhein, 1980). Therefore, glyphosate was originally considered safe to humans and was classified as a category E compound, i.e., non-carcinogenicity for humans (USEPA, 1993).

1.1.3 Application Rate and Environmental Occurrence of Glyphosate

Glyphosate has been increasingly applied worldwide in agriculture as well as horticulture ever since its industrialization, and especially after the introduction of genetically modified glyphosate-resistant crops such as soybean and corn, in more than 160 countries and on more than 100 types of crops (Franz et al., 1997; Monsanto, 2005). According to the statistics reported by United States Geological Survey (USGS), the application rate of glyphosate in agricultural lands in the U.S. skyrocketed significantly from less than 9×10^6 Kg yr^{-1} in 1992 to 127×10^6 Kg yr^{-1} in 2015, within which more than 70 % was applied to corn and soybean crops, with very heavy application in agricultural areas in the mid-east regions of the U.S. (Figure 1.2a,b) (Baker and Stone, 2015; USGS, 2015). The non-agricultural application of glyphosate in the U.S. increased from 2.27×10^6 Kg in 1993 to 9.53×10^6 Kg in 2007 (Aspelin, 1997; Battaglin et al., 2014; Donaldson et al., 2002; Grube et al., 2011; Kiely et al., 2004).

a)

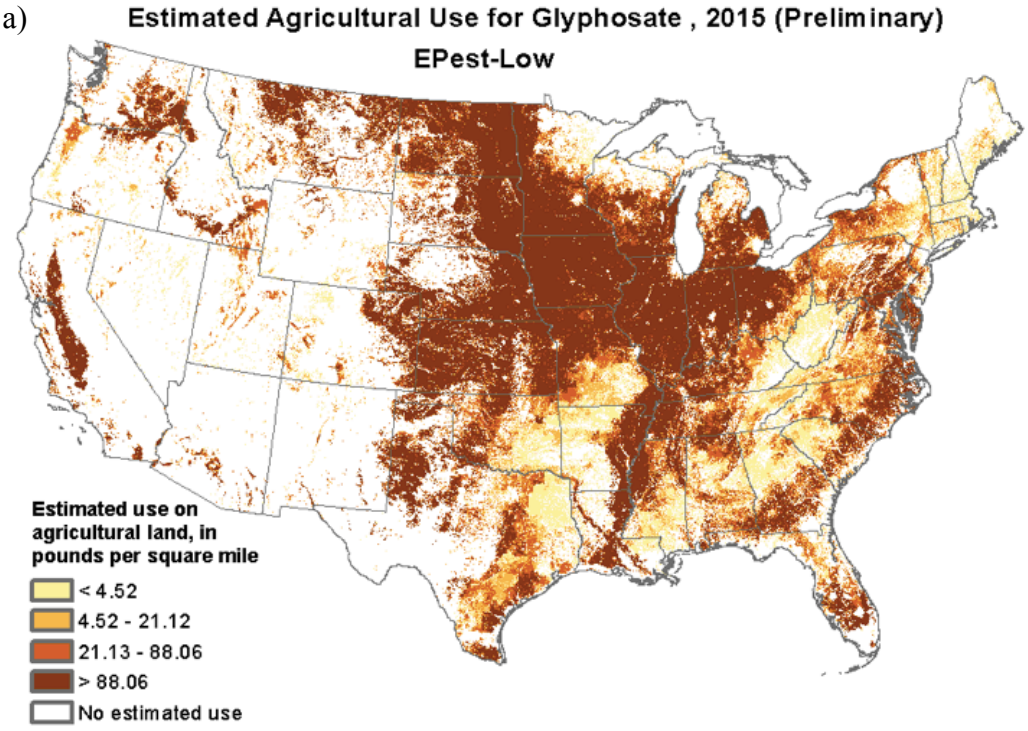

b)

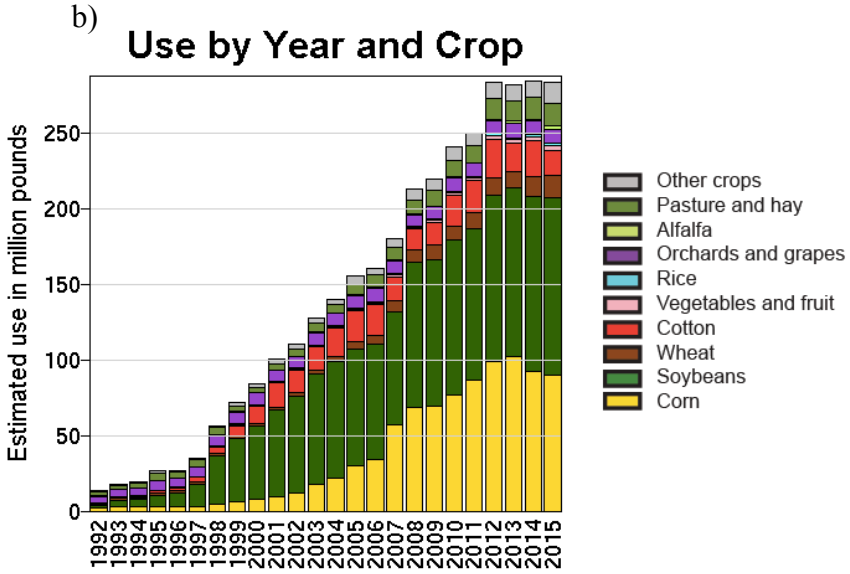

Figure 1.2. Estimated application of glyphosate in 2015 (a) and proportions in the agricultural crops over years (b) (USGS, 2015).

Drifts of glyphosate from urban and agricultural application and transport out of target applications have contributed to the increasingly frequent occurrence of glyphosate and its degradation products (e.g., AMPA) in various environments, including atmosphere, soils and sediments, ditches and drains, and rivers and streams (Battaglin et al., 2014; Chang et al., 2011; Kolpin et al., 2006; Meyer et al., 2009). For example, glyphosate was detected at concentrations above 0.1 μg L^{-1} (with a maximum of 9 μg L^{-1}) in more than 30 % of water samples collected from 51 streams in nine Midwestern states in the U.S. (Battaglin et al., 2005). Similarly, detectable glyphosate was found in more than 50 % of sediments, rivers, and streams collected from 38 states in the U.S. from 2001 to 2010 (Battaglin et al., 2014). In most natural water and sediment samples, glyphosate was detected along with AMPA, which is normally present at higher abundance (Battaglin et al., 2005; Battaglin et al., 2014). The higher environmental occurrence of AMPA than glyphosate is probably ascribed to its longer residence time, which ultimately depends on the source proximity, complexation in soils and sediments, and degradation rates (Battaglin et al., 2005; Battaglin et al., 2014). Moreover, residual glyphosate was also detected in crops and hence foods, including glyphosate-resistant soybeans, cereals, fruits, and vegetables, and even in human urine (Acquavella et al., 2003; Anson Moye et al., 1983; Bohn et al., 2014; Granby et al., 2003).

1.1.4 Environmental and Health Effects of Glyphosate

The United States Environmental Protection Agency (USEPA) had set up a relatively high *maximum contaminant level* of glyphosate as 700 μg L^{-1}, which is 10 times higher than that of 2,4-D (70 μg L^{-1}), more than 300 times higher than alachlor (2 μg L^{-1}), and more than 200 times higher than atrazine (3 μg L^{-1}) (USEPA, 2009),

among which the latter three are other widely used herbicides in the U.S. (Thelin and Stone, 2013). The *maximum contaminant level* of glyphosate in the U.S. is unusually much higher than that in Canada (65 μg L^{-1}) and European Union (0.1 μg L^{-1}) (Kjaer, 2005).

In spite of the high regulatory limit of glyphosate in the U.S., recent studies have documented negative environmental effects and toxicity of glyphosate and AMPA even at low concentrations such as in zebrafish and navigational honey bees, and potential risks to soil nematodes (such as *Caenorhabditis elegans*), thus putting the safety of glyphosate and its widespread application under greater scrutiny (Balbuena et al., 2015; McVey et al., 2016; Roy et al., 2016). Similarly, glyphosate is suspected to affect the synthesis of DNA in sea urchins (Marc et al., 2004) and influence estrogenic activities in human beings (Thongprakaisang et al., 2013). Several glyphosate degradation products are more toxic or persistent than glyphosate itself. For example, AMPA has been reported to have adverse effects on DNA in fish and has potential genotoxicity (Guilherme et al., 2014). This compound is more persistent in the environment, thus poses higher toxicity than glyphosate (Giesy et al., 2000; Grunewald et al., 2001; Rueppel et al., 1977). Though glyphosate itself has relatively low toxicity (Durkin, 2011), commercial formulations contain polyoxyethylene amine, a surfactant used to enhance glyphosate contact on the foliar surface of plants after spraying (Gaskin and Holloway, 1992), thus inducing greater toxicity (Navarro and Martinez, 2014; Tsui and Chu, 2003).

Several recent findings listed above have pointed towards the major safety concern of glyphosate and put the current practice of widespread application under greater scrutiny (Balbuena et al., 2015; McVey et al., 2016; Roy et al., 2016). Based

on the toxicity data, glyphosate was re-classified as Group 2A '*probable carcinogenic to humans*' by the International Agency for Research on Cancer (IARC) of the World Health Organization in 2015 (IARC, 2015). This classification dramatically raised the public concern about the safety of the heavily applied glyphosate. Thereafter, the USEPA initiated a reevaluation of the risks posed to humans from the exposure to glyphosate. The initial review memorandum in 2017 suggested glyphosate classification as "not likely to be carcinogenic to humans" (USEPA, 2017). Moreover, the toxicity statement made by IARC was questionable due to a flawed and incomplete summary that the initial assessment was based largely on animal studies and several studies that showed no cancer link were ignored or edited out (Kelland, 2017a,b; Tarone, 2018). Given this prevailing uncertainty on the toxicity of glyphosate and widespread application and hence frequent occurrence of glyphosate and its degradation products in various environments, studies on the fate of glyphosate in the environment are necessary and urgent.

1.2 Fate of Glyphosate in Soils and Other Environments

1.2.1 Sorption and Desorption of Glyphosate

The mobility and bioavailability of glyphosate in soils are strongly influenced by its complexation with soil components via sorption and desorption (Sprankle et al., 1975). Glyphosate can be strongly fixed through sorption to soil minerals, in particular, Fe-oxides and Al-oxides (Borggaard and Gimsing, 2008; Gimsing et al., 2007). Sorption of glyphosate is significantly influenced by mineral characteristics (e.g., specific surface area and surface charge), pH, and competition with orthophosphate for sorption sites (Borggaard and Gimsing, 2008; Gimsing and Borggaard, 2007; Gimsing

et al., 2007). Most common Fe-oxides have a point of zero charge above 7, and therefore are mostly positively charged in common neutral soil pH conditions (Sparks, 2002), enabling their high sorption affinity to negatively charged glyphosate and orthophosphate. Glyphosate contains three polar functional groups—carboxyl, amine, and phosphonate groups—among which the phosphonate group is the main linkage between glyphosate and the mineral surface (Ahmed et al., 2018; Franz et al., 1997; Sheals et al., 2002). Similar to orthophosphate, glyphosate is readily bound to soil minerals through ligand exchange with coordinated water molecules or hydroxyl functional groups on mineral surfaces or via specific sorption predominantly as monodentate surface complexation and less commonly as bidentate complexation (McBride and Kung, 1989; Sheals et al., 2002; Tribe et al., 2006; Waiman et al., 2013). The major sorption complexation of orthophosphate is bidentate and it has higher affinity than glyphosate (Gimsing et al., 2007). It means orthophosphate over competes glyphosate during competitive sorption and desorb glyphosate and occupy active surface sites on mineral surfaces (Gimsing and Borggard, 2001; McBride and Kung, 1989). Moreover, increased negative charges on mineral surfaces after orthophosphate sorption may further decrease sorption capability of soils for the negatively charged glyphosate anion (Gimsing et al., 2007). Therefore, orthophosphate-saturated soils are not expected to retain excessive unreacted glyphosate, resulting in leaching of glyphosate to surface water and groundwater and furthering environmental problems.

1.2.2 Degradation of Glyphosate

Glyphosate can be rapidly degraded by soil microorganisms into AMPA, glyoxylate, and sarcosine, and these intermediate products are ultimately degraded to

inorganic products including orthophosphate, carbon dioxide, and ammonia (Kishore and Jacob, 1987; Pipke and Amrhein, 1988; Sviridov et al., 2015). The half-life of glyphosate normally ranges between 2–142 days, with an average of 32 days in soils and 7–14 days in forest waters (Goldsborough and Brown, 1993; Newton et al., 1994). The half-life of AMPA ranges between 76–240 days in soils and 7–14 days in waters (Giesy et al., 2000; Monsanto, 2014).

The degradation of glyphosate in soils is predominately driven by biotic routes mediated by autochthonous or introduced bacteria and fungi (Rueppel et al., 1977). Therefore, biotic degradation has been the main focus of most past studies of glyphosate degradation (Sviridov et al., 2015). Enzymes involved in the degradation of glyphosate include C–P lyase and hydrolases, which are capable of breaking the C–P bonds to generate sarcosine and orthophosphate (Ternan et al., 1998; Wackett et al., 1987) and oxidoreductase breaking the C–N bonds to form AMPA (Obojska et al., 2002; Sprankle et al., 1975). However, abiotic degradation may also occur in the presence of manganese oxides and/or light (photolysis) (Barrett and McBride, 2005; Li et al., 2016; Sandy et al., 2013). Naturally occurring minerals (Ascolani Yael et al., 2014; Barrett and McBride, 2005; Paudel et al., 2015), mineral-activated carbon composite (Cui et al., 2012), UV-photo oxidation (Sandy et al., 2013), and nanoparticles (Chen et al., 2015) have been found to be capable of degrading glyphosate. Mn-oxides (among which birnessite is the most abundant) are commonly present in soils (Post, 1999; Post and Veblen, 1990; Taylor et al., 1964) and are strong candidates for abiotic glyphosate degradation.

Glyphosate degradation occurs either through the cleavage of a C–N bond to form AMPA and glyoxylic acid (the AMPA pathway), or through the cleavage of the

C–P bond to form sarcosine and orthophosphate (the sarcosine pathway) (Franz et al., 1997; Rueppel et al., 1977; Sviridov et al., 2015). The focus of most past studies on the biotic degradation of glyphosate has been restricted to these two major degradation pathways. Biotic degradation of glyphosate in soils has been found to accumulate AMPA (Bento et al., 2016; Franz et al., 1997; Rueppel et al., 1977). Sarcosine, however, is less commonly detected as a product. For instance, the apparent formation of glycine was detected in the absence of sarcosine during biotic degradation of ^{14}C labeled glyphosate in soils (Rueppel et al., 1977). Glycine formation without sarcosine was also observed during the incubation of *Achromobacter* sp. MPS 12 in the presence of a sarcosine oxidase inhibitor (Sviridov et al., 2012). Similarly, sarcosine was not detected as a precursor to glycine during abiotic glyphosate degradation catalyzed by either manganese oxide (Barrett and McBride, 2005) or photo-electrochemically generated hydroxyl radicals on a TiO_2 surface under alkaline conditions (Muneer and Boxall, 2008). These studies generally attributed the absence of sarcosine to its rapid degradation rate and did not consider the possibility that glycine might also form as a direct degradation product of glyphosate. However, one study with *Pseudomonas* sp. cultures suggested that glycine might form directly (Jacob et al., 1985). These findings have elevated the fore notion that the sarcosine pathway may be circumvented by an unrecognized direct glycine pathway. However, direct evidence of the absence of sarcosine and the existence of the glycine pathway (through direct C–N bond cleavage) is needed. In fact, glyphosate degradation may proceed through one of the two C–N bond positions: cleavage of the first C–N bond position results in the formation of AMPA, which is known to be more persistent in the environment (Bento et al., 2016; Giesy et al., 2000; Li et al., 2016), while cleavage of the second may result in the

direct formation of comparatively benign products (e.g., glycine). Therefore, the existence of this less toxic abiotic glyphosate degradation pathway carries both scientific and environmental significance.

Research focused on degradation pathways and intermediate products will allow identification of the specific pathway that generates less toxic and low persistent products in the environment. It will allow further research on improving or modifying glyphosate with both high efficiency and environmental safety or otherwise exploit a particular pathway of degradation for lesser harm to the environment.

1.3 Analytical Techniques for Glyphosate and Its Degradation Products

1.3.1 Phosphate Oxygen Isotope Ratios

Phosphorus (P) only has one stable isotope (^{31}P); however, P is always strongly bound to O in the environment, and occurs majorly in one oxidation state (+5) and primarily as orthophosphate (PO_4) under Earth's surface conditions, thus enabling utilization of stable isotope ratios of oxygen in orthophosphate ($\delta^{18}O_P$) as an effective stable isotope tracer for P to investigate P sources, track P cycling, and deduce biogeochemical processes (Blake et al., 1997; Kendall, 1998; McLaughlin et al., 2006). The oxygen isotopic composition in orthophosphate is calculated using the following equation:

$$\delta^{18}O_P = \left(\frac{(^{18}O/^{16}O)_{sample}}{(^{18}O/^{16}O)_{standard}} - 1 \right) \times 1000.$$

The oxygen isotope ratios are measured against reference standard samples and denoted in the form of conventional delta notation in parts per thousand, relative to the Vienna Standard Mean Ocean Water (VSMOW).

There are two major processes that can induce isotope fractionation: ionic exchange and isotope exchange reactions. Ionic exchange is caused by kinetic exchange among intact orthophosphate ions that carry different $\delta^{18}O_P$ values; while isotope exchange is caused by oxygen atom exchange between orthophosphate and water or other sources, resulting in equilibrium fractionation (Longinelli et al., 1976; Kendall, 1998; Jaisi et al., 2010). Oxygen isotope exchange between orthophosphate and ambient water is insignificant in abiotic conditions at low temperature (<80 °C) and neutral pH conditions (Blake et al., 1997; Blake et al., 1998; Jaisi et al., 2010; Lecuyer et al., 1999). Thus, the oxygen isotopes in orthophosphate remain quite inert and resistant during abiotic processes; it means the original source signature is preserved during reactions such as sorption, desorption, and precipitation under soil environments (Blake et al., 2001; Jaisi et al., 2010; Longinelli et al., 1976; Tudge, 1960). Microbial turnover of orthophosphate in living cells results in intensive oxygen isotope exchange between orthophosphate and water inside the cells during intracellular enzymatic hydrolysis (Blake et al., 2001; Blake et al., 2005). This process results in the isotopic equilibrium of orthophosphate with ambient water, which is temperature dependent and can be expressed by the following equations:

$$T = 111.4 - 4.3 \times (\delta^{18}O_P - \delta^{18}O_W)$$

or $1000 \times \ln\alpha_{(PO4\text{-}H2O)} = 14.43(\pm 0.39) \times 1000/T - 26.54(\pm 1.33)$ (Chang and Blake, 2015; Longinelli and Nuti, 1973).

Furthermore, various extracellular phosphoenzymes are capable of hydrolyzing organophosphorus compounds—a reaction that causes partial incorporation of foreign oxygen into the released orthophosphate (Blake et al., 1997; Blake et al., 2005; Liang and Blake, 2009). Analyses of $\delta^{18}O_P$ values of released orthophosphate from

enzymatically hydrolyzed phosphomonoesters and phosphodiesters have shown incorporation of one (25%) or two (50%) O atoms from water into each orthophosphate, respectively (Liang and Blake, 2006, 2009). Therefore, $\delta^{18}O_P$ values of orthophosphate are frequently used to investigate specific biogeochemical reactions and verify the presence and extent of microbial activities (Blake et al., 2001; Blake et al., 1997; Jaisi et al., 2010; McLaughlin et al., 2006). Glyphosate undergoes both biotic and abiotic pathways of degradation in natural environments. Therefore, a distinct trend of $\delta^{18}O_P$ value evolution may help approximate relative contributions of abiotic and biotic reactions.

Isotope labeling and natural abundance studies can be utilized to investigate glyphosate degradation pathways and to identify isotope signatures of glyphosate as well as its metabolites generated during degradation. The isotopic compositions of C, N, and O in the glyphosate molecule depend mainly on (i) the original reagents used (original isotopic composition) for synthesis and (ii) the synthesis procedures (that causes bond cleavage/formation reactions). While there are several methods to synthesize glyphosate (Dill et al., 2010; Zhou et al., 2012), two major methods appear to be common in the current manufacturing industry: (i) alkyl ester method from glycine, dimethylphosphite, and paraformaldehyde, and (ii) phosphonomethyl method where phosphoric acid and formaldehyde form iminodiacetic acid hydrochloride and then one of the two carboxymethyl groups is cleaved to form glyphosate (Dill et al., 2010). A broad range of $\delta^{13}C$ values, varying from –24 to –34 ‰, has been reported for various commercial glyphosate sources in the literature (Kujawinski et al., 2013). The $\delta^{15}N$ values of nitrogen, however, have not been reported in the literature. A combination of the isotope labeling of triple isotopes $\delta^{13}C$, $\delta^{15}N$, and $\delta^{18}O_P$ in

glyphosate and its degradation products will contribute great advantages in tracking these compounds in the environment and discriminate glyphosate-derived products in the environment.

1.3.2 Nuclear Magnetic Resonance (NMR) and High-Performance Liquid Chromatography (HPLC) Techniques

Glyphosate degradation generates various intermediates and final products, including AMPA, glyoxylic acid, sarcosine, glycine, orthophosphate, carbon dioxide, and ammonium salts. These products have different half-lives; therefore, their concentrations vary during progressive degradation of glyphosate. The 2,4,6-trinitrobenzene sulfonic acid (TNBSA) colorimetric method for quantifying primary amines is a sensitive and selective method (Brown, 1968; Paudel et al., 2015b). Glyphosate, as a secondary amine, however, cannot be quantified using this method. Besides, this colorimetric method is the measure of total primary amines but does not discriminate different primary amines. Thus, advanced techniques such as NMR and HPLC become necessary to resolve the identity of each specific individual component and concentration. The NMR technique provides compound-related information based on bond structures and atomic interactions and has a relatively straightforward sample treatment method (Mehrsheikh et al., 2006). Specifically, measurement of the changes in chemical shifts and peak areas in the NMR spectra allows monitoring the dynamic changes of the reactant and products during the reaction. The HPLC method allows better identification of quantitation of glyphosate and its products because it separates compounds based on distinct molecular weight and polarity. It further has a low limit of detection (LOD). A major limitation, however, is the requirement for derivatization. Overall, HPLC allows monitoring of products during progressive degradation, and this

information can be used to deduce the degradation pathways as well as to calculate half-lives of products.

1.4 Research Objectives

This dissertation research aimed to investigate the mechanisms and pathways of glyphosate degradation and explore the persistence of glyphosate and its degradation products. Major research objectives are listed as follows:

Objective 1. Investigate the integrity of orthophosphate during sorption and desorption processes on common minerals (Chapter 2)

Major research questions to be addressed under this objective are:

1. Does the P–O bond of orthophosphate break during sorption and desorption reactions on common Fe- and Mn-oxide minerals?
2. Do sorption and desorption of orthophosphate induce equilibrium isotope fractionation?

Objective 2. Connect glyphosate sources and degradation products by using stable oxygen isotopes ($\delta^{18}O_P$) and develop a method for source tracking of glyphosate and its degradation products (Chapter 3)

1. What are the roles of environmentally relevant factors on the kinetics of glyphosate degradation?
2. What is the isotope fractionation during degradation of glyphosate catalyzed by Mn-oxides?
3. How distinct are the stable oxygen isotopes ($\delta^{18}O_P$) of orthophosphate derived from commercial glyphosate sources? Are they sufficiently distinct from other natural sources and allow isotope source tracking of glyphosate?

Objective 3. Identify the intermediate products generated during glyphosate degradation by birnessite and reassess the half-lives of glyphosate and the major intermediate products (Chapter 4)

1. What are the major intermediate products generated during the degradation of glyphosate catalyzed by birnessite? What are the ranges of their half-lives?

2. What are the dominant mechanisms and pathways of degradation of glyphosate?

Objective 4. Identify and quantify the intermediate products generated during glyphosate degradation by δ-MnO_2 coated on ferrihydrite and determine the effect of coating on the rate and the pathways of degradation (Chapter 5)

1. How do the different Mn/Fe molar ratios in core-shell structure affect the degradability and degradation kinetics of glyphosate?

2. Does the coating of Mn minerals impact the composition of major intermediate products and pathways of degradation impacted? If so, what are the environmental implications?

These objectives were sought to be achieved by running a series of controlled experiments using commercial and stable isotope labeled glyphosate. A combination of i) stable isotopes [phosphate oxygen ($\delta^{18}O_P$)], ii) spectroscopic methods [NMR: 1-D (^{1}H, ^{13}C, and ^{31}P) and 2-D correlation spectroscopies, and HPLC], and iii) molecular simulation using density functional theory (DFT) were used to generate the most accurate data to date on the fate of glyphosate in abiotic degradation.

REFERENCES

Acquavella, J.F., Alexander, B.H., Mandel, J.S., Gustin, C., Baker, B., Chapman, P. and Bleeke, M., 2003. Glyphosate biomonitoring for farmers and their families: Results from the farm family exposure study. Environ. Health Perspect., 112: 321–326.

Ahmed, A.A., Leinweber, P. and Kuhn, O., 2018. Unraveling the nature of glyphosate binding to goethite surfaces by ab initio molecular dynamics simulations. Phys. Chem. Chem. Phys., 20: 1531–1539.

Amrhein, N., Deus, B., Gehrke, P. and Steinrucken, H.C., 1980. The site of the inhibition of the shikimate pathway by glyphosate: II. Interference of glyphosate with chorismate formation in vivo and in vitro. Plant Physiol., 66: 830–834.

Anson Moye, H., Miles, C.J. and Scherer, S.J., 1983. A simplified high-performance liquid chromatographic residue procedure for the determination of glyphosate herbicide and (aminomethyl)phosphonic acid in fruits and vegetables employing postcolumn fluorogenic labeling. J. Agric. Food Chem., 31: 69–72.

Ascolani Yael, J., Fuhr, J.D., Bocan, G.A., Daza Millone, A., Tognalli, N., Dos Santos Afonso, M. and Martiarena, M.L., 2014. Abiotic degradation of glyphosate into aminomethylphosphonic acid in the presence of metals. J. Agric. Food Chem., 62: 9651–9656.

Aspelin, A.L., 1997. Pesticide industry sales and usage: 1994 and 1995 market estimates. U.S. Environmental Protection Agency, Office of Pesticide Programs., EPA-733-R-97-002: 35.

Bailey, W.A., Poston, D.H., Wilson, H.P. and Hines, T.E., 2002. Glyphosate interactions with manganese. Weed Technol., 16: 792–799.

Baker, N.T. and Stone, W.W., 2015. Estimated annual agricultural pesticide use for counties of the conterminous united states. 2008–12. USGS Report DS 907. U.S. Geological Survey, Reston, Virginia.

Balbuena, M.S., Tison, L., Hahn, M.L., Greggers, U., Menzel, R. and Farina, W.M., 2015. Effects of sublethal doses of glyphosate on honeybee navigation. J. Exp. Biol., 218: 2799–2805.

Barrett, K.A. and McBride, M.B., 2005. Oxidative degradation of glyphosate and aminomethylphosphonate by manganese oxide. Environ. Sci. Technol., 39: 9223–9228.

Battaglin, W.A., Kolpin, D.W., Scribner, E.A., Kuivila, K.M. and Sandstrom, M.W., 2005. Glyphosate, other herbicides, and transformation products in midwestern streams, 2002. J. Am. Water Res. Assoc., 41: 323–332.

Battaglin, W.A., Meyer, M.T., Kuivila, K.M. and Dietze, J.E., 2014. Glyphosate and its degradation product AMPA occur frequently and widely in U.S. soils, surface water, groundwater, and precipitation. J. Am. Water Res. Assoc., 50: 275–290.

Bentley, R. and Haslam, E., 1990. The shikimate pathway—A metabolic tree with many branches. Crit. Rev. Biochem. Mol. Biol., 25: 307–384.

Bento, C.P., Yang, X., Gort, G., Xue, S., van Dam, R., Zomer, P., Mol, H.G., Ritsema, C.J. and Geissen, V., 2016. Persistence of glyphosate and aminomethylphosphonic acid in loess soil under different combinations of temperature, soil moisture and light/darkness. Sci. Total Environ., 572: 301–311.

Bernards, M.L., Thelen, K.D., Penner, D., Muthukumaran, R.B. and McCracken, J.L., 2005. Glyphosate interaction with manganese in tank mixtures and its effect on glyphosate absorption and translocation. Weed Sci., 53: 787–794.

Blake, R.E., Alt, J.C. and Martini, A.M., 2001. Oxygen isotope ratios of PO_4: An inorganic indicator of enzymatic activity and P metabolism and a new biomarker in the search for life. Proc. Natl. Acad. Sci. USA, 98: 2148–2153.

Blake, R.E., O'Neil, J.R. and Garcia, G.A., 1997. Oxygen isotope systematics of biologically mediated reactions of phosphate: I. Microbial degradation of organophosphorus compounds. Geochim. Cosmochim. Acta, 61: 4411–4422.

Blake, R.E., O'Neil, J.R. and Garcia, G.A., 1998. Effects of microbial activity on the $\delta^{18}O$ of dissolved inorganic phosphate and textural features of synthetic apatites. Am. Mineral., 83: 1516–1531.

Blake, R.E., O'Neil, J.R. and Surkov, A.V., 2005. Biogeochemical cycling of phosphorus: Insights from oxygen isotope effects of phosphoenzyme. Am. J. Sci., 305: 596–620.

Bohlke, J.K. and Denver, J.M., 1995. Combined use of groundwater dating, chemical and isotopic analyses to resolve the history and fate of nitrate contamination in two agricultural watersheds, Atlantic coastal plain, Maryland. Water Resour. Res., 31: 2319–2339.

Bohn, T., Cuhra, M., Traavik, T., Sanden, M., Fagan, J. and Primicerio, R., 2014. Compositional differences in soybeans on the market: Glyphosate accumulates in Roundup Ready GM soybeans. Food Chem., 153: 207–215.

Borggaard, O.K. and Gimsing, A.L., 2008. Fate of glyphosate in soil and the possibility of leaching to ground and surface waters: A review. Pest Manag. Sci., 64: 441–456.

Brown, H.H., 1968. A study of 2,4,6-trinitrobenzenesulfonic acid for automated amino acid chromatography. Clin. Chem., 14: 967–978.

Caceres-Jensen, L., Gan, J., Baez, M., Fuentes, R. and Escudey, M., 2009. Adsorption of glyphosate on variable-charge, volcanic ash-derived soils. J. Environ. Qual., 38: 1449–1457.

Chang, F.C., Simcik, M.F. and Capel, P.D., 2011. Occurrence and fate of the herbicide glyphosate and its degradate aminomethylphosphonic acid in the atmosphere. Environ. Toxicol. Chem., 30: 548–555.

Chang, S.J. and Blake, R.E., 2015. Precise calibration of equilibrium oxygen isotope fractionations between dissolved phosphate and water from 3 to 37 °C. Geochim. Cosmochim. Acta, 150: 314–329.

Chen, X., Liu, F., Liu, B., Tian, L., Hu, W. and Xia, Q., 2015. A novel route to graphite-like carbon supporting SnO_2 with high electron transfer and photocatalytic activity. J. Hazard. Mater., 287: 126–132.

Cui, H., Li, Q., Qian, Y., Zhang, Q. and Zhai, J., 2012. Preparation and adsorption performance of MnO_2/PAC composite towards aqueous glyphosate. Environ. Technol., 33: 2049–2056.

De Roos, A.J., Blair, A., Rusiecki, J.A., Hoppin, J.A., Svec, M., Dosemeci, M., Sandler, D.P. and Alavanja, M.C., 2004. Cancer incidence among glyphosate-exposed pesticide applicators in the agricultural health study. Environ. Health Perspect., 113: 49–54.

Dill, G.M., Douglas Sammons, R., Feng, P.C.C., Kohn, F., Kretzmer, K., Mehrsheikh, A., Bleeke, M., Honegger, J.L., Farmer, D., Wright, D. and Haupfear, E.A., 2010. Glyphosate resistance in crops and weeds: History, development, and management. Wiley.

Donaldson, D., Kiely, T. and Grube, A., 2002. Pesticide industry sales and usage: 1998 and 1999 market estimates. U.S. Environmental Protection Agency, Office of Pesticide Programs., EPA-733-R-02-001: 33.

Durkin, P.R., 2011. Glyphosate—human health and ecological risk assessment. Syracuse Environmental Research Associates, Inc., Manlius, New York., SERA TR-052-22-03b.

Franz, J.E., Mao, M.K. and Sikorski, J.A., 1997. Glyphosate: A unique global herbicide. American Chemical Society: Washington, DC.

Freedman, L.D. and Doak, G.O., 1957. The preparation and properties of phosphonic acids. Chem. Rev., 57: 479–523.

Gaskin, R.E. and Holloway, P.J., 1992. Some physicochemical factors influencing foliar uptake enhancement of glyphosate-mono(isopropylammonium) by polyoxyethylene surfactants. Pestic. Sci., 34: 195–206.

Giesy, J.P., Dobson, S. and Solomon, K., 2000. Ecotoxicological risk assessment for Roundup herbicide. Rev. Environ. Contam. Toxicol., 167: 35–120.

Gimsing, A.L. and Borggaard, O.K., 2007. Phosphate and glyphosate adsorption by hematite and ferrihydrite and comparison with other variable-charge minerals. Clays Clay Miner., 55: 108–114.

Gimsing, A.L. and Borggaard, O.K., 2001. Effect of KCl and $CaCl_2$ as background electrolytes on the competitive adsorption of glyphosate and phosphate on goethite. Clays Clay Miner., 49: 270–275.

Gimsing, A.L., Szilas, C. and Borggaard, O.K., 2007. Sorption of glyphosate and phosphate by variable-charge tropical soils from Tanzania. Geoderma, 138: 127–132.

Goldsborough, L.G. and Brown, D.J., 1993. Dissipation of glyphosate and aminomethylphosphonic acid in water and sediments of boreal forest ponds. Environ. Toxicol. Chem., 12: 1139–1147.

Granby, K., Johannesen, S. and Vahl, M., 2003. Analysis of glyphosate residues in cereals using liquid chromatography–mass spectrometry (LC–MS/MS). Food Addit. Contam., 20: 692–698.

Grube, A., Donaldson, D., Kiely, T. and Wu, L., 2011. Pesticide industry sales and usage: 2006 and 2007 market estimates. U.S. Environmental Protection Agency, Biological and Economic Analysis Division, Office of Pesticide Programs, Office of Prevention, Pesticides, and Toxic Substances., EPA 733-R-11-001: 33.

Grunewald, K., Schmidt, W., Unger, C. and Hanschmann, G., 2001. Behavior of glyphosate and aminomethylphosphonic acid (AMPA) in soils and water of reservoir Radeburg II catchment (Saxony/Germany). J. Plant Nutr. Soil Sci., 164: 65–70.

Guilherme, S., Santos, M.A., Gaivao, I. and Pacheco, M., 2014. DNA and chromosomal damage induced in fish (Anguilla anguilla L.) by aminomethylphosphonic acid (AMPA)—the major environmental breakdown product of glyphosate. Environ. Sci. Pollut. Res. Int., 21: 8730–8739.

Herrmann, K.M. and Weaver, L.M., 1999. The shikimate pathway. Annu. Rev. Plant Physiol. Plant Mol. Biol., 50: 473–503.

International Agency for Research on Cancer, 2015. IARC Monographs: Evaluation of five organophosphate insecticides and herbicides., 112.

Jacob, G.S., Schaefer, J., Stejskal, E.O. and McKay, R.A., 1985. Solid-state NMR determination of glyphosate metabolism in a *Pseudomonas* sp. J. Biol. Chem., 260: 5899–5905.

Jaisi, D.P., Blake, R.E. and Kukkadapu, R.K., 2010. Fractionation of oxygen isotopes in phosphate during its interactions with iron oxides. Geochim. Cosmochim. Acta, 74: 1309–1319.

Kelland, K., 2017a. Cancer agency left in the dark over glyphosate evidence. Reuters Investigates. https://www.reuters.com/investigates/special-report/glyphosate-cancer-data/. Accessed on 6/14/2017.

Kelland, K., 2017b. In glyphosate review, WHO cancer agency edited out "non-carcinogenic" findings. Reuters Investigates. https://www.reuters.com/investigates/special-report/who-iarc-glyphosate/. Accessed on 10/19/2017.

Kendall, C., 1998. Tracing nitrogen sources and cycling in catchments. In C. Kendall and J. J. McDonnell ed. Isotope tracers in catchment hydrology. Elsevier Science: 519–576.

Kiely, T., Donaldson, D. and Grube, A., 2004. Pesticide industry sales and usage: 2000 and 2001 market estimates. U.S. Environmental Protection Agency, Office of Prevention, Pesticides, and Toxic Substances (7503C). EPA-733-R-04-001: 34.

Kishore, G.M. and Jacob, G.S., 1987. Degradation of glyphosate by *Pseudomonas* sp. PG 2982 via a sarcosine intermediate. J. Biol. Chem., 262: 12164–12168.

Kjaer, J., 2005. No restriction of autumn use of glyphosate in Denmark. The Danish Pesticide Leaching Assessment Programme., Monitoring Results May 1999–June 2002. 3rd Report. ISBN 87-7871-115-0.

Kolpin, D.W., Thurman, E.M., Lee, E.A., Meyer, M.T., Furlong, E.T. and Glassmeyer, S.T., 2006. Urban contributions of glyphosate and its degradate AMPA to streams in the United States. Sci. Total Environ., 354: 191–197.

Kujawinski, D.M., Wolbert, J.B., Zhang, L., Jochmann, M.A., Widory, D., Baran, N. and Schmidt, T.C., 2013. Carbon isotope ratio measurements of glyphosate and AMPA by liquid chromatography coupled to isotope ratio mass spectrometry. Anal. Bioanal. Chem., 405: 2869–2878.

Lecuyer, C., Grandjean, P. and Sheppard, S.M.F., 1999. Oxygen isotope exchange between dissolved phosphate and water at temperatures <135 °C: Inorganic versus biological fractionations. Geochim. Cosmochim. Acta, 63: 855–862.

Li, H., Joshi, S.R. and Jaisi, D.P., 2016. Degradation and isotope source tracking of glyphosate and aminomethylphosphonic acid. J. Agric. Food Chem., 64: 529–538.

Liang, Y. and Blake, R.E., 2006. Oxygen isotope signature of Pi regeneration from organic compounds by phosphomonoesterases and photooxidation. Geochim. Cosmochim. Acta, 70: 3957-3969.

Liang, Y. and Blake, R.E., 2009. Compound- and enzyme-specific phosphodiester hydrolysis mechanisms revealed by $\delta^{18}O$ of dissolved inorganic phosphate: Implications for marine P cycling. Geochim. Cosmochim. Acta, 73: 3782–3794.

Longinelli, A., Bartelloni, M. and Cortecci, G., 1976. The isotopic cycle of oceanic phosphate, I. Earth Planet. Sci. Lett., 32: 389–392.

Longinelli, A. and Nuti, S., 1973. Revised phosphate–water isotopic temperature scale. Earth Planet. Sci. Lett., 19: 373–376.

Marc, J., Belle, R., Morales, J., Cormier, P. and Mulner-Lorillon, O., 2004. Formulated glyphosate activates the DNA-response checkpoint of the cell cycle leading to the prevention of G2/M transition. Toxicol. Sci., 82: 436–442.

McBride, M.B. and Kung, K.H., 1989. Complexation of glyphosate and related ligands with iron(III). Soil Sci. Soc. Am. J., 53: 1668–1673.

McLaughlin, K., Cade-Menun, B.J. and Paytan, A., 2006. The oxygen isotopic composition of phosphate in Elkhorn Slough, California: A tracer for phosphate sources. Estuarine, Coastal Shelf Sci., 70: 499–506.

McVey, K.A., Snapp, I.B., Johnson, M.B., Negga, R., Pressley, A.S. and Fitsanakis, V.A., 2016. Exposure of C. elegans eggs to a glyphosate-containing herbicide leads to abnormal neuronal morphology. Neurotoxicol. Teratol., 55: 23–31.

Mehrsheikh, A., Bleeke, M., Brosillon, S., Laplanche, A. and Roche, P., 2006. Investigation of the mechanism of chlorination of glyphosate and glycine in water. Water Res., 40: 3003–3014.

Meyer, M.T., Loftin, K.A., Lee, E.A., Hinshaw, G.H., Dietze, J.E. and Scribner, E.A., 2009. Determination of glyphosate, its degradation product aminomethylphosphonic acid, and glufosinate, in water by isotope dilution and online solid-phase extraction and liquid chromatography/tandem mass spectrometry. U.S. Geological Survey, Reston, Virginia.

Monsanto, 1996. Glyphosate fact sheet. Pesticides News, 33: 28–29.

Monsanto, 2005. Backgrounder: History of Monsanto's glyphosate herbicides. https://monsanto.com/app/uploads/2017/06/back_history.pdf. Accessed on 07/16/2018.

Monsanto, 2014. Backgrounder: Glyphosate and environmental fate studies. http://www.monsantoglobal.com/global/jp/products/Documents/glyphosate-and-environmental-fate-studies.pdf. Accessed on 07/16/2018.

Muneer, M. and Boxall, C., 2008. Photocatalyzed degradation of a pesticide derivative glyphosate in aqueous suspensions of titanium dioxide. Int. J. Photoenergy, 2008: 1–7.

Navarro, C.D. and Martinez, C.B., 2014. Effects of the surfactant polyoxyethylene amine (POEA) on genotoxic, biochemical and physiological parameters of the freshwater teleost Prochilodus lineatus. Comp. Biochem. Physiol. C: Toxicol. Pharmacol., 165: 83–90.

Newton, M., Horner, L.M., Cowell, J.E., White, D.E. and Cole, E.C., 1994. Dissipation of glyphosate and aminomethylphosphonic acid in North American forests. J. Agric. Food Chem., 42: 1795–1802.

Nowack, B., 1997. Determination of phosphonates in natural waters by ion-pair high-performance liquid chromatography. J. Chromatogr. A, 773: 139–146.

Obojska, A., Ternan, N.G., Lejczak, B., Kafarski, P. and Mc Mullan, G., 2002. Organophosphonate utilization by the thermophile Geobacillus caldoxylosilyticus T20. Appl. Environ. Microbiol., 68: 2081–2084.

Paudel, P., Negusse, A. and Jaisi, D.P., 2015. Birnessite-catalyzed degradation of glyphosate: A mechanistic study aided by kinetics batch studies and NMR spectroscopy. Soil Sci. Soc. Am. J., 79: 815–825.

Pipke, R. and Amrhein, N., 1988. Degradation of the phosphonate herbicide glyphosate by *arthrobacter atrocyaneus* ATCC 13752. Appl. Environ. Microbiol., 54: 1293–1296.

Post, J.E., 1999. Manganese oxide minerals: Crystal structures and economic and environmental significance. Proc. Natl. Acad. Sci. USA, 96: 3447–3454.

Post, J.E. and Veblen, D.R., 1990. Crystal structure determination of synthetic sodium, magnesium, and potassium birnessite using TEM and the Rietveld method. Am. Mineral., 75: 477–489.

Roy, N.M., Ochs, J., Zambrzycka, E. and Anderson, A., 2016. Glyphosate induces cardiovascular toxicity in *Danio rerio*. Environ. Toxicol. Pharmacol., 46: 292–300.

Rueppel, M.L., Brightwell, B.B., Schaefer, J. and Marvel, J.T., 1977. Metabolism and degradation of glyphosate in soil and water. J. Agric. Food Chem., 25: 517–528.

Sandy, E.H., Blake, R.E., Chang, S.J., Jun, Y. and Yu, C., 2013. Oxygen isotope signature of UV degradation of glyphosate and phosphonoacetate: Tracing sources and cycling of phosphonates. J. Hazard. Mater., 260: 947–954.

Sheals, J., Sjoberg, S. and Persson, P., 2002. Adsorption of glyphosate on goethite: Molecular characterization of surface complexes. Environ. Sci. Technol., 36: 3090–3095.

Sparks, D.L., 2002. Environmental soil chemistry. 2nd Edition. Academic Press, San Diego, CA. Elsevier.

Sprankle, P., Meggitt, W.F. and Penner, D., 1975. Adsorption, mobility, and microbial degradation of glyphosate in soil. Weed Sci., 23: 229–234.

Steinrticken, H.C. and Amrhein, N., 1980. The herbicide glyphosate is a potent inhibitor of 5-enolpyruvyl-shikimaic acid-3-phosphate synthase. Biochem. Biophys. Res. Commun., 94: 1207–1212.

Sviridov, A.V., Shushkova, T.V., Ermakova, I.T., Ivanova, E.V., Epiktetov, D.O. and Leontievsky, A.A., 2015. Microbial degradation of glyphosate herbicides (Review). Appl. Biochem. Microbiol., 51: 188–195.

Sviridov, A.V., Shushkova, T.V., Zelenkova, N.F., Vinokurova, N.G., Morgunov, I.G., Ermakova, I.T. and Leontievsky, A.A., 2012. Distribution of glyphosate and methylphosphonate catabolism systems in soil bacteria *Ochrobactrum anthropi* and *Achromobacter* sp. Appl. Microbiol. Biotechnol., 93: 787–796.

Tarone, R.E., 2018. On the international agency for research on cancer classification of glyphosate as a probable human carcinogen. Eur. J. Cancer Prev., 27: 82–87.

Taylor, R.M., McKenzie, R.M. and Norrish, K., 1964. The mineralogy and chemistry of manganese in some Australian soils. Aust. J. Soil Res, 2: 235–248.

Ternan, N.G., Mc Grath, J.W., Mc Mullan, G. and Quinn, J.P., 1998. Review: Organophosphonates: Occurrence, synthesis and biodegradation by microorganisms. World J. Microbiol. Biotechnol., 14: 635–647.

Thelin, G.P. and Stone, W.W., 2013. Estimation of annual agricultural pesticide use for counties of the conterminous United States, 1992–2009. U.S. Geological Survey Scientific Investigations Report 2013-5009: 54 p.

Thongprakaisang, S., Thiantanawat, A., Rangkadilok, N., Suriyo, T. and Satayavivad, J., 2013. Glyphosate induces human breast cancer cells growth via estrogen receptors. Food Chem. Toxicol., 59: 129–136.

Tribe, L., Kwon, K.D., Trout, C.C. and Kubicki, J.D., 2006. Molecular orbital theory study on surface complex structures of glyphosate on goethite: Calculation of vibrational frequencies. Environ. Sci. Technol., 40: 3836–3841.

Tsui, M.T.K. and Chu, L.M., 2003. Aquatic toxicity of glyphosate-based formulations: Comparison between different organisms and the effects of environmental factors. Chemosphere, 52: 1189–1197.

Tudge, A.P., 1960. A method of oxygen isotopes in orthophosphate and its use in measurement of paleotemperatures. Geochim. Cosmochim. Acta, 18: 81–93.

United States Environmental Protection Agency, 1993. Prevention, pesticides and toxic substances (7508W). R.E.D FACTS. Glyphosate., EPA-738-F-93-011.

United States Environmental Protection Agency, 2009. National primary drinking water regulations. http://water.epa.gov/drink/contaminants/upload/mcl-2.pdf. EPA 816-F-09-004.

United States Environmental Protection Agency, 2017. Glyphosate. Draft human health risk assessment in support of registration review. Washington, D. C. 20460.

United States Geological Survey, 2015. http://water.usgs.gov/nawqa/pnsp/usage/maps/show_map.php?year=2015&map=GLYPHOSATE&hilo=L&disp=Glyphosate. Accessed on 07/16/2018.

Wackett, L.P., Shames, S.L., Venditti, C.P. and Walsh, C.T., 1987. Bacterial carbon–phosphorus lyase: Products, rates, and regulation of phosphonic and phosphinic acid metabolism. J. Bacteriol., 169: 710–717.

Waiman, C.V., Avena, M.J., Regazzoni, A.E. and Zanini, G.P., 2013. A real time in situ ATR-FTIR spectroscopic study of glyphosate desorption from goethite as induced by phosphate adsorption: Effect of surface coverage. J. Colloid Interface Sci., 394: 485–489.

Wang, Z., Fingas, M., Landriault, M., Sigouin, L., Castle, B., Hostetter, D., Zhang, D. and Spencer, B., 1998. Identification and linkage of tarballs from the coasts of Vancouver island and Northern California using GC/MS and isotopic techniquess. J. High Resol. Chromatogr., 21: 383–395.

Wester, R.C., Quan, D. and Maibach, H.I., 1996. In vitro percutaneous absorption of model compounds glyphosate and malathion from cotton fabric into and through human skin. Food Chem. Toxicol., 34: 731–735.

Zhou, J., Li, J., An, R., Yuan, H. and Yu, F., 2012. Study on a new synthesis approach of glyphosate. J. Agric. Food Chem., 60: 6279–6285.

Chapter 2

AN ISOTOPE LABELING TECHNIQUE TO INVESTIGATE ATOM EXCHANGE DURING ORTHOPHOSPHATE SORPTION AND DESORPTION

Reproduced with permission from

An Isotope Labeling Technique to Investigate Atom Exchange during Phosphate Sorption and Desorption

Hui Li and Deb P. Jaisi

Soil Sci. Soc. Am. J., 2015, 79:1340–1351

DOI: 10.2136/sssaj2015.04.0158

https://dl.sciencesocieties.org/publications/sssaj/abstracts/79/5/1340

2.1 Abstract

Iron and manganese oxides are common minerals in a wide range of soils, and they largely control the fate of phosphorus. It is often implicitly assumed that orthophosphate does not exchange oxygen atoms with minerals and water during adsorption, desorption, and precipitation reactions, but this has not yet been fully verified. In this study, we applied an ^{18}O stable isotope labeling technique to individually label oxygen atoms in Fe- and Mn-oxides, water, and orthophosphate, and tested the exchange of O among them during orthophosphate sorption and desorption reactions. Physicochemical properties of ^{18}O-labeled goethite, hematite, hausmannite, and birnessite minerals were characterized using X-ray diffraction, Brunauer–Emmett–Teller (BET) surface area, particle size distribution, and scanning electron

microscopy. All sorption and desorption results showed fast initial kinetics, with hausmannite having the highest sorption capacity, followed by a relatively slower sorption–desorption reaction before reaching equilibrium. Oxygen isotope ratios ($\delta^{18}O$) in Fe- and Mn-oxides, orthophosphate, and water showed no exchange of O between orthophosphate and mineral or water during either sorption or desorption reactions. These results attest to the integrity of the P–O bond during these reactions and thus enable the phosphate oxygen isotope composition to be used as a reliable tool for tracing orthophosphate sources in soils and other environments.

ABBREVIATIONS: XRD: X–ray diffraction; BET: Brunauer–Emmett–Teller; DLS: dynamic light scattering; $\delta^{18}O$: oxygen isotope ratios; $\delta^{18}O_P$: phosphate oxygen isotope ratios; $\delta^{18}O_W$: water oxygen isotope ratios; $\delta^{18}O_{FeO/MnO}$: oxygen isotope ratios in Fe- or Mn-oxide; PZC: point of zero charge; SEM: scanning electron microscope; SSA: specific surface area; VSMOW: Vienna standard mean oxygen water.

2.2 Introduction

Iron (Fe) and manganese (Mn) oxides are common minerals in soils. These minerals influence physicochemical properties of soils and thereby control the distribution and transport of nutrients (Ulery and Drees, 2008). The fate of phosphorus (P), an essential and often limiting nutrient for all life forms (Jaisi and Blake, 2010), is largely controlled by different reactions with minerals such as adsorption, desorption, and co-precipitation (Emerson, 1978; Paige et al., 1997; Schwertmann and Taylor, 1989). Because of the low stoichiometric biological need for P among other major nutrients (106C: 16N: 1P) (Redfield, 1958), a small increase in P concentration could cause severe impacts on water quality. Therefore, partitioning of P as sorbed and

mobile species has attracted intense research efforts in various disciplines, including soil fertility and water quality.

It is generally agreed that orthophosphate adsorbs onto Fe-oxides, such as goethite and hematite, that are positively charged at neutral pH as inner-sphere bidentate binuclear or monodentate mononuclear complexes (via ligand exchange) where one or two oxygen atoms of orthophosphate anions are assumed to bind directly to one or two Fe atoms, forming $(FeO)_2(OH)PO$ or $(FeO)(OH)_2PO$, respectively (Arai and Sparks, 2007; Elzinga and Sparks, 2007; Tejedor-Tejedor and Anderson, 1990). On the other hand, Mn-oxides are negatively charged at neutral pH and thus are effective for metal cations sorption (Li et al., 2015; Post, 1999; Yin et al., 2014) but have limited capacity to sorb anions such as orthophosphate because of electrostatic repulsion. However, δ- and β-MnO_2 and nano-sized hydrous manganese oxides have been reported to adsorb orthophosphate and probably form both outer-sphere and inner-sphere complexes (Pan et al., 2014; Yao and Millero, 1996). In these complexation reactions, one O has to be removed either from mineral or from orthophosphate to establish a P–O–Fe/Mn bond. It is commonly assumed that O (or OH) from the mineral, but not from orthophosphate, is removed during this reaction. The underlying reason for this assumption is that the P–O bond is strong compared with Fe–O(–OH)/H_2O or Mn–O(–OH)/H_2O bonds (Gibbs et al., 2008; Luo, 2007). This assumption applies analogously to desorption reactions where O (or OH) from water is incorporated into the mineral surface following the removal of intact PO_4. While there is a general consensus on the dominance of bond type and nature (mono-, bi-, or tridentate) of the complexes formed, O atom exchange has been ignored.

Stable isotope ratios of nutrients such as nitrogen ($\delta^{15}N$), carbon ($\delta^{13}C$) and oxygen ($\delta^{18}O$) in N and C compounds have been routinely used as a tool to track nutrient sources and cycling (Bohlke and Denver, 1995; Kendall, 1998; Wang et al., 1998). Oxygen isotopic compositions of phosphate ($\delta^{18}O_P$) can analogously be used to identify different P sources and to disentangle specific biogeochemical reactions among different P pools and forms at different interfaces (Blake et al., 1997; Jaisi and Blake, 2010; McLaughlin et al., 2006). This is because phosphate oxygen isotope ratios have a reaction-specific isotope effect, in particular: (i) in abiotic reactions such as sorption, desorption, transport, and mineral transformation, phosphate does not undergo any significant changes in its O isotopic composition (Jaisi et al., 2010; Jaisi et al., 2011; O'Neil et al., 2003; Tudge, 1960; Winter et al., 1940); (ii) in biological reactions, rapid O isotope exchange occurs between dissolved orthophosphate and water, and this may result in complete isotope exchange and thus produce temperature-dependent equilibrium O isotope fractionation (Blake et al., 1997; Blake et al., 2005; Longinelli and Nuti, 1973). Phosphorus undergoes both biotic and abiotic pathways of cycling in natural environments; however, a distinct trend of $\delta^{18}O_P$ evolution may help approximate the relative extent of biotic and abiotic cycling (Jaisi and Blake, 2010; Jaisi et al., 2011; Joshi et al., 2015).

Several biogeochemical reactions that involve P in soils and other environments often affect both the concentration and isotopic composition of orthophosphate. While abiotic interactions, in general, at low temperature do not impart significant isotope fractionation (see above), more detailed aspects of this isotope effect, including different minerals and interfaces, in all potential O sources are still unknown and thus require validation before any generalization can be made.

In particular, it remains unknown whether there is any O isotopic exchange among orthophosphate, water, and minerals during abiotic interactions of orthophosphate with Fe- and Mn-oxides. This is particularly important because inner-sphere complexation of orthophosphate on mineral surfaces requires O removal (see above). An in-depth understanding of these reactions will (i) identify the specific bond cleavage site during orthophosphate sorption and desorption reactions and help better elucidate the mechanism of sorption–desorption onto Fe- and Mn-oxides, and (ii) further enhance the use of phosphate oxygen isotopes as a geochemical indicator of reactions involving P in natural environments. The objectives of this research, therefore, were to determine any oxygen isotope exchange during orthophosphate adsorption and desorption reactions on four common Fe- and Mn-oxide minerals—goethite, hematite, hausmannite, and birnessite—under room temperature (22±1 ^{o}C) and neutral pH (pH=7.00±0.05) conditions, and to identify the O source to be removed during the sorption and received during the desorption reaction.

2.3 Materials and Methods

2.3.1 Mineral Synthesis

Two Fe minerals (goethite and hematite) and two Mn minerals (hausmannite and birnessite) were synthesized. The Fe mineral synthesis followed the method of Schwertmann and Cornell (Schwertmann and Cornell, 1991). Goethite (FeOOH) was prepared by rapidly adding 180 mL of 5 mol L^{-1} KOH to a stirred 100 mL solution of 1 mol L^{-1} $Fe(NO_3)_3 \cdot 9H_2O$. The solution was immediately diluted to 2000 mL and was kept at 70 °C for 60 h. Similarly, hematite (Fe_2O_3) was prepared by adding 16.6 g of $Fe(NO_3)_3 \cdot 9H_2O$ to a vigorously stirred and heated 2000 mL solution of 2 mmol L^{-1}

HCl at 98 °C. The suspension was gently stirred and aged for seven days at the same temperature to achieve the bright red hematite precipitate.

Hausmannite [$(Mn^{2+}Mn^{3+}_2)O_4$] was prepared following the McArdell et al. (McArdell et al., 1998) method. In brief, 1000 mL of 60 mmol L^{-1} $MnSO_4$ solution was heated to 60 °C followed by adding 20.5 mL of 8.8 mol L^{-1} H_2O_2 and 300 mL of 0.2 mol L^{-1} NH_4OH. The resulting brown suspension was quickly heated to 95 °C, and maintained at this temperature for 6 h with continuous stirring. Similarly, K^+-birnessite [$K_x(Mn^{4+}, Mn^{3+})_2O_4$; where $x<1$] was prepared by adding 45 mL of 6 mol L^{-1} HCl at a constant rate to a vigorously boiling solution of 300 mL of 0.667 mol L^{-1} $KMnO_4$ (McKenzie, 1971). The constant rate of HCl addition was maintained by using an ISMATEC IPC high precision multichannel dispenser pump (Cole Parmer, IL, USA).

We used three different ^{18}O-labeled waters (with $\delta^{18}O_W$ = -5.5, +44, and +88 ‰ VSMOW) appropriately diluted from 10% ^{18}O-enriched water (Cambridge Isotope Laboratories, Tewksbury, MA) in each mineral synthesis so that structural oxygen atoms in each mineral were correspondingly labeled with distinct ^{18}O values. These three isotope-labeled minerals are indicated by A, B, and C suffixes (from lighter to heavier isotopic composition, such as Goe-A, Goe-B, and Goe-C, respectively, for goethite). During the synthesis reactions, the temperature was frequently monitored and controlled within ±3 °C of the targeted temperature, and triple-folded aluminum foil tightly covered the top of the reactor to minimize water evaporation. After completion of the reactions, the synthesized mineral precipitates were washed five times in deionized water, then freeze-dried, gently ground, and stored until further use.

2.3.2 Mineral Characterization

X-ray diffraction (XRD) analysis of each synthetic mineral was performed on a D8 Discover Diffractometer (Bruker, Germany) using Ni-filtered, Cu Kα radiation (wavelength λ = 0.15418 nm). The diffractometer was operated at a voltage of 40 kV and a current of 40 mA and each XRD measurement included 1.0 s counting time per 0.02° 2θ step. Similarly, the micromorphology and crystallinity of the minerals, including the degree of purity, was probed by a field emission capable scanning electron microscope (JEOL JSM-7400F, Japan) after coating a thin layer of mineral powder with a thin gold film.

The specific surface area (SSA) of each mineral was measured using the BET (Brunauer-Emmett-Teller) method by using a Micromeritics ASAP 2020 Surface Area and Porosity Analyzer (Georgia, USA). Mineral samples (0.1–0.2 g) were first degassed for 3 h under vacuum before running N_2 adsorption–desorption isotherms to calculate the SSA. Similarly, a Wyatt Möbiuζ Dynamic Light Scattering instrument (DLS; Santa Barbara, California) was used to determine the particle size distribution of each synthetic mineral.

2.3.3 Synthesis of ^{18}O Labeled Orthophosphate

The ^{18}O-labeled orthophosphate was synthesized using the method described by Melby et al. (Melby et al., 2011) and Stout et al. (Stout et al., 2014) by reacting PCl_5 with ^{18}O-labeled water:

$$PCl_5 + 4H_2O = H_3PO_4 + 5HCl \quad [1]$$

Because this reaction is exothermic, the PCl_5 was finely powdered and added to the ^{18}O-labeled water in small masses (< 1.0 g), waiting until the heat produced in the reaction was completely dissipated before adding fresh PCl_5. We were able to

synthesize highly concentrated (~3 mol L^{-1}) labeled orthophosphate following this method due to the high solubility of orthophosphate in water. After synthesis, the pH of the solution was neutralized (pH 7.0±0.1), and the solution was stored until use.

2.3.4 Orthophosphate Sorption and Desorption Experiments

A series of orthophosphate sorption experiments was performed to determine the equilibrium orthophosphate distribution as well as O-isotopic fractionation between aqueous and sorbed orthophosphate (Table 2.1). Suspensions containing 5 g L^{-1} of each of three different ^{18}O-labeled minerals were prepared in 10 mmol L^{-1} KCl ionic strength at pH=7.00 (±0.05). The batch sorption reaction was initiated by adding ^{18}O-labeled orthophosphate. Initial orthophosphate concentrations used in the experiments were 1200, 500, 800, and 500 μmol L^{-1} for goethite, hematite, hausmannite, and birnessite, respectively. Each reaction was performed in triplicate at room temperature (22±1 ^{o}C) and several of these experiments were repeated to test the reproducibility of the results. A magnetic stirrer was used at a speed of 200 rpm in each batch experiment to ensure homogeneous mineral mixing of the suspension during the reaction. The pH was periodically measured and maintained at 7.00±0.05, adjusted by using 1 mol L^{-1} NaOH or 1 mol L^{-1} HCl, as needed. Maximum orthophosphate adsorption by Fe- and Mn-oxides has been reported under acidic conditions (Shang et al., 1992; Yao and Millero, 1996). However, we chose pH 7.0 in this experiment to represent common natural soil pH conditions. In each experiment, 50 μmol L^{-1} sodium azide (NaN_3) was added to suppress microbial activities. At selected time points (1 min, 5 min, 10 min, 20 min, 30 min, 40 min, 1 h, 2 h, 3 h, 5 h, 8 h, 12 h, 1 d, 2 d, 3 d...>30 d), sample aliquots were removed, and aqueous and

sorbed orthophosphate were separated by centrifugation (7,000 ×g for 0.5 h). Sorption kinetic data were fitted with a pseudo-second-order sorption model:

$$q_t = \frac{q_e^2 Kt}{1+q_e Kt} \quad [2]$$

where q_e represents the maximum sorption capacity at equilibrium, q_t is the sorbed orthophosphate at any time t, and K is the rate coefficient for the pseudo-second-order sorption reaction.

After the completion of the sorption experiment, minerals with sorbed orthophosphate were washed with the DI water three times to remove aqueous orthophosphate. Each mineral suspension was then dispersed in new 10 mmol L^{-1} KCl at the same original concentration (5 g L^{-1}) and pH balanced to 7.00 (±0.05). The desorption experiment was initiated by adding 1 mmol/L Na- or K-citrate. Na-citrate was used for Mn minerals and K-citrate was used for Fe-oxides for easy quantification of released structural ions induced by citrate-promoted dissolution. Sample aliquots were removed at predetermined time intervals and separated into aqueous and sorbed phases (as above).

To extract sorbed orthophosphate from minerals (both in sorption and desorption experiments) for isotope analysis, the pelleted mineral-orthophosphate samples were first freeze-dried and then dissolved in 12 mol L^{-1} HCl or 1 mol L^{-1} hydroxylamine hydrochloride. Goethite, hematite, and hausmannite minerals fully dissolved in hydrochloric acid but hydroxylamine hydrochloride was additionally added to birnessite for complete dissolution. Concentrations of aqueous and sorbed orthophosphate were measured colorimetrically by using a UV/vis spectrophotometer (Murphy and Riley, 1962) and a P mass balance was calculated to accurately account for P speciation, particularly to ensure complete removal of sorbed P from minerals.

Table 2.1. Initial experimental set up with different $\delta^{18}O$ values (A, B, and C) of the mineral, orthophosphate, and water.

Oxides	Label	$\delta^{18}O$ (‰)		
		Mineral	Orthophosphate	H_2O
Goethite FeO(OH)	A	-9.45±0.02	36.29±0.19	-7.10±0.05
	B	32.61±0.00	15.58±0.31	-7.17±0.03
	C	69.74±0.03	15.58±0.31	-7.16±0.03
Hematite Fe_2O_3	A	-9.00±0.02	36.29±0.19	-7.16±0.05
	B	36.56±0.01	15.58±0.31	-7.17±0.07
	C	77.31±0.01	15.58±0.31	-7.16±0.03
Hausmannite $(Mn^{2+}Mn^{3+}{}_2)O_4$	A	-10.55±0.01	36.29±0.19	-7.11±0.04
	B	33.38±0.02	19.50±0.18	-7.14±0.06
	C	67.91±0.03	19.50±0.18	-7.20±0.07
Birnessite $K_xMn_2O_4$	A	-3.69±0.03	36.29±0.19	-7.13±0.05
	B	55.31±0.02	19.50±0.18	-7.11±0.07
	C	94.79±0.02	19.50±0.18	-7.10±0.04

2.3.5 Sample Processing and The Measurement of Oxygen Isotope Ratios in Orthophosphate, Water, and Minerals

Both aqueous and sorbed orthophosphate samples collected at different times during the sorption and desorption experiments were processed and ultimately converted to silver phosphate for O-isotopic measurement. Several steps were taken to remove reagents and purify orthophosphate. Dissolved orthophosphate was first precipitated into ammonium phosphomolybdate (APM), then dissolved by ammonium citrate and then recrystallized as magnesium ammonium phosphate (MAP) following published methods (Jaisi and Blake, 2010; Jaisi and Blake, 2014; Jaisi et al., 2010). The MAP was dissolved in nitric acid and further treated with a cation resin to remove cations. The purified orthophosphate was then precipitated as silver phosphate with addition of a silver amine reagent. Two phosphate standards with known $\delta^{18}O_P$ values

were processed in parallel with the experimental samples to test the validity of the sample processing method and isotope results. The silver phosphate precipitate, the ultimate analyte, was roasted at 110 °C for 24 h to remove any trapped water. Silver capsules containing 200–250 μg of silver phosphate were prepared in triplicate for O isotope measurement.

Phosphate O isotope ratios were measured in the stable isotope facility at the University of Delaware. Silver phosphate was pyrolyzed at 1460 °C by online high-temperature thermal decomposition using a Thermo Chemolysis/Elemental Analyzer (TC/EA) coupled with a Delta V continuous-flow isotope ratio monitoring mass spectrometer (IRMS; Thermo, Bremen, Germany) with a precision of ±0.3 ‰. All samples and standards were run at least in triplicate. The $\delta^{18}O_P$ values of the silver phosphate samples were calibrated against two silver phosphate standards (YR1-1 aR02 and YR3-2) with $\delta^{18}O_P$ values of -5.49 and +33.63 ‰, respectively (Vennemann et al., 2002).

To determine the changes in O isotope ratios of the waters used in the experiments, 1 mL of solution was extracted at the start and the end of each experiment. Water samples of 0.3 mL were injected into a 12 mL pressurized borosilicate Exetainer® (Labco; Buckinghamshire, England) prefilled with 300 ppm CO_2 in He. Equilibration between CO_2 and H_2O was allowed for 24 h at 26.2 °C, and the O isotope ratios in CO_2 ($\delta^{18}O_{CO2}$) were measured using a GasBench device connected to an IRMS. The $\delta^{18}O_W$ values in H_2O were then calculated from $\delta^{18}O_{CO2}$ values based on the fractionation factor following the method of Cohn and Urey (Cohn and Urey, 1938) as described in Upreti et al. (Upreti et al., 2015). All samples and standards were run at least in duplicate. Measured $\delta^{18}O_W$ values of the waters were

calibrated against two USGS water standards ($\delta^{18}O_W$ values of -1.97 and -9.15‰). The standard deviation of isotope measurement was within the range of ±0.02 ‰.

The O isotope ratios of Fe- and Mn-oxide minerals were determined using laser fluorination. The minerals were first heated in a BrF_5 atmosphere in a 30 W CO_2 laser fluorination device to liberate structural oxygen from the minerals (Bao et al., 2000; Peng et al., 2011). Isotope ratios of the molecular oxygen produced were measured in dual-inlet mode on an MAT253 IRMS at Louisiana State University. For each mineral, isotope ratios were measured in triplicate. The standard deviation of the measurement was within the range of ±0.05 ‰. Please note that the laser fluorination method has potential limitations for accurate $\delta^{18}O$ measurement for several reasons including partial O yield for more crystalline minerals and premature removal of oxygen from specific sites (e.g. removal of surface hydroxyl group) during prefluorination of amorphous minerals. Potential effects of these issues on measured isotope values were tested carefully by comparing measured $\delta^{18}O_{FeO/MnO}$ and water $\delta^{18}O_W$ values used during the synthesis of the minerals. Given that the results from replicate sample measurements were similar and within the ranges expected from the water $\delta^{18}O_W$ values, the impact of these potential sources of errors on the measured isotope composition were expected to be minimal. All oxygen isotope data (in orthophosphate, water, and minerals) in this study are reported as $\delta^{18}O$ ‰ (with appropriate subscript) relative to Vienna standard mean ocean water (VSMOW) as a reference standard.

2.4 Results

2.4.1 Mineral Characterization

The powder XRD patterns of the synthetic minerals are shown in Figure 2.1. All minerals were mostly single-phase Fe- and Mn-oxides, with no identifiable ancillary phases that showed peaks in XRD patterns. The K^+-birnessite showed more diffuse *hkl* peaks, indicating lesser crystalline structure similar to that in a previous study (Jaisi et al., 2009). SEM analyses of these minerals showed uniform characteristic morphologies (Figure 2.1). For example, goethite existed as acicular crystals, while hematite as well as hausmannite showed spherical crystal morphology. The K^+-birnessite had a distinct morphology, with flaky crystals that piled up to three-dimensional hierarchical microspheres and appeared like sponge- or flower-like structures. A close inspection of the SEM images showed that the layer or sheet structure of individual crystallite in birnessite radiated from the center of the crystal to form a flower-shaped structure. The K^+-birnessite forms a hexagonal layered structure and has a low degree of stacking among phyllomanganate sheets (Drits et al., 1997; Post and Veblen, 1990). No difference in morphology was observed due to changes in $\delta^{18}O_{FeO/MnO}$ for a mineral that was synthesized using different ^{18}O-labeled waters.

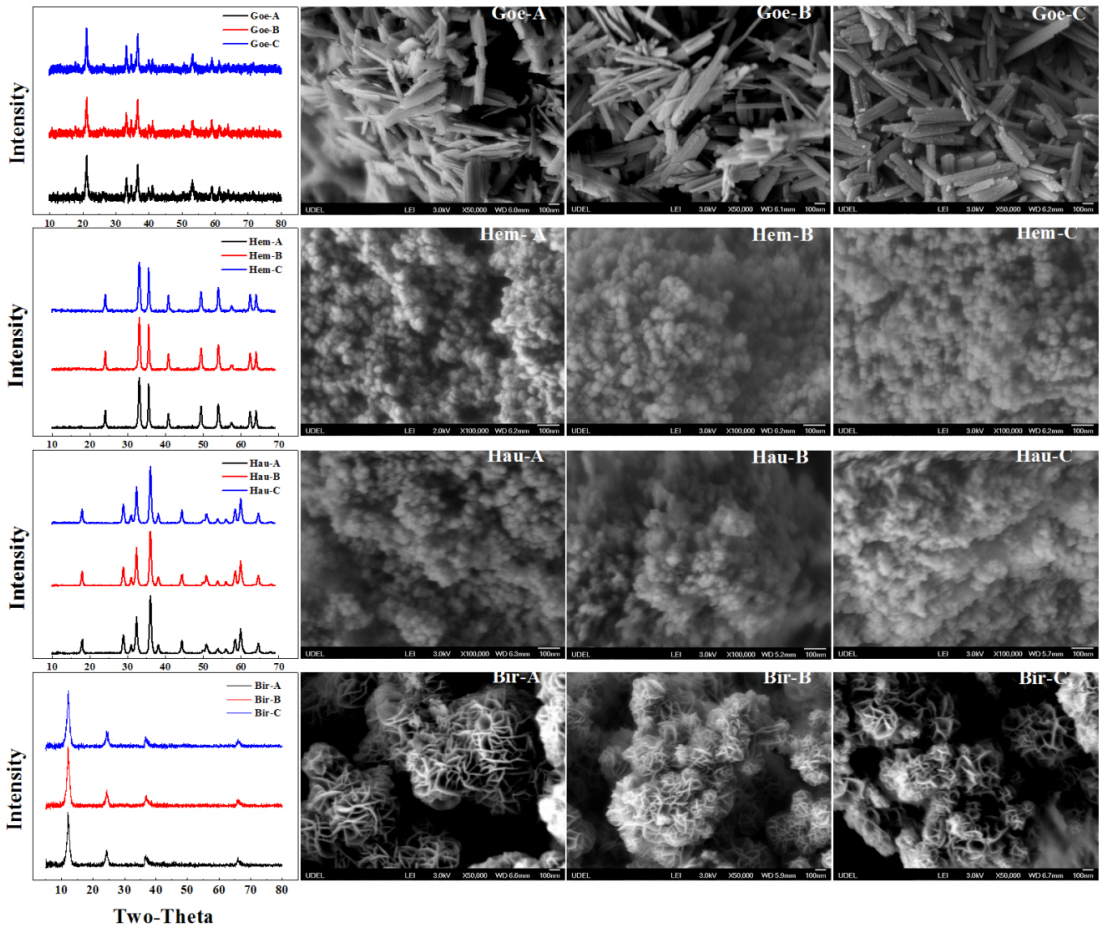

Figure 2.1. X-ray diffraction (XRD) patterns and scanning electron microscope (SEM) images of synthesized goethite (Goe), hematite (Hem), hausmannite (Hau), and birnessite (Bir) minerals. Three SEM images in a row identified, for example, as Goe-A, Goe-B, and Goe-C, refer to goethite minerals with different ^{18}O labeling (see Table 2.1 and 2.2).

The specific surface area (SSA) of the synthetic minerals varied from 26.67 to 54.30 m^2/g (Table 2.2), with average surface areas of 41.75 (±6.43) $m^2\ g^{-1}$. This range of surface areas is within the ranges reported in the literature (Feng et al., 2007; Jaisi

et al., 2009) for the minerals synthesized using the same methods. Furthermore, the SSA of a mineral with three different isotopic compositions of its structural oxygen was essentially the same. Therefore, we do not expect any significant change in mineral properties due to structural ^{18}O labeling or on orthophosphate sorption and desorption kinetics and corresponding isotope fractionation. The particle size distribution of different minerals, as measured by DLS, varied within a narrow range (Table 2.2). For example, the size range varied between 100 and 150 nm for goethite and 50 to 70 nm for hematite. Similarly, the size ranges for Mn-oxides were between 140–190 nm and 100–260 nm for birnessite and hausmannite, respectively.

Table 2.2. Characterization of synthesized minerals with different ^{18}O labeling (A, B, and C) using successively enriched ^{18}O composition in the mineral structure. NA means not available because the isotope composition was not measured.

Oxides	Label	$\delta^{18}O$ (‰)		SSA (m^2/g)	DLS Particle Size (nm)
		Mineral Structure	H_2O used in synthesis		
Goethite [FeO(OH)]	A	-9.45±0.02	NA	44.54± 0.21	117.83±0.97
	B	32.61±0.00	NA	47.55± 0.27	139.1±5.31
	C	69.74±0.03	NA	54.30± 0.39	133.7±10.46
Hematite (Fe_2O_3)	A	-9.00±0.02	NA	41.15± 0.12	71.63±4.12
	B	36.56±0.01	41.57±0.10	38.23 ± 0.12	49.40±1.28
	C	77.31±0.01	84.41±0.08	40.51 ± 0.15	55.83±0.64
Hausmannite ($Mn^{2+}Mn^{3+}{}_2)O_4$	A	-10.55±0.01	-6.44±0.06	43.70 ± 0.16	248.90±29.60
	B	33.38±0.02	38.11±0.10	42.95 ± 0.12	201.87±22.30
	C	67.91±0.03	84.57±0.06	43.18 ± 0.13	136.33±11.49
Birnessite ($K_xMn_2O_4$)	A	-3.69±0.03	-5.71±0.08	41.26 ± 0.29	143.35±4.54
	B	55.31±0.02	67.23±0.10	40.96 ± 0.25	185.70±7.99
	C	94.79±0.02	139.59±0.06	26.67 ± 0.20	167.77±3.43

SSA represents for Specific Surface Area; DLS represents for Dynamic Light Scattering method.

The $\delta^{18}O_{FeO/MnO}$ values of structural oxygen in the ^{18}O labeled synthetic minerals were within three ranges, -10.55 to -3.69 ‰, 32.61 to 55.31 ‰, and 67.91 to 94.79 ‰, that were determined by the ^{18}O-labeled waters used for synthesis and the associated fractionation factors (Table 2.2). Triplicate isotope measurements in each mineral showed a negligible difference in isotope values (±0.05 ‰), suggesting uniform labeling of structural oxygen in all minerals. This also means that the potential isotope exchange, if any, during sorption–desorption reactions would be uniform and representative for the particular mineral.

2.4.2 Phosphate Sorption and Desorption Kinetics

The orthophosphate sorption and desorption kinetics of all synthetic minerals are shown in Figure 2.2. As shown, all sorption reactions initially proceeded by a rapid sorption (within 1 h) on the mineral surface. It was followed by a slower and gradual increase of orthophosphate sorption before reaching a stable sorption equilibrium, consistent with published results (Parfitt and Atkinson, 1976; Torrent et al., 1992). On the other hand, Fe-oxides showed a fast initial release of sorbed orthophosphate in desorption reactions, followed by a slower release before reaching equilibrium. Mn-oxides presented slightly different trends during orthophosphate desorption. For example, hausmannite minerals initially released >20% of the sorbed orthophosphate within 2 h. The amount of released orthophosphate then started to decrease gradually and reached a new equilibrium. In general, after a rapid initial release of orthophosphate, desorption reached equilibrium for all minerals for all experiments, albeit at different times.

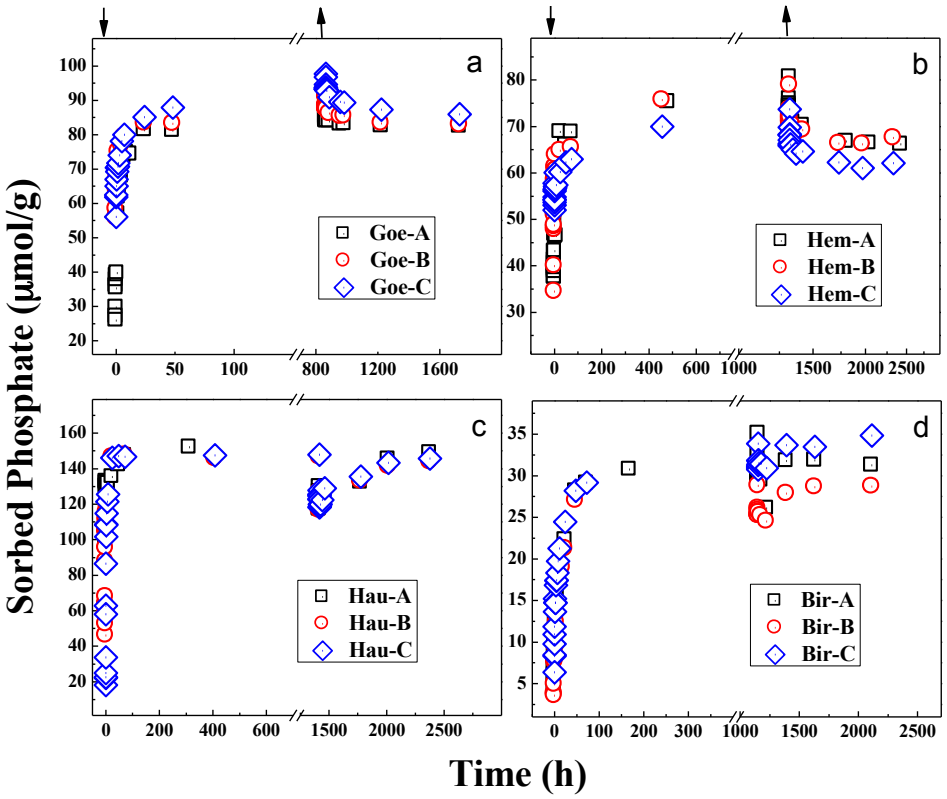

Figure 2.2. Orthophosphate sorption and desorption kinetics on ^{18}O-labeled goethite (Goe), hematite (Hem), hausmannite (Hau), and birnessite (Bir) minerals. Arrows pointing down indicate the start of sorption reactions and arrows pointing up indicate desorption reactions. Experiments were performed using starting orthophosphate $\delta^{18}O_P$ values of 15.58, 19.50 and 36.29 ‰ and $\delta^{18}O_W$ values of water about -7 ‰ at 21 ºC, pH=7.00±0.05.

The fitting of the measured data using the pseudo-second-order sorption model (eq. 2) is shown in Figure 2.3. Based on the fitting results, the decreasing order of maximum equilibrium sorption (q_e) for orthophosphate among all the minerals was as follows: hausmannite (~130 μmol g^{-1}) > goethite (~80 μmol g^{-1}) > hematite (~60 μmol g^{-1}) > birnessite (~30 μmol g^{-1}). Comparing these results with the SSA of the minerals,

the order remained the same: hausmannite (~3 μmol m^{-2}) > goethite (~1.7 μmol m^{-2}) > hematite (~1.5 μmol m^{-2}) > birnessite (~0.7 μmol m^{-2}). The decreasing order of desorption by citrate was: hematite (~15%) > goethite (9%) ≈ birnessite (9%) > hausmannite (2%). This extent of desorption was still low to insignificant, indicating strong orthophosphate retention on these minerals, consistent with a past study (Zeng et al., 2004). These results, overall, indicate major roles played by these minerals on limiting P availability in soil environments.

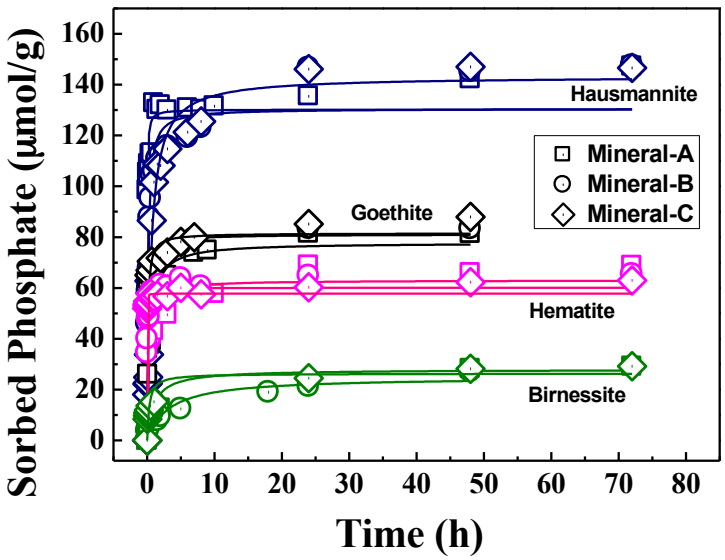

Figure 2.3. Fitting of sorption kinetics into Pseudo-second-order model using three different ^{18}O labelings (A, B, and C) of each mineral. The fitted parameters are included in Table 2.3.

Table 2.3. Fitted parameters for orthophosphate sorption on goethite (Goe), hematite (Hem), hausmannite (Hau), and birnessite (Bir) minerals with three different ^{18}O labelings (A, B, and C) using a Pseudo-second-order sorption model.

	Parameters					
Mineral	K ($g\ \mu mol^{-1}\ h^{-1}$)	q_e ($\mu mol\ g^{-1}$)	q_e ($\mu mol\ m^{-2}$)	Average q_e ($\mu mol\ g^{-1}$)	Standard Deviation	R^2
Goe-A	0.03	77.76	1.75			0.94
Goe-B	0.09	81.05	1.70	80.11	2.05	0.99
Goe-C	0.12	81.53	1.50			0.98
Hem-A	0.06	63.00	1.53			0.91
Hem-B	0.82	60.07	1.57	60.29	2.61	0.93
Hem-C	6.52	57.79	1.43			0.97
Hau-A	0.34	130.23	2.98			0.93
Hau-B	0.05	130.56	3.04	134.68	7.42	0.89
Hau-C	0.01	143.24	3.32			0.97
Bir-A	0.02	30.73	0.74			0.92
Bir-B	0.01	28.83	0.70	28.62	2.23	0.92
Bir-C	0.13	26.29	0.99			0.89

q_e, maximum amount of sorbed orthophosphate at sorption equilibrium status; K, the equilibrium rate constant for pseudo-second-order sorption reaction.

2.4.3 Changes in Phosphate Oxygen Isotope Ratios during Sorption and Desorption

The changes in $\delta^{18}O_P$ values during sorption and desorption reactions on the synthetic minerals are shown in Figure 2.4. With less energy required for light isotopes, lighter phosphate ($P^{16}O_4$ i.e., with lighter $\delta^{18}O_P$ values) is more reactive (Siebert et al., 2003) and is preferentially sorbed onto mineral surfaces first, leaving aqueous orthophosphate enriched with heavier isotopes (i.e., higher $\delta^{18}O_P$ values). Analogously, $P^{16}O_4$ tended to be preferentially desorbed first from the minerals, leaving residual orthophosphate on the mineral surfaces enriched with heavier isotopes (Jaisi et al., 2010). This lighter $P^{16}O_4$ preference in both reactions would cause

differences in the $\delta^{18}O_P$ values and result in isotope fractionation between sorbed and aqueous orthophosphate. Therefore, small differences in isotopic compositions observed at the initial stage of reaction in some experiments (e.g., Goe-A and Hem-A) was due to kinetic fractionation between aqueous and sorbed orthophosphates, consistent with similar studies on ferrihydrite (Jaisi et al., 2010). Please note that the maximum fractionation between these two P pools is significant only at the initial stage of sorption and desorption and is not apparent in some minerals due to dispersed data points or due to technical limitation of quick sampling in minerals with fast sorption–desorption kinetics. The $\delta^{18}O_P$ values of both pools in sorption and desorption reactions probably reached isotope equilibrium, as shown by small but insignificant differences between the two pools at the conclusion of the experiment. Interestingly, the $\delta^{18}O_P$ values of orthophosphate at the end of the experiment were close to that of the starting orthophosphate, and the equilibrium fractionation between sorbed and aqueous orthophosphate was small, similar to past studies on ferrihydrite (Jaisi et al., 2010).

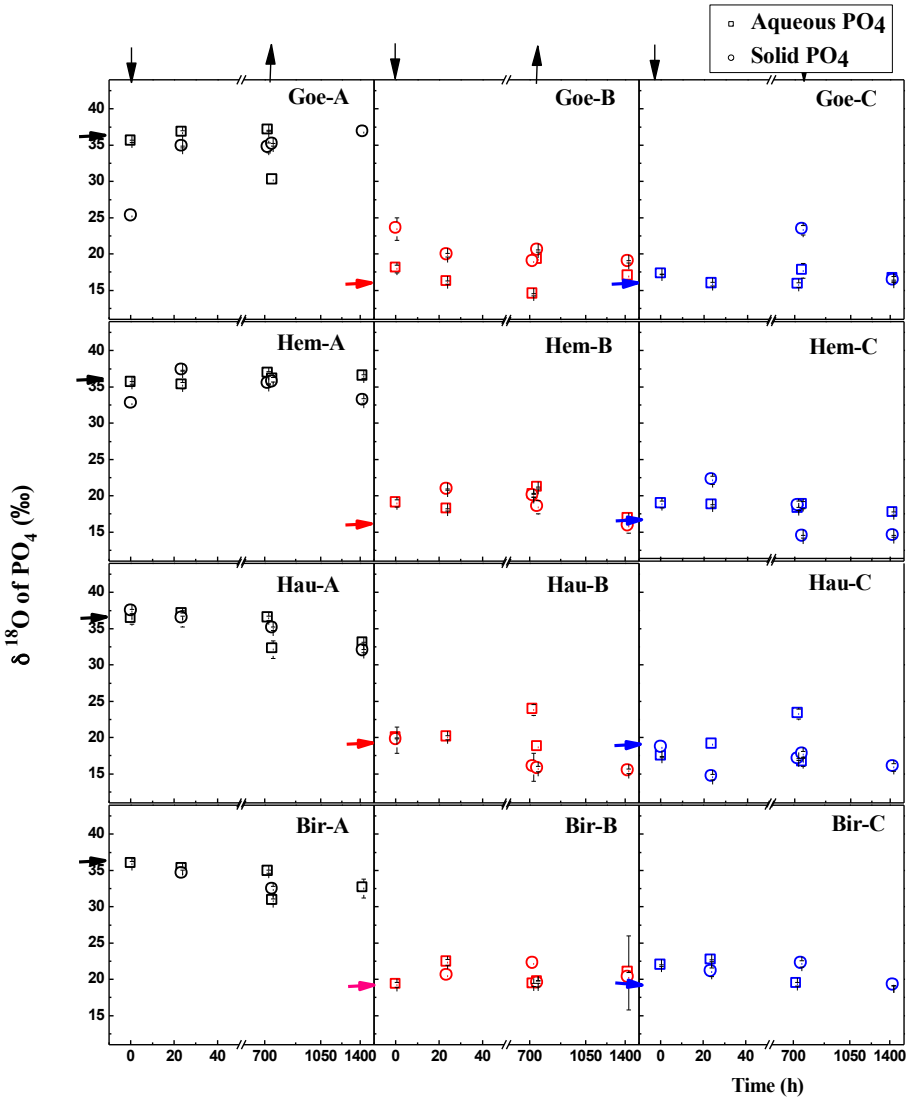

Figure 2.4. Kinetic fractionation of phosphate $\delta^{18}O_P$ values between sorbed and aqueous orthophosphate species during sorption–desorption reactions on three different ^{18}O labelings (A, B, and C) of goethite (Goe), hematite (Hem), hausmannite (Hau), and birnessite (Bir) minerals. Vertical arrows pointing down indicate the start of the sorption reactions, and arrows pointing up indicate desorption reactions. The horizontal arrows indicate the starting phosphate $\delta^{18}O_P$ values used in the experiments. Please note that the sizes of the error bars are mostly within the symbols.

The initial difference in the $\delta^{18}O$ values of minerals, orthophosphates, and waters in our experiments was >15 ‰ (in some cases it was as high as 51‰; Table 2.1). In all cases, the difference in initial isotopic composition was chosen to be different from equilibrium fractionation of O between mineral and water and that of orthophosphate and water. For example, this difference in the $\delta^{18}O$ values between orthophosphate and minerals and between orthophosphate and water was more than 45 and 43‰, respectively, for Goe-A. Thus, the isotope labeling allowed easy detection of any O isotope exchange among minerals, orthophosphates, and waters, if it occurred, due to the large difference in starting $\delta^{18}O$ values among them. Taking Goe-A as an example, the incorporation of one O from either mineral or water would result in the formation of new orthophosphate with $\delta^{18}O_P$ values of 25‰, thus dramatically shifting its original $\delta^{18}O_P$ value (36.29 ‰) by >10 ‰. Interestingly, the difference in the $\delta^{18}O_P$ values of all orthophosphate pools (i.e., sorbed, desorbed, and aqueous) remained within small ranges (usually less than ±2.1‰) (Figure 2.4). These results confirmed that no O atom exchange took place between orthophosphate and water or between mineral and orthophosphate. This means that the orthophosphate ion remained as an intact molecule (irrespective of $P^{16}O_4$ or $P^{18}O_4$ or different combinations of $P^{16}O_4$ and $P^{18}O_4$).

2.5 Discussion

2.5.1 Orthophosphate Sorption and Desorption

Orthophosphate sorption kinetics analyzed for four minerals in this study showed a high sorption capacity, with an initial step of rapid sorption followed by a slow but continued sorption reaction (Figure 2.2). Desorption also followed a similar

pattern. The rapid reaction at the first phase is explained as a combination of nonspecific adsorption and ligand exchange reactions (Bohn et al., 1979; Bohn et al., 2001), whereas the second stage, the slow reaction, is explained as a result of the gradual penetration of orthophosphate ions into the mineral aggregates. Ligand exchange is a rapid exothermic reaction in which a bridging binuclear complex of type M–O–P–O–M (where M represents Fe or Mn) is formed and OH^- is subsequently released. These changes have been confirmed in the past by monitoring changes in pH during the sorption reaction (Parfitt and Atkinson, 1976; Wang et al., 2013), isothermal calorimetry (Penn et al., 2014), or modeling (Arai and Sparks, 2007). The extent of orthophosphate sorbed is also affected by the surface charge of the minerals (Bowden et al., 1977). The point of zero charge (PZC) of Fe-oxides is usually >7.0; however, that of Mn-oxides is normally <7.0, which results in positively charged surfaces on Fe-oxide minerals and negatively charged surfaces on Mn-oxide minerals at circumneutral pH. Thus, electrostatic interactions as well as ligand exchange reactions both contribute to orthophosphate sorption onto Fe-oxides (Bowden et al., 1977; Feng et al., 2004; Parfitt and Atkinson, 1976), resulting in a higher capacity for orthophosphate sorption onto Fe-oxides than Mn-oxides. Some synthetic hydrous manganese oxides with similar PZC (~2.0) values to birnessite have been found to sorb a negligible amount of orthophosphate at pH 7.0 (Kawashima et al., 1986). However, hausmannite showed a much higher orthophosphate sorption capacity than goethite and hematite in our study. This might be due to two major reasons: (i) besides pure sorption, surface precipitation of sorbed P also results in a higher apparent sorption capacity. This, however, would require additional testing to confirm the presence of a precipitation reaction, and (ii) hausmannite has a much higher PZC

(which is > pH 10 for both natural and synthetic hausmannite) than other Mn-oxides and even higher than Fe-oxides. Thus, electrostatic and surface complexation reactions together enhance its sorption capacity (Matocha et al., 2001; Shaughnessy et al., 2003). The higher orthophosphate sorption capacity of goethite than hematite might be due to more singly coordinated OH^- groups on the *(110)* crystal faces on goethite and a smaller proportion of reactive surface sites on hematite (Barron et al., 1988; Torrent and Schwertmann, 1990).

Citrate was found to have a stronger ability to desorb orthophosphate from mineral surfaces than other reagents through ligand exchange reactions (Yan et al., 2014). While KCl and NaF have also been used in desorption studies, our comparative analyses found that orthophosphate desorption by citrate was much higher than that by KCl and NaF (results not shown). In desorption reactions, Mn-oxides showed slightly different desorption kinetics than Fe-oxides. For example, the sharp increase in initial desorption from Mn-oxides was probably induced from the increase in pH after adding citrate, which itself decreases the sorption capacity and thus contributes to additional orthophosphate desorption from mineral surfaces. It is unclear, however, whether pH changes, adjustment and migration of sorbed orthophosphate, or other factors caused the small increase in sorption in the later phase of the desorption experiments.

2.5.2 Effect of Partial Mineral Dissolution on Isotope Values

Besides being a strong desorbing agent, citrate can also induce limited mineral dissolution and thus release more orthophosphate concurrently with ligand exchange promoted desorption. The extent of dissolution depends on several factors including mineral crystallinity, ionic strength, redox potential, and pH conditions, with pH being a more significant factor for ferrihydrite dissolution than for goethite or hematite

dissolution (Earl et al., 1979; Wang et al., 2013). Mineral dissolution in our study, calculated based on the amount of released cations (Fe and Mn), was found to be insignificant (≤0.77%; Table 2.3) but variable among minerals. The extent of dissolution decreased in the following order: hausmannite > goethite≈hematite > birnessite, indicating that citrate could effectively dissolve more hausmannite than other minerals. The amount of dissolution reported here could, however, be underestimated because of potential resorption of released cations onto residual minerals. Nonetheless, our results indicate that the amount of orthophosphate released through citrate-enhanced dissolution was negligible for the minerals studied.

2.5.3 Isotope Equilibria during Sorption and Desorption

The oxygen isotopic composition of sorbed orthophosphate, aqueous orthophosphate, and water at different times during the sorption and desorption reactions remained largely constant, that is, close to the initial $\delta^{18}O_p$ values (Figure 2.4). Due to less energy required for a lighter molecular mass (Siebert et al., 2003), $P^{16}O_4$ can be more preferably sorbed and released by minerals compared with $P^{18}O_4$. Therefore, small differences in isotopic compositions at the initial stage of both sorption and desorption reactions (e.g. Hem-A) is due to kinetic fractionation between aqueous and sorbed orthophosphates, consistent with the results of Jaisi et al. (Jaisi et al., 2010).

Potential O isotope exchange among orthophosphate, minerals, and water can also be discussed in terms of O isotope fractionation factors. Because of a small fractionation factor between Fe-oxides and water (i.e. fractionation factor $\alpha \approx 1$) (Bao and Koch, 1999; Becker and Clayton, 1976; Yapp, 1990), and rapid isotope exchange between mineral-O (particularly surface hydroxyl functional groups) and water-O

(Woutersen and Bakker, 2006), an equilibrium isotope fractionation between these two pools is always expected to be attained. This means that the $\delta^{18}O_{FeO/MnO}$ values of oxides are always off by 1 ‰ from the $\delta^{18}O_W$ values of water because water-O dominates the system. Please note that the lattice structure of the minerals still retains its original $\delta^{18}O_{FeO/MnO}$ values (at the time of synthesis) because of limited isotope exchange between the surface functional groups and the lattice structure due to the high percentage of structural oxygen in minerals (as evidenced from constant $\delta^{18}O_{FeO/MnO}$ values, Table 2.2). While the fractionation factor between orthophosphate-O and water-O is high ($\alpha \approx 21$ at 21 ^{o}C), none of our data show the $\delta^{18}O_P$ values of sorbed and aqueous orthophosphate approaching equilibrium isotopic composition. Considering the OH^- ion, the O fractionation factor between water and aqueous OH^- is around 30−45 at 15−20 °C (Green and Taube, 1963). Furthermore, isotope exchange of surface OH^- and water is very fast (Woutersen and Bakker, 2006), enabling easy detection of any $OH-PO_4$ isotope exchange from corresponding changes in the $\delta^{18}O_P$ values. Given the high molar ratio of water/mineral as well as water/hydroxyl in all experiments, the $\delta^{18}O_{OH}$ values of hydroxyl groups on mineral surfaces should be influenced by water $\delta^{18}O_W$ values and become much lighter than that of ambient water. Accounting for these possibilities in O exchange and corresponding fractionation factors, and the fact that $\delta^{18}O_P$ values of both sorbed and aqueous orthophosphate in this study are off from the expected isotopic composition, our data provide strong evidence that isotope exchange did not occur in these reactions.

The role of partial mineral dissolution and the potential effect on isotopes merits a discussion here. Because the isotopic preference for $P^{16}O_4$ or $P^{18}O_4$ does not exist during partial dissolution (Jaisi et al., 2010), the released orthophosphate during

mineral dissolution should carry the same isotopic signature as that of sorbed orthophosphate. This mechanism, therefore, helps minimize differences in the $\delta^{18}O_P$ values between sorbed and aqueous orthophosphate. However, due to the low extent of mineral dissolution in this study (<1% w/w), the contribution of this mechanism to the measured isotope values is expected to be insignificant. All these lines of evidence verified that no P–O bond cleavage and hence no O exchange between orthophosphate and water or orthophosphate and minerals occurred during these reactions at the mineral–water interface.

Table 2.4. Concentration of dissolved cations (Fe and Mn) and extent of dissolution of three different ^{18}O labelings (A, B, and C) of goethite (Goe), hematite (Hem), hausmannite (Hau), and birnessite (Bir) minerals by citrate, the desorption reagent used in the experiments.

Mineral	Fe Concentration (μmol L^{-1})				Mineral	Mn Concentration (μmol L^{-1})			
	1 d	30 d	Mineral matrix	Dissolution in 30 d (%)		1d	30 d	Mineral matrix	Dissolution in 30 d (%)
Goe-A	0.06	0.18	298.07	0.06	Hau-A	1.62	2.08	326.38	0.63
Goe-B	0.23	0.35	284.76	0.12	Hau-B	1.72	2.63	339.06	0.77
Goe-C	0.45	0.36	299.93	0.12	Hau-C	1.81	2.45	333.00	0.73
Hem-A	0.11	0.12	356.72	0.03	Bir-A	0.12	0.00	254.79	0.00
Hem-B	0.20	0.57	345.13	0.16	Bir-B	0.08	0.01	264.07	0.00
Hem-C	0.25	0.38	345.87	0.11	Bir-C	0.06	0.00	246.30	0.00

2.5.4 Discrimination of Isotope Effect between Biotic and Abiotic Reactions

Two major reactions that can change the isotope compositions of orthophosphate are: (i) ionic exchange and (ii) isotope exchange. Ion exchange is caused by the selectivity of PO_4 ions (i.e., preference of ^{18}O or ^{16}O or the different combinations of ^{18}O and ^{16}O in PO_4) in sorption or desorption reactions (as indicated

by our data in the early phase of sorption and desorption reactions in Goe-A and Hem-A, Figure 2.4), but the PO_4 ions remain intact. Over time, this isotope difference decreases because of efficient ion exchange between two pools and could become insignificant compared with differences between different O sources (>10 ‰) (Jaisi et al., 2010). On the other hand, isotope exchange is caused by O atom exchange between orthophosphate and water, in which P−O bonds are broken and reformed such as in enzyme-catalyzed hydrolysis–condensation reactions (Blake et al., 1997; Jaisi et al., 2011; Winter et al., 1940), and may achieve isotopic equilibrium determined by the water $\delta^{18}O_W$ values and the ambient temperature (Blake et al., 1997; Longinelli and Nuti, 1973). It is well recognized that O-isotopic exchange, which results from the difference in the $\delta^{18}O$ values between orthophosphate and water and P–O bond cleavage, only takes place in biological (enzyme-catalyzed) systems, rather than in abiotic reactions at low temperature (<80 °C) and neutral pH (Blake et al., 1997; Blake et al., 1998; Jaisi and Blake, 2010). In the case of organic P hydrolysis, a disequilibrium isotope effect was observed (Blake et al., 2005). The P–O–C or P–C bond breakage in organic P compounds always incorporates external O sources. For example, analyses of the $\delta^{18}O_P$ values of released orthophosphate from enzymatically hydrolyzed phosphomonoesters and diesters have been found to include one (25%) or two (50%) O atoms from water, respectively (Liang and Blake, 2006; Liang and Blake, 2009), and thus shift the $\delta^{18}O_P$ values of the released orthophosphate towards the value of the ambient water.

The P–O bond in the orthophosphate molecule remains quite resistant to cleavage in abiotic reactions at most surface temperatures (<80 °C) and pressures on Earth (Blake et al., 2001; Blake et al., 1997; Longinelli et al., 1976; Tudge, 1960).

Therefore, the observed variability in the O isotopic composition of orthophosphate in abiotic reactions such as sorption and desorption should be induced solely by an ionic exchange reaction between aqueous and sorbed orthophosphate pools. No isotopic exchange between O atoms from orthophosphate and water was detected during sorption and desorption reactions on ferrihydrite, which meant no P–O bond cleavage occurred, and orthophosphate sorbed or desorbed intact on mineral surfaces under conditions with temperature <80 °C (Jaisi et al., 2010). Isotope fractionation due to ion exchange observed in the early stages of sorption and desorption reactions gradually decreased and became insignificant compared with differences between different O sources. Based on the changes in isotope values of two P pools, we have developed a conceptual model of O atom exchange between orthophosphate and minerals (Figure 2.5). As shown, intact PO_4 ions sorb and desorb. Without P–O bond cleavage at mineral–water interfaces, the $\delta^{18}O_P$ values of both aqueous and sorbed orthophosphate remain close to that of the starting orthophosphate at equilibrium for the sorption–desorption reactions without any shift of the $\delta^{18}O_p$ values towards either that of water or minerals or that expected from fractionation factors (Figure 2.4). The variation of ambient pH conditions would change the amount of variable surface charge on the minerals and thus influence the initial uptake capacity of the minerals for lighter orthophosphate and isotopic fractionation at initial stages, whereas sufficient time for efficient ion exchange between preferentially sorbed lighter orthophosphate and relatively heavier orthophosphate in solution would result in an insignificant difference in the isotope composition of these two P pools (i.e., becomes close to that of the original orthophosphate).

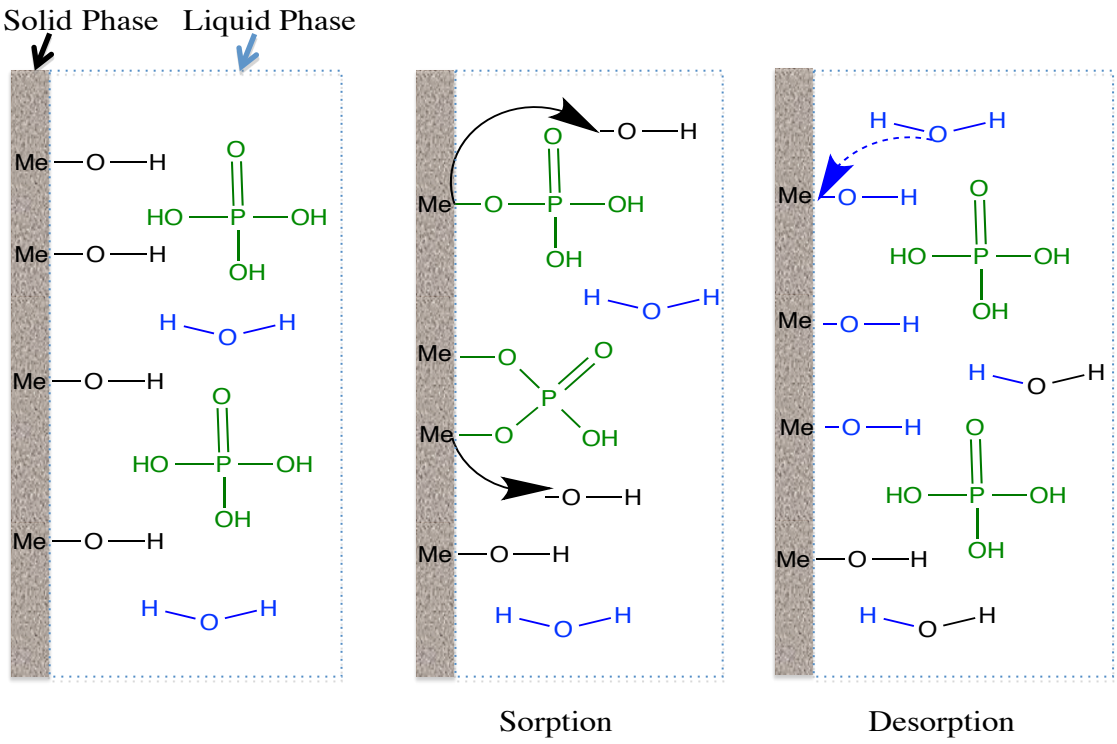

Figure 2.5. Schematic representation of the behavior of O during orthophosphate sorption and desorption reactions. The symbol Me represents an Fe or Mn atom in the mineral structure.

2.6 Conclusions and Implications

A series of orthophosphate sorption and desorption experiments was performed on four minerals (goethite, hematite, hausmannite, and K^+-birnessite) at room temperature and neutral pH conditions. This research revealed the bond cleavage Fe–O(OH) [not P–O(OH)] during orthophosphate sorption and desorption reactions, which was not previously validated. Our results consistently showed similar equilibrium isotopic composition of sorbed and aqueous orthophosphate to the starting

orthophosphate, after small changes in isotope values at the early stage of reactions due to kinetic isotope exchange (efficient ionic exchange between aqueous and sorbed orthophosphate). These minerals have a strong sorption capacity for orthophosphate but desorb a limited amount of orthophosphate in the presence of strong desorption reagents. Therefore, the $\delta^{18}O_p$ values of orthophosphate in soils could be preserved as sorbed onto minerals, thus enabling tracing of original orthophosphate sources. This means that isotope evolution may occur with time due to the interaction with different orthophosphate sources or other biological reactions. Reaction-specific isotopic composition increases the possibility of tracing original sources or decoupling different sources or biogeochemical processes that change the original isotopic composition.

Acknowledgments

This research was supported by research grants from the U.S. Department of Agriculture (NIFA award 2012-67019-19320). We would like to acknowledge the Advanced Material Characterization Lab at the University of Delaware for providing XRD, BET, and SEM analyses of Fe-/Mn-oxide minerals. We would also like to extend our gratitude to Jiangqi Wu (University of Delaware) and Justin Hayles (Louisiana State University) for their contribution during different stages of these experiments and isotope data collection.

REFERENCES

Arai, Y. and Sparks, D.L., 2007. Phosphate reaction dynamics in soils and soil components: A multiscale approach. Adv. Agron., 94: 135–179.

Bao, H. and Koch, P.L., 1999. Oxygen isotope fractionation in ferric oxide-water systems: Low temperature synthesis. Geochim. Cosmochim. Acta, 63: 599–613.

Bao, H., Koch, P.L. and Thiemens, M.H., 2000. Oxygen isotopic composition of ferric oxides from recent soil, hydrologic, and marine environments. Geochim. Cosmochim. Acta, 64: 2221–2231.

Barron, V., Herruzo, M. and Torrent, J., 1988. Phosphate adsorption by aluminous hematites of different shapes. Soil Sci. Soc. Am. J., 52: 647–651.

Becker, R.H. and Clayton, R.N., 1976. Oxygen isotope study of a precambrian banded iron-formation, Hamersley Range, Western Australia. Geochim. Cosmochim. Acta, 40: 1153–1165.

Blake, R.E., Alt, J.C. and Martini, A.M., 2001. Oxygen isotope ratios of PO_4: An inorganic indicator of enzymatic acitivity and P metabolism and a new biomarker in the search for life. Proc. Natl. Acad. Sci. USA, 98: 2148–2153.

Blake, R.E., O'Neil, J.R. and Garcia, G.A., 1997. Oxygen isotope systematics of biologically mediated reactions of phosphate: I. Microbial degradation of organophosphorus compounds. Geochim. Cosmochim. Acta, 61: 4411–4422.

Blake, R.E., O'Neil, J.R. and Garcia, G.A., 1998. Effects of microbial activity on the $\delta^{18}O$ of dissolved inorganic phosphate and textural features of synthetic apatites. Am. Mineral., 83: 1516–1531.

Blake, R.E., O'Neil, J.R. and Surkov, A.V., 2005. Biogeochemical cycling of phosphorus: Insights from oxygen isotope effects of phosphoenzymes. Am. J. Sci., 305: 596–620.

Bohlke, J.K. and Denver, J.M., 1995. Combined use of groundwater dating, chemical and isotopic analyses to resolve the history and fate of nitrate contamination in two agricultural watersheds, Atlantic coastal plain, Maryland. Water Resour. Res., 31: 2319–2339.

Bohn, H.B., McNeal, B. and O'Conner, G., 1979. Soil chemistry. Wiley Interscience, New York.

Bohn, H.B., McNeal, B. and O'Conner, G., 2001. Soil chemistry. 3rd ed. Wiley Interscience, New York.

Bowden, J.W., Posner, A.M. and Quirk, J.P., 1977. Ionic adsorption on variable charge mineral surfaces. Theoretical-charge development and titration curves. Aust. J. Soil Res., 15: 121–136.

Cohn, M. and Urey, H.C., 1938. Oxygen exchange reactions of organic compounds and water. J. Am. Chem. Soc., 60: 679–687.

Drits, V.A., Silvester, E., Gorshkov, A.I. and Manceau, A., 1997. Structure of synthetic monoclinic Na-rich birnessite and hexagonal birnessite: I. Results from X-ray diffraction and selected-area electron diffraction. Am. Mineral., 82: 946–961.

Earl, K.D., Syers, J.K. and McLaughlin, J.R., 1979. Origin of the effects of citrate, tartrate, and acetate on phosphate sorption by soils and synthetic gels. Soil Sci. Soc. Am. J., 43: 674–678.

Elzinga, E.J. and Sparks, D.L., 2007. Phosphate adsorption onto hematite: An in situ ATR-FTIR investigation of the effects of pH and loading level on the mode of phosphate surface complexation. J. Colloid Interface Sci., 308: 53–70.

Emerson, S., 1978. Early diagenesis in anaerobic lake sediments. II. Thermodynamic and kinetic factors controlling the formation of iron phosphate. Geochim. Cosmochim. Acta, 42: 1307–1316.

Feng, X.H., Liu, F., Tan, W.F. and Liu, X.W., 2004. Synthesis of birnessite from the oxidation of Mn^{2+} by O_2 in alkali medium: Effects of synthesis conditions. Clays Clay Miner., 52: 240–250.

Feng, X.H., Zhai, L.M., Tan, W.F., Liu, F. and He, J.Z., 2007. Adsorption and redox reactions of heavy metals on synthesized Mn oxide minerals. Environ. Pollut., 147: 366–373.

Gibbs, G.V., Downs, R.T., Cox, D.F., Rosso, K.M., Ross, N.L., Kirfel, A., Lippmann, T., Morgenroth, W. and Crawford, T.D., 2008. Experimental bond critical point and local energy density properties determined for Mn–O, Fe–O, and Co–O bonded interactions for tephroite, Mn_2SiO_4, fayalite, Fe_2SiO_4, and Co_2SiO_4 olivine and selected organic metal complexes: Comparison with properties calculated for non-transition and transition metal M–O bonded interactions for silicates and oxides. J. Phys. Chem. A, 112: 8811–8823.

Green, M. and Taube, H., 1963. Isotopic fractionation in the OH–H_2O exchange reaction. J. Phys. Chem., 67: 1565–1566.

Jaisi, D.P. and Blake, R.E., 2010. Tracing sources and cycling of phosphorus in Peru Margin sediments using oxygen isotopes in authigenic and detrital phosphates. Geochim. Cosmochim. Acta, 74: 3199–3212.

Jaisi, D.P. and Blake, R.E., 2014. Advances in using oxygen isotope ratios of phosphate to understand phosphorus cycling in the environment. Adv. Agron., 125: 1–53.

Jaisi, D.P., Blake, R.E. and Kukkadapu, R.K., 2010. Fractionation of oxygen isotopes in phosphate during its interactions with iron oxides. Geochim. Cosmochim. Acta, 74: 1309–1319.

Jaisi, D.P., Dong, H.L., Plymale, A.E., Fredrickson, J.K., Zachara, J.M., Heald, S. and Liu, C.X., 2009. Reduction and long-term immobilization of technetium by Fe(II) associated with clay mineral nontronite. Chem. Geol., 264: 127–138.

Jaisi, D.P., Kukkadapu, R.K., Stout, L.M., Varga, T. and Blake, R.E., 2011. Biotic and abiotic pathways of phosphorus cycling in minerals and sediments: Insights from oxygen isotope ratios in phosphate. Environ. Sci. Technol., 45: 6254–6261.

Joshi, S.R., Kukkadapu, R.K., Burdige, D.J., Bowden, M.E., Sparks, D.L. and Jaisi, D.P., 2015. Organic matter remineralization predominates phosphorus cycling in the mid-bay sediments in the chesapeake bay. Environ. Sci. Technol., 49: 5887–5896.

Kawashima, M., Tainaka, Y., Koyama, M. and Takamatsu, T., 1986. Phosphate adsorption onto hydrous manganese(IV) oxide in the presence of divalent cations. Wat. Res., 20: 471–475.

Kendall, C., 1998. Tracing nitrogen sources and cycles in catchments. In C. Kendall and J. J. McDonnell ed. Isotope tracers in catchment hydrology. Elsevier Science: 519–576.

Li, H., Liu, F., Zhu, M., Feng, X., Zhang, J. and Yin, H., 2015. Structure and properties of Co-doped cryptomelane and its enhanced removal of Pb^{2+} and Cr^{3+} from wastewater. J. Environ. Sci., 34: 77–85.

Liang, Y. and Blake, R.E., 2006. Oxygen isotope signature of Pi regeneration from organic compounds by phosphomonoesterases and photooxidation. Geochim. Cosmochim. Acta, 70: 3957–3969.

Liang, Y. and Blake, R.E., 2009. Compound- and enzyme-specific phosphodiester hydrolysis mechanisms revealed by $\delta^{18}O$ of dissolved inorganic phosphate: Implications for marine P cycling. Geochim. Cosmochim. Acta, 73: 3782–3794.

Longinelli, A., Bartelloni, M. and Cortecci, G., 1976. The isotopic cycle of oceanic phosphate, I. Earth Planet. Sci. Lett., 32: 389–392.

Longinelli, A. and Nuti, S., 1973. Revised phosphate–water isotopic temperature scale. Earth Planet. Sci. Lett., 19: 373–376.

Luo, Y.R., 2007. Chemical bond energies. CRC Press, Boca Raton, FL.

Matocha, C.J., Elzinga, E.J. and Sparks, D.L., 2001. Reactivity of Pb(II) at the Mn(III, IV) (oxyhydr)oxide–water interface. Environ. Sci. Technol., 35: 2967–2972.

McArdell, C.S., Stone, A.T. and Tian, J., 1998. Reaction of EDTA and related aminocarboxylate chelating agents with $Co^{III}OOH$ (heterogenite) and $Mn^{III}OOH$ (manganite). Environ. Sci. Technol., 32: 2923–2930.

McKenzie, R.M., 1971. The influence of cobalt on the reactivity of manganese dioxide. Aust. J. Soil Res., 9: 55–58.

McLaughlin, K., Cade-Menun, B.J. and Paytan, A., 2006. The oxygen isotopic composition of phosphate in Elkhorn Slough, California: A tracer for phosphate sources. Estuarine, Coastal Shelf Sci., 70: 499–506.

Melby, E.S., Soldat, D.J. and Barak, P., 2011. Synthesis and detection of oxygen-18 labeled phosphate. PLoS One, 6: e18420.

Murphy, J. and Riley, J.P., 1962. A modified single solution method for the determination of phosphate in natural waters. Anal. Chim. Acta, 27: 31–36.

O'Neil, J.R., Vennemann, T.W. and McKenzie, W.F., 2003. Effects of speciation on equilibrium fractionations and rates of oxygen isotope exchange between $(PO_4)_{aq}$ and H_2O. Geochim. Cosmochim. Acta, 67: 3135–3144.

Paige, C.R., Snodgrass, W.J., Nicholson, R.V., Scharer, J.M. and He, Q.H., 1997. The effect of phosphate on the transformation of ferrihydrite into crystalline products in alkaline media. Water, Air, Soil Pollut., 97: 397–412.

Pan, B., Han, F., Nie, G., Wu, B., He, K. and Lu, L., 2014. New strategy to enhance phosphate removal from water by hydrous manganese oxide. Environ. Sci. Technol., 48: 5101–5107.

Parfitt, R.L. and Atkinson, R.J., 1976. Phosphate adsorption on goethite (α-FeOOH). Nature, 264: 740–742.

Peng, Y., Bao, H., Zhou, C. and Yuan, X., 2011. ^{17}O-depleted barite from two Marinoan cap dolostone sections, South China. Earth Planet. Sci. Lett., 305: 21–31.

Penn, C., Heeren, D., Fox, G. and Kumar, A., 2014. Application of isothermal calorimetry to phosphorus sorption onto soils in a flow-through system. Soil Sci. Soc. Am. J., 78: 147–156.

Post, J.E., 1999. Manganese oxide minerals: Crystal structures and economic and environmental significance. Proc. Natl. Acad. Sci. USA, 96: 3447–3454.

Post, J.E. and Veblen, D.R., 1990. Crystal structure determination of synthetic sodium, magnesium, and potassium birnessite using TEM and the Rietveld method. Am. Mineral., 75: 477–489.

Redfield, A.C., 1958. The biological control of chemical factors in the environment. Am. Sci., 46: 205–221.

Schwertmann, U. and Cornell, R.M., 1991. Iron oxides in the laboratory: Preparation and characterization. VCH Publisher, Inc., New York.

Schwertmann, U. and Taylor, R.M., 1989. Iron oxides. In J. B. Dixon and S. B. Weed (ed.) Minerals in soil environments. 2nd ed. Soil Sci. Soc. Am., Madison, WI, USA.

Shang, C., Srewart, J.W.B. and Huang, P.M., 1992. PH effect on kinetics of adsorption of organic and inorganic phosphates by short-range ordered aluminum and iron precipitates. Geoderma, 53: 1–14.

Shaughnessy, D.A., Nitsche, H., Booth, C.H., Shuh, D.K., Waychunas, G.A., Wilson, R.E., Gill, H., Cantrell, K.J. and Serne, R.J., 2003. Molecular interfacial reactions between Pu(VI) and manganese oxide minerals manganite and hausmannite. Environ. Sci. Technol., 37: 3367–3374.

Siebert, C., Nagler, T.F., Von Blanckenburg, V. and Kramers, J.D., 2003. Molybdenum isotope records as a potential new proxy for paleoceanography. Earth Planet. Sci. Lett., 211: 159–171.

Stout, L.M., Joshi, S.R., Kana, T.M. and Jaisi, D.P., 2014. Microbial activities and phosphorus cycling: An application of oxygen isotope ratios in phosphate. Geochim. Cosmochim. Acta, 138: 101–116.

Tejedor-Tejedor, M.I. and Anderson, M.A., 1990. Protonation of phosphate on the surface of goethite as studied by CIR-FTIR and electrophoretic mobility. Langmuir, 6: 602–611.

Torrent, J. and Schwertmann, U., 1990. Phosphate adsorption and desorption by goethites differing in crystal morphology. Soil Sci. Soc. Am. J., 54: 1007–1012.

Torrent, J., Schwertmann, U. and Barron, V., 1992. Fast and slow phosphate sorption by goethite-rich natural materials. Clays Clay Miner., 40: 14–21.

Tudge, A.P., 1960. A method of oxygen isotopes in orthophosphate and its use in measurement of paleotemperatures. Geochim. Cosmochim. Acta, 18: 81–93.

Ulery, A.L. and Drees, L.R., 2008. Methods of soil analysis. Part 5—Mineralogical methods. Soil Sci. Soc. Am. Book Ser. 5, Madison, WI, USA.

Upreti, K., Joshi, S.R., McGrath, J.W. and Jaisi, D.P., 2015. Factors controlling phosphorus mobilization in a coastal plain tributary to the Chesapeake Bay. Soil Sci. Soc. Am. J., 79: 826–837.

Vennemann, T.W., Fricke, H.C., Blake, R.E., O'Neil, J.R. and Colman, A., 2002. Oxygen isotope analysis of phosphates: A comparison of techniques for analysis of Ag_3PO_4. Chem. Geol., 185: 321–336.

Wang, X., Liu, F., Tan, W.F., Li, W., Feng, X.H. and Sparks, D.L., 2013. Characteristics of phosphate adsorption-desorption onto ferrihydrite. Soil Sci., 178: 1–11.

Wang, Z., Fingas, M., Landriault, M., Sigouin, L., Castle, B., Hostetter, D., Zhang, D. and Spencer, B., 1998. Identification and linkage of tarballs from the coasts of Vancouver island and Northern California using GC/MS and isotopic techniquess. J. High Resol. Chromatogr., 21: 383–395.

Winter, E.S., Carlton, M. and Briscoe, H.A., 1940. The interchange of heavy oxygen between water and inorganic oxy-anions. J. Chem. Soc., 32: 131–138.

Woutersen, S. and Bakker, H.J., 2006. Ultrafast vibrational and structural dynamics of the proton in liquid water. Phys. Rev. Lett., 96: 138305.

Yan, Y., Wan, B., Liu, F., Tan, W., Liu, M. and Feng, X., 2014. Adsorption-desorption of myo-inositol hexakisphosphate on hematite. Soil Sci., 179: 476–485.

Yao, W. and Millero, F.J., 1996. Adsorption of phosphate on manganese dioxide in seawater. Environ. Sci. Technol., 30: 536–541.

Yapp, C.J., 1990. Oxygen isotopes in iron(III) oxides: Mineral water fractionation factors. Chem. Geol., 85: 329–335.

Yin, H., Li, H., Wang, Y., Ginder-Vogel, M., Qiu, G., Feng, X.H., Zheng, L. and Liu, F., 2014. Effects of Co and Ni co-doping on the structure and reactivity of hexagonal birnessite. Chem. Geol., 381: 10–20.

Zeng, L., Li, X. and Liu, J., 2004. Adsorptive removal of phosphate from aqueous solutions using iron oxide tailings. Water Res., 38: 1318–1326.

Chapter 3

DEGRADATION AND ISOTOPE SOURCE TRACKING OF GLYPHOSATE AND AMINOMETHYLPHOSPHONIC ACID

Reproduced with permission from

Degradation and Isotope Source Tracking of Glyphosate and Aminomethylphosphonic Acid

Hui Li, Sunendra R. Joshi, and Deb P. Jaisi

J. Agric. Food Chem., 2016, 64(3), pp 529–538

DOI: 10.1021/acs.jafc.5b04838

https://pubs.acs.org/doi/abs/10.1021/acs.jafc.5b04838

3.1 Abstract

Glyphosate (N-phosphonomethyl glycine), an active ingredient of the herbicide Roundup, and its main metabolite, aminomethylphosphonic acid (AMPA), have been frequently reported to be present in soils and other environments, and thus have heightened public concerns on their potential adverse effects. Understanding the fate of these compounds and differentiating them from other naturally occurring compounds require a toolbox of methods that can go beyond conventional methods. Here, we applied an individual isotope labeling technique whereby each compound or mineral involved in the glyphosate and AMPA degradation reaction was either synthesized or chosen to have distinct $^{18}O/^{16}O$ ratios so that the source of incorporated oxygen in the generated orthophosphate and corresponding isotope effect during the C–P bond cleavage could be identified. Furthermore, we measured original isotope

signatures of a few commercial glyphosate sources to identify their source-specific isotope signatures. Our degradation kinetics results showed that the rate of glyphosate degradation was higher than that of AMPA in all experimental conditions, and both the rate and extent of degradation of glyphosate were lowest under anoxic conditions. Oxygen isotope ratios ($\delta^{18}O_P$) of orthophosphate generated from glyphosate and AMPA degradation suggested that one external oxygen atom from ambient water, not from dissolved oxygen or mineral, was incorporated into orthophosphate with the other three oxygen atoms inherited from the parent molecule. Interestingly, the $\delta^{18}O_P$ values of all commercial glyphosate products studied here were found to be the lightest among all orthophosphates known so far. Furthermore, isotope composition was found to be unaffected due to variable degradation kinetics, light/dark, and oxic/anoxic conditions. These results highlight the importance of phosphate oxygen isotope ratios as a nonconventional tool to potentially distinguish glyphosate sources and products from other organophosphorus compounds and orthophosphate in the environment.

KEYWORDS: glyphosate, aminomethylphosphonic acid, isotope source tracking, orthophosphate

3.2 Introduction

Glyphosate (N-phosphonomethyl glycine) is one of the most common synthetic phosphonate compounds and is used as an active ingredient of Roundup herbicide in agricultural and urban applications (Franz et al., 1997; Sikorski and Gruys, 1997). Widespread adoption of glyphosate-resistant technology for weed control has brought significant economic advantages in agriculture production. An effective increase in agricultural productivity, however, relies on the application of

new technologies that are sound and safe and at the same time ensure sustainability of the ecosystem. The primary functioning mechanism of glyphosate is through blockage of the shikimate pathway—present in plants and some fungi and bacteria, but not in animals and human beings—which inhibits the synthesis of aromatic amino acids (Steinrticken and Amrhein, 1980). Thus, glyphosate was originally considered to be safe for humans and was classified as a category E compound (i.e., noncarcinogenicity for humans) by the U.S. Environmental Protection Agency (United States Environmental Protection Agency, 1993). Several follow-up studies, however, have reported negative environmental impacts and toxicity of glyphosate and its metabolites. For example, glyphosate may affect DNA synthesis in sea urchins (Marc et al., 2004) and influence estrogenic activity in humans (Thongprakaisang et al., 2013). Some glyphosate degradation products are more toxic or persistent than glyphosate itself. For example, aminomethylphosphonic acid (AMPA) has been reported to have adverse effects on DNA in fish and have potential genotoxicity (Guilherme et al., 2014), and is more persistent in the environment than glyphosate (Grunewald et al., 2001). Although the toxicity results are much disputed, increasing urban and agricultural applications of glyphosate have resulted in the widespread presence of glyphosate and AMPA in soils, streams, and other environments (Battaglin et al., 2014; Meyer et al., 2009). Thus, the common occurrence of glyphosate coupled with elevated public concern over potential toxicity highlights the importance as well as the urgency of scientific investigation on the fate and persistence of glyphosate and its degradation products in soils and other environments.

The presence of glyphosate in agricultural watersheds where other more bioavailable forms of phosphorus (P) are often in excess above biological P demand

implies that abiotic degradation could be an important degradation pathway. In fact, glyphosate interacts strongly with soil components and forms chelation complexes with minerals; thus, its mobility is restricted in soils (Franz et al., 1997). The degradation of glyphosate involves either cleavage of a C–N bond that produces AMPA first, or the cleavage of a C–P bond that produces sarcosine first (Barrett and McBride, 2005; Franz et al., 1997; Paudel et al., 2015). Both of these intermediate products degrade further and eventually generate inorganic compounds (PO_4, NH_3, H_2O, and CO_2). Naturally occurring minerals (Barrett and McBride, 2005; Paudel et al., 2015), mineral-activated carbon composite (Cui et al., 2012), and UV–photo-oxidation (Sandy et al., 2013) have been found to be capable of degrading glyphosate. Because Mn-oxide minerals (among which birnessite is the most abundant) are commonly present in soils (Post, 1999; Taylor et al., 1964) where glyphosate ultimately deposits after application for weed control, it is important and logical to better understand the degradation of glyphosate catalyzed by Mn-oxides. In fact, birnessite often plays an important role in redox and ion exchange reactions in soils due to its various valence states and characteristic structural vacancies (Post, 1999). These properties enable birnessite to adsorb and degrade organic contaminants (Remucal and Ginder-Vogel) including glyphosate and its metabolites such as AMPA. However, orthophosphate outcompetes phosphonates on mineral sorption sites, probably because of the differences in sorption affinity affected by size and composition of phosphonate (Nowack and Stone, 2006).

Bond cleavage and atom transfer induce isotope exchange (Marcus, 1957). Oxygen isotope ratios of orthophosphate ($\delta^{18}O_P$) have been increasingly used to unravel biogeochemical reactions at interfaces and to identify various sources and

pathways of P cycling (Blake et al., 1997; Jaisi and Blake, 2014; Joshi et al., 2015). The ester bond (P–O–C or P–C bonds) cleavage in organophosphorus compounds always incorporates foreign oxygen (O) sources. For example, enzymatic hydrolysis of selected phosphomonoesters and diesters has been found to incorporate one (25%, i.e., one out of four oxygens in orthophosphate) and two (50%) O atoms from water, respectively (Liang and Blake, 2006b; Liang and Blake, 2009). The cleavage of the C−P bond in glyphosate is expected to incorporate one O atom from external O sources into the generated orthophosphate and three O atoms inherited from glyphosate itself. Thus, the oxygen isotope ratios in orthophosphate generated from glyphosate degradation could be an important proxy for tracing the source of glyphosate by discriminating inherited oxygen or for understanding the bond cleavage mechanism and corresponding isotope effect. In this research, we aimed to identify the roles of environmentally relevant factors on the degradation kinetics of glyphosate and AMPA catalyzed by birnessite and to develop phosphate oxygen isotope ratios as a proxy to identify sources of commercial glyphosate and its degradation products. Understanding glyphosate degradation and linking source and product/s through a particular isotope effect could provide a framework to initiate research on source tracking of glyphosate and other organophosphorus compounds in the environment.

3.3 Materials and Methods

3.3.1 Mineral Synthesis

To understand glyphosate degradation catalyzed by manganese oxide, birnessite mineral [$K_x(Mn^{4+}, Mn^{3+})_2O_4$; where x<1] was synthesized following the McKenzie method by dropwise addition of 45 mL of 6 mol L^{-1} HCl to a boiling

solution of 300 mL of 0.667 mol L^{-1} $KMnO_4$ (Foster et al., 2003; McKenzie, 1971). An ISMATEC IPC high-precision multichannel dispenser pump (Cole Parmer, Vernon Hills, IL, USA) was used to maintain the constant flow of HCl reagent. Three ^{18}O-labeled water solutions with different isotopic compositions ($\delta^{18}O_W$ = -5.7, 67.2, 139.6 ‰ relative to Vienna standard mean ocean water, VSMOW), prepared by diluting 10% ^{18}O-enriched water (Cambridge Isotope Laboratories, Tewksbury, MA, USA) using deionized (DI) water, were used to label structural oxygen atoms of corresponding birnessite minerals so that the same mineral but with distinct ^{18}O values would be produced. These three isotope-labeled minerals are identified as MnO_2-A, MnO_2-B, and MnO_2-C with lighter to heavier oxygen isotope ratios ($\delta^{18}O_{MnO2}$ = -3.69±0.03, 55.31±0.02, 94.79±0.02 ‰), respectively. All synthetic birnessite mineral precipitates were washed five times with DI water, freeze-dried and homogenized by grinding before characterization and use in degradation experiments.

3.3.2 Mineral Characterization

To determine the purity and uniformity of ^{18}O-labeled minerals, X-ray diffraction (XRD) analysis was carried out on a Bruker D8 Discover Diffractometer (Germany) using Ni-filtered, Cu Kα radiation (λ = 0.15418 nm). The diffractometer was operated under voltage of 40 kV and current of 40 mA with 1.0 s counting time per 0.02° 2θ step. Analogously, field emission scanning electron microscope (FE-SEM; JEOL JSM-7400F microscope, Japan) was used to probe micromorphology, crystallinity, and purity of minerals. To minimize surface charging during high voltage emission in SEM, each mineral was coated with a thin gold film. The specific surface area (SSA) of synthetic minerals was measured using a Micromeritics ASAP 2020 Surface Area and Porosity Analyzer (Micromeritics Instrument Corporation, Norcross,

GA, USA). Mineral precipitates (0.1–0.2 g) were degassed in a vacuum atmosphere at 373 K for 3 h, and surface area was measured by using the BET (Brunauer-Emmett-Teller) method. Furthermore, Möbiuζ Dynamic Light Scattering (DLS) (Wyatt Technology, Santa Barbara, CA, USA) was used to determine the particle size distribution.

3.3.3 Glyphosate and AMPA Degradation Experiments

A series of glyphosate and AMPA (Sigma Aldrich, St Louis, MO, USA) degradation experiments was carried out to investigate the roles of environmentally relevant factors on degradation kinetics. Homogenous suspensions of 5 g L^{-1} ^{18}O-labeled birnessite were prepared in 10 mM MOPS (4-morpholinepropane sulfonic acid) buffer at pH=7.00±0.05 and room temperature (22±1 °C). The degradation experiment was initiated by adding glyphosate (or AMPA) stock (to achieve final concentration of 3000 μmol L^{-1}) to the birnessite suspension. Control experiments included glyphosate or AMPA under the same experimental conditions but without the presence of birnessite mineral. Each experiment was conducted in triplicate, and each reactor was continually stirred to maintain uniform distribution of reactants. At selected time points, a sample aliquot was removed from the reactor into 15 mL centrifuge tubes that contained a predetermined concentration of $CuSO_4$ so that the molar ratio of Cu^{2+} to glyphosate was at ~1.1:1 for complete glyphosate complexation. We used Cu^{2+} to inhibit further glyphosate degradation after sampling because Cu^{2+} complexes strongly with glyphosate and limits coordination of glyphosate onto reactive surface sites on minerals (Barrett and McBride, 2005) but the Cu^{2+} concentration was not high enough to interfere with the phosphomolybdate blue method for orthophosphate quantitation (Galhardo and Masini, 2000). Aqueous and

solid phases were separated by centrifugation (7150 ×g for 0.5 h) and filtration (0.22 μm nylon filter). The orthophosphate concentration in the solution was measured colorimetrically by using a UV/vis spectrophotometer following the phosphomolybdate blue method (Murphy and Riley, 1962).

The first set of glyphosate and AMPA degradation experiments was carried out to investigate the degradation kinetics and influence of air (oxygen) and light. Three conditions were included: (i) ambient laboratory conditions (aerobic and under light); (ii) anaerobic and under light; and (iii) aerobic and dark conditions. The illumination intensity of fluorescent lamps in laboratory light conditions was ~ 812.7 lx (~ 81.3 μ E m^{-2} sec^{-1}) measured by using Quantum/radiometer/photometer (model LI-185B) from LI-COR corporation (Lincoln, NE, USA) (Ge et al., 2010). To generate oxygen-free media, de-ionized (DI) water was first boiled and then degassed with Ar gas twice prior to transferring to a glovebox. The oxygen-free DI water was kept inside the glovebox filled with nitrogen and hydrogen gas for over 24 h before running the experiment. The dissolved O_2 in the DI water was determined using a CHEMets colorimetric kit R-7540 (2.5 ppb sensitivity). All experimental solutions including glyphosate and AMPA stocks were prepared using the oxygen-free DI water, and all anoxic experiments were run in triplicate inside the glovebox under an N_2 atmosphere. Dark condition experiments were conducted on the benchtop by using thick aluminum foil wrapped around each reactor. The dark condition was maintained during sampling until the reaction was quenched in $CuSO_4$ solution (as above).

The second set of experiments was conducted in a series of ^{18}O-labeled oxygen sources. Three potential oxygen sources (water, dissolved oxygen, and mineral) were included to identify external O sources incorporated into orthophosphate. The $\delta^{18}O_W$

values of labeled water used in the experiments increased from -7.41(±0.09) to 138.57(±0.57) ‰. Similarly, the $\delta^{18}O_{O2}$ values of labeled dissolved oxygen varied from 110.15(±0.92) to 2082.41(±2.37) ‰ (diluted from 98% ^{18}O-enriched air, ICON Isotopes, Summit, NJ, USA). The $\delta^{18}O_{MnO2}$ values of birnessite minerals synthesized by using different ^{18}O-labeled water were -3.69(±0.03), 55.31(±0.02), and 94.79(±0.02) ‰.

The third set of experiments was designed to identify isotope signatures of different commercial glyphosate sources and to investigate the potential impact of inactive ingredients in commercial formulations during degradation and processing for isotope measurements. Commercial grade glyphosate is formulated with different concentrations of inactive and active ingredients for specified applications. Five different commercial glyphosate products collected from various sources were used, and the degradation experiments were conducted similarly to the first set of experiments (see above). Aqueous and solid phases were separated by centrifugation (7150 ×*g* for 0.5 h) and filtration (0.22 μm filters). The experiments were conducted in duplicate using DI water (-7.34 ‰). Non-ionic, macro-porous DAX 8 Superlite resin was used to trap organic compounds present in the formulation on the resin column. The samples were further purified and processed to measure the $\delta^{18}O$ values (see below).

3.3.4 Sample Processing and Oxygen Isotope Ratios Measurement in Orthophosphate, Water, and Mineral

The oxygen isotope ratios of released orthophosphate during glyphosate and AMPA degradation, water used in experiments, and synthetic birnessite were measured after processing samples to remove contaminants. For orthophosphate

samples, the silver phosphate precipitation method described in Jaisi and Blake (Jaisi and Blake, 2010; Jaisi and Blake, 2014) was followed. Independent tests confirmed that glyphosate and AMPA used in this research did not hydrolyze in reagent-promoted acidic conditions; therefore, pretreatment to remove residual glyphosate/AMPA was not necessary. However, their presence hindered the precipitation of ammonium phosphomolybdate (APM). In brief, orthophosphate was first precipitated as APM at acidic pH, dissolved, and then precipitated as magnesium ammonium phosphate (MAP) at high pH. The MAP precipitate was then dissolved and treated with cation resin (AG50W-X8, Bio-Rad, Hercules, CS, USA) to remove cations, primarily Mg^{2+} and NH_4^+. The purified solution was evaporated to concentrate orthophosphate and ultimately precipitated as silver phosphate. Although this method has been routinely used for isotope processing, a separate orthophosphate sample with known isotopic composition was processed along with actual samples to verify the validity of the sample processing procedure. Silver phosphate precipitates were then heated at 110 °C for 24 h to remove remaining and physically trapped/sorbed water.

All O isotopic compositions of orthophosphate were measured in the stable isotope facility at the University of Delaware. Silver capsules containing 200−300 μg of silver phosphate (in triplicate) were pyrolyzed at 1460 ^{o}C in a Thermo Chemolysis/Elemental Analyzer (TC/EA). Oxygen isotope ratios were measured in a Delta V continuous flow isotope ratio mass spectrometer (IRMS; Thermo-Finnigan, Bremen, Germany). Measured $\delta^{18}O_P$ values of orthophosphate were calibrated against two silver phosphate standards (YR1-1aR02 and YR3-2) with $\delta^{18}O_P$ values of -5.49 and +33.63 ‰, respectively.

To measure the O isotopic compositions of waters used in the experiments, 0.3 mL water samples were injected into a 12 mL borosilicate Exetainer® (Labco, Buckinghamshire, UK) pressurized with 300 ppm of CO_2 in He. After equilibration between CO_2 and H_2O for 24 h at 26.2 °C, the O isotopic composition in CO_2 was measured using a GasBench peripherally connected to an IRMS (Thermo-Finnigan, Bremen, Germany) at the University of Delaware. Given that the fractionation factor between CO_2 and H_2O is well established, the $\delta^{18}O_W$ values of H_2O were then calculated using the $\delta^{18}O_{CO2}$ values of CO_2 following the method by Cohn and Urey (Cohn and Urey, 1938). All standards and samples were measured at least in duplicate. Measured $\delta^{18}O_W$ values of waters were calibrated against two U.S. Geological Survey water standards ($\delta^{18}O_W$ values of -9.25 and -1.25 ‰). Standard deviation of water samples was within the range of ±0.02 ‰.

The O isotopic composition of structural oxygen in ^{18}O-labeled birnessite minerals was measured using a laser fluorination method at the isotope facility at Louisiana State University. Minerals were heated in a BrF_5 atmosphere in the 30 W CO_2–laser fluorination equipment for liberating structural oxygen atoms. The $\delta^{18}O$ values of liberated molecular oxygen were then measured in dual-inlet mode on an MAT253 (Bao et al., 2000; Peng et al., 2011). While the standard deviation of samples measured was found to be low (within the range of ±0.05 ‰), the uncertainty of measuring the $\delta^{18}O$ values by using laser fluorination on synthetic and less crystalline minerals (in contrast to geological materials) could be high because of potential removal of surface hydroxyl groups during the pre-fluorination step. Similarly, potential partial yield during fluorination may induce unpredictable shifts in the $\delta^{18}O$ values.

3.4 Results and Discussion

3.4.1 Mineral Characterization

The powder XRD patterns of synthetic birnessite indicate single-phase birnessite with no identifiable contaminant minerals (Figure 3.1a). The peak position and intensity of XRD patterns are comparable to those of turbostratic birnessite (Drits et al., 1997). In SEM, synthetic birnessite shows uniform flower-like morphologies (Figure 3.1b−d). Birnessite normally forms a hexagonal layered structure (Post, 1999) that under further aggregation forms three-dimensional hierarchical microspheres. No significant difference was observed among birnessite minerals synthesized using different ^{18}O-labeled waters. Specific surface areas (SSA) of synthetic minerals with varying ^{18}O-labeling were ~40 m^2 g^{-1}, with MnO_2-C being an exception (SSA of 26.67 m^2 g^{-1}). This difference might be due to different grain size distribution or the presence of denser aggregates of hexagonal layers. The SSA values are comparable to the reported ranges in previous studies (Jaisi et al., 2009; Yin et al., 2014), in which birnessite minerals were synthesized following similar methods. Particle size distribution of different ^{18}O-labeled birnessite minerals varied within a narrow range between 143 and 186 nm. All of these similar physical properties of minerals suggest that the role of ^{18}O-labeling is insignificant in glyphosate degradation kinetics and corresponding isotope effect.

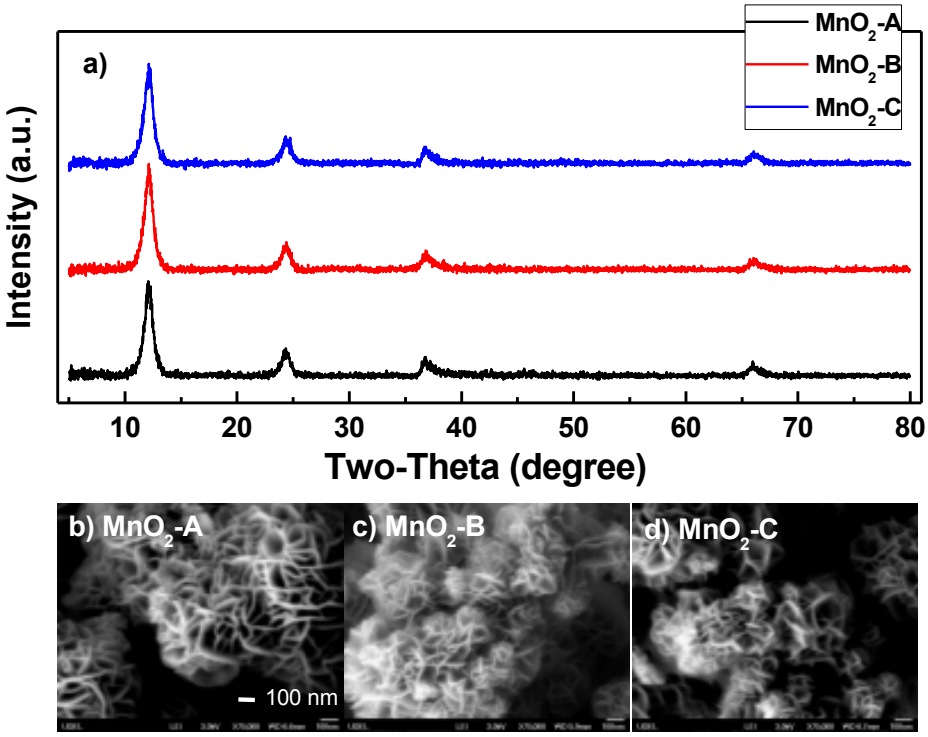

Figure 3.1. X-ray diffraction (XRD) patterns (a) and scanning electron microscope (SEM) images (b,c,d) of synthesized birnessite (MnO_2) minerals. MnO_2-A, MnO_2-B, and MnO_2-C refer to birnessite minerals with different $\delta^{18}O_{MnO2}$ values ($\delta^{18}O_{MnO2}$ = -3.69±0.03, 55.31±0.02, 94.79±0.02 ‰) in their structural oxygen atoms. The scale bar in SEM images represents 100 nm.

The $\delta^{18}O_{MnO2}$ values of structural oxygen in three synthetic birnessite (MnO_2) minerals were -3.69 (±0.03), 55.31(±0.02), and 94.79 (±0.02) ‰, respectively. Triplicate measurements of each sample showed little fluctuation of oxygen isotope ratios (standard deviation <0.05 ‰), indicating homogeneous isotope labeling of oxygen atoms in birnessite samples and reproducibility of isotope measurement using

laser fluorination method. Therefore, the isotope effects induced by atom exchange with other oxyanions should be representative of distinctly labeled oxygen in the mineral.

3.4.2 Glyphosate and AMPA Degradation Kinetics

Degradation kinetics of glyphosate and AMPA (Figure 3.2) followed typical biphasic kinetics similar to the degradation of organic compounds (Remucal and Ginder-Vogel), with a rapid initial rate followed by a gradual slower rate before approaching maximum degradation. No effects of different ^{18}O-labeled minerals or waters, however, were found regarding degradation kinetics. Both the rate and extent of degradation of AMPA were lower than that of glyphosate, which were calculated on the basis of the comparison of orthophosphate released to moles of P in parent compounds. For example, glyphosate reached ~70 % degradation in 24 h, but AMPA required 7 days for that extent of degradation. When comparing reaction rates at the same glyphosate/AMPA:birnessite ratio, the initial rate of glyphosate degradation (567.6 μmol L^{-1} h^{-1}) was ~4.5 times higher than that of AMPA (122.5 μmol L^{-1} h^{-1}). The faster initial rate and higher percentage of glyphosate degradation compared to AMPA degradation, consistent with previous studies (Barrett and McBride, 2005), may result from their different sorption affinities to the surface functional groups of birnessite. The weaker coordination of AMPA onto birnessite may be attributed to the absence of a carboxyl functional group in AMPA. Sustained increase in AMPA degradation after 100 h may result from (i) further degradation that gradually reaches maximum degradation capacity of minerals, due to weaker coordination of AMPA to birnessite and (ii) gradual release of adsorbed orthophosphate from the mineral surface.

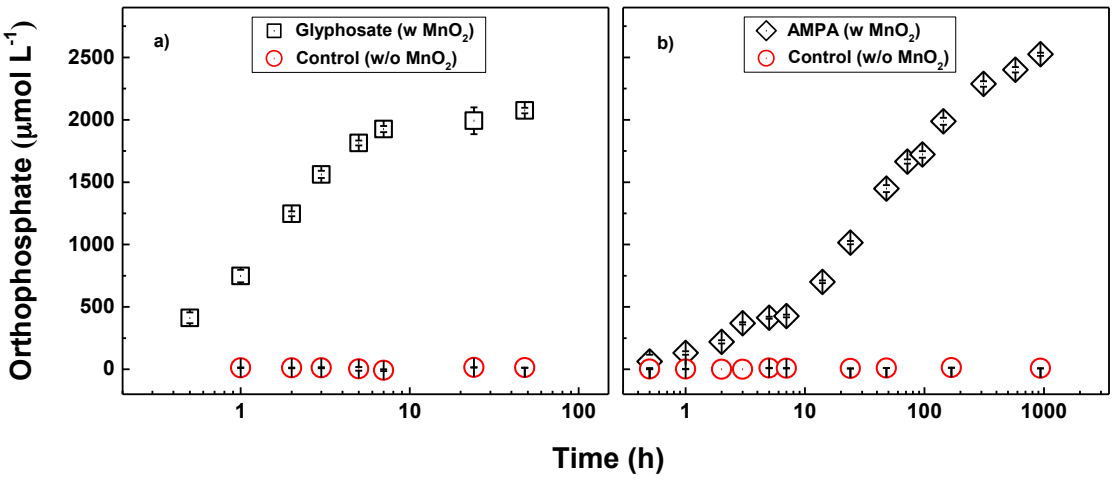

Figure 3.2. Degradation kinetics of glyphosate (a) and AMPA (b) catalyzed by birnessite (MnO_2) mineral (please note the longer degradation time for AMPA than that for glyphosate). Experiments were performed using a starting glyphosate/AMPA concentration of 3000 μmol L^{-1} at 22±1 °C and pH=7.00±0.05. Controls represent experiments without birnessite minerals.

The amount of orthophosphate produced was negligible in control experiments containing glyphosate or AMPA but without birnessite, indicating their stability in the media. This result alternatively indicated the absence of microbial degradation of these compounds within the time range of experiments that is important for interpretation of isotope results (see below). After 48 h of reaction, the pH value increased slightly to ~7.5, which could result from the consumption of H^+ during degradation (Barrett and McBride, 2005) and the release of hydroxyl groups from mineral surfaces due to ligand exchange with orthophosphate. During glyphosate degradation, Mn(IV) is reduced to Mn^{2+} and released into the media. However, inductively coupled plasma (ICP) measurement of Mn^{2+} in the solution showed no significant increase in Mn

concentration. The negligible concentration of Mn in the solution indicates rapid resorption of reduced Mn^{2+} onto mineral surfaces at layer vacancies or edge sites which may undergo further oxidation to Mn^{3+} (see discussion below). This re-oxidization could be induced either by Mn^{4+} in birnessite (Lefkowitz et al., 2013; Perez-Benito, 2002), or by dissolved oxygen (Nowack and Stone, 2000). Even without Mn(IV), Mn^{2+} has been found to be capable of catalyzing degradation of other phosphonates such as nitrilotris(methylene)phosphonic acid (NTMP), with O_2 involved in the oxidative degradation reaction (Nowack and Stone, 2000).

The rate of glyphosate degradation in the dark condition was slightly lower than that in the light condition (Figure 3.3a). Photochemical reactions are known to accelerate the degradation of organic compounds (Liang and Blake, 2006b) such as through the generation of reactive radicals and thus affect the reaction rate. Although we did not validate reasons for this potential difference, the difference in degradation in dark and light conditions might affect glyphosate degradation in soils and subsoils once it spreads or percolates into soils. The extent of degradation, however, was not affected by the presence or absence of light.

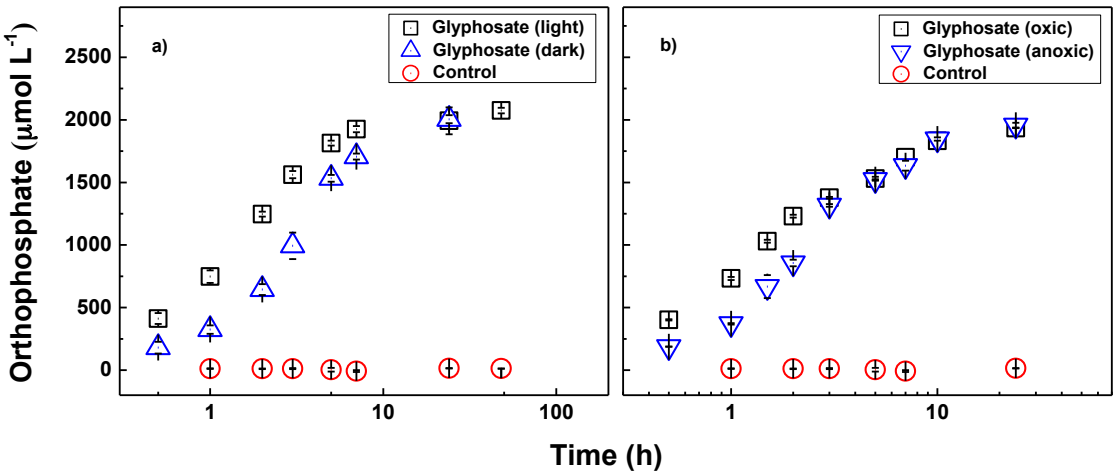

Figure 3.3. Degradation kinetics of glyphosate catalyzed by birnessite mineral in light/dark (a) and oxic/anoxic (b) conditions. Experiments were performed using a starting glyphosate concentration of 3000 μmol L^{-1} at 22±1 °C, pH=7.00±0.05. Control represents the experiments without birnessite minerals.

The rate of glyphosate degradation slightly decreased when the experiments were performed in the anaerobic conditions (Figure 3.3b). After ~5 h, however, the extent of degradation became close to that of the aerobic conditions. The higher degradation rate under aerobic conditions might mean that O_2 could have played a role in accelerating the reaction by potentially re-oxidizing reduced Mn^{2+} to a new Mn-oxide or Mn-glyphosate/AMPA complex that participates in the reaction. On the other hand, electron transfer between sorbed Mn^{2+} and structural Mn^{4+} can generate Mn^{3+} and then induce partial conversion of birnessite into feitknechtite (β-MnOOH) that can further transform into manganite (γ-MnOOH), as has been reported in anoxic conditions and circumneutral pH similar to those used in our experiments (Lefkowitz

et al., 2013). The reductive transformation of birnessite into manganite may also be possible. In general, manganite has a lower degradation rate than birnessite due to the lower valence state of Mn. The highest oxidizing capacity of Mn-oxides, however, was reported to be that containing Mn^{3+}, and, in particular, those containing Mn^{3+} and Mn^{2+} (Weaver et al., 2002). The speciation of Mn including valance state was not measured in this study as it was out of the scope of this research. Nonetheless, the overall rate of degradation was found to be affected by the absence of oxygen.

Surface catalysis of a mineral depends on the presence of reactive surface in the mineral and the formation of reactive complexes. Given that sorption is an essential step in glyphosate degradation (Barrett and McBride, 2005; Paudel et al., 2015), formation of a new mineral and the influence of new surface on the rate and extent of degradation depend on whether the existing surface is saturated or poisoned by degradation products. According to studies on birnessite synthesized using similar methods and with comparable SSA, the approximate greatest surface active site density at edges, which are the primary reactive positions for sorption or degradation reactions, can be calculated on the basis of the height of each phyllomanganate layer (0.19 nm) and the Mn–Mn distance (0.287 nm) (Villalobos et al., 2005; Villalobos et al., 2014). According to the above calculation, the edge site density becomes close to 1 site/(0.19 nm × 0.287 nm)=18.3 sites nm^{-2}. If we arbitrarily assume that 60 % of measured SSA belongs to the edge surface, then the reactive surface site density should be 18.3 sites nm^{-2} × 0.6 × 40 × 10^{18} nm^2 g^{-1} ×5 g L^{-1} = 22 × 10^{20} sites L^{-1}. The amount of initial glyphosate molecules used in this study is equal to 3 × 10^{-3} mol L^{-1} × 6.02 × 10^{23} molecules mol^{-1} = 18.06 × 10^{20} molecules L^{-1}. This means that >80 % of reactive surface sites of birnessite were initially saturated by glyphosate/AMPA. If the

reactive surface area decreased to 30%, which is more realistic for 2×4×1 geometry of birnessite with the unit cell parameters of 5.3, 3.05 and 7.79 Å (Cygan et al.), glyphosate clearly oversaturates the reactive surface. Therefore, the re-oxidation of Mn^{2+} into higher valence minerals to form new reactive surfaces or the formation of reactive complexes is required to enhance the extent of degradation in aerobic conditions. Even though the reactive surface sites and Mn^{4+} centers are sufficient for glyphosate coordination and degradation, with a low glyphosate:birnessite ratio (600 $\mu M\ g^{-1}$), enhanced degradation in the aerobic conditions indicates an important role for molecular oxygen in oxidation of Mn^{2+} and accelerating redox reactions. In addition, Mn^{2+} could also form complexes with glyphosate/AMPA, which can be rapidly oxidized into Mn^{3+}–complexes by superoxide ions generated from O_2 as has been interpreted in other phosphonates (Nowack and Stone, 2000; Nowack and Stone, 2002). These Mn^{3+} complexes also contribute to oxidative degradation without interaction or electron transport between mineral structural Mn^{4+} and glyphosate/AMPA, and thus could indicate a different degradation pathway in the presence of oxygen from that in the absence of oxygen. Overall, light and O_2 could be important rate-limiting factors in glyphosate degradation reactions.

Sorption of degradation products onto catalytic surface sites in the mineral decreases both the rate and extent of the reaction. Glyphosate and generated orthophosphate can both adsorb onto reactive surface sites of birnessite through complexation or ligand exchange reactions (Barrett and McBride, 2005), with orthophosphate outcompeting glyphosate (Cui et al., 2012). Therefore, orthophosphate speciation during degradation reactions can provide additional insights into the temporal change in reactivity. Interestingly, speciation of the generated

orthophosphate was found to be literally independent (Figure 3.4) during the progress of the degradation reaction. For example, the concentration of adsorbed orthophosphate rapidly increased within 15 h, then decreased and reached an equilibrium at ~40 μmol g^{-1}. The adsorbed orthophosphate accounts for ~11 % of total P as orthophosphate, demonstrating that almost 80 % degradation was achieved.

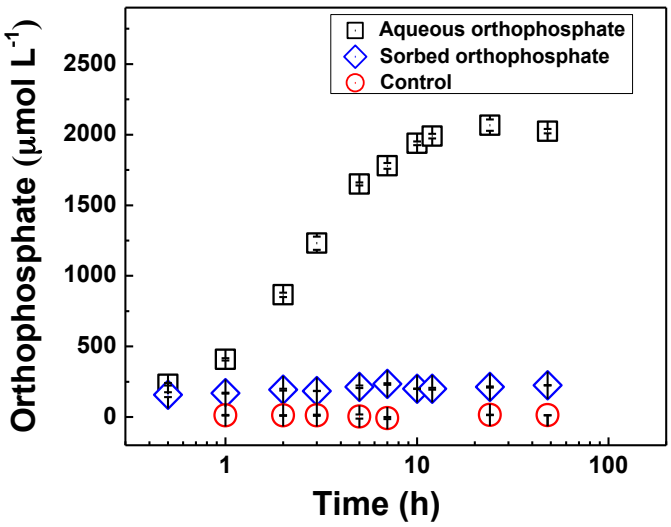

Figure 3.4. Orthophosphate partitioning between aqueous and sorbed phases as a function of time during glyphosate degradation. The starting glyphosate concentration was 3000 μmol L^{-1}.

3.4.3 Sources of Oxygen Incorporated into Orthophosphate

Given that the phosphorus atom is covalently bonded with carbon (i.e., the C−P sigma bond) in glyphosate and AMPA, cleavage at the C−P bonds in both compounds requires at least one oxygen atom from external sources to be incorporated

into the released orthophosphate. Glyphosate and AMPA degradation experiments performed under a series of $\delta^{18}O_W$ values (-7.41 to 138.57 ‰) of the ambient water showed that the $\delta^{18}O_P$ values of generated orthophosphate increased correspondingly with the increase in the $\delta^{18}O_W$ values (Figure 3.5a,b). This corresponding increase means that an oxygen atom from ambient water is incorporated into generated orthophosphate. The changes in the $\delta^{18}O_W$ values between waters before and after experiments were found to be within the detection limit of the equipment (0.02 ‰). The constant $\delta^{18}O_W$ values are expected due to the higher concentration of oxygen atoms in water than that of oxygen atoms in orthophosphate (in the order of molar to micromolar concentrations, respectively). The slope between the $\delta^{18}O_P$ values of generated orthophosphate and the $\delta^{18}O_W$ values of ambient water in hydrolysis reactions of different phosphomonoester and phophodiester compounds has been used to identify sources and number of water O atoms incorporated into the released orthophosphate (Liang and Blake, 2006a; Liang and Blake, 2006b; Liang and Blake, 2009). The slope of the fitting curve varies within 95% confidence intervals (0.20, 0.22) and (0.20, 0.21) for glyphosate and AMPA, respectively. For both glyphosate and AMPA in this study, the slope was found to be ~0.21, representing the incorporation of less than one oxygen atom (out of four oxygen atoms) from ambient water.

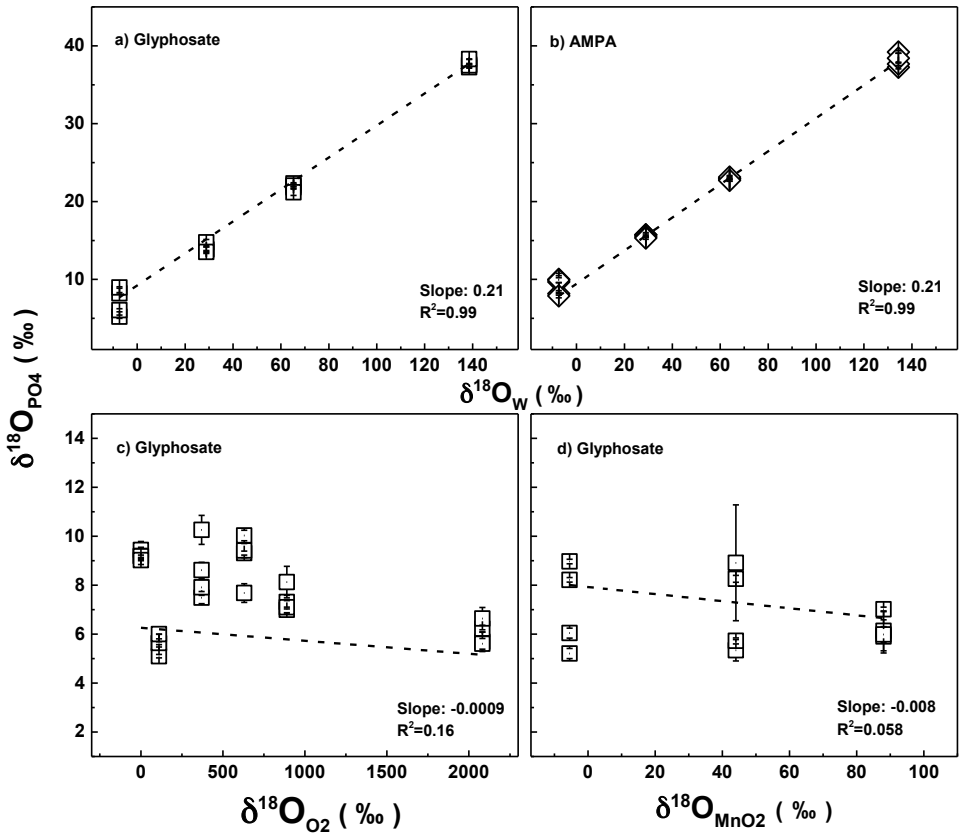

Figure 3.5. Plot of the $\delta^{18}O_P$ values of released orthophosphate (P_i) in labeled O experiments in water, dissolved oxygen, and minerals: (a,b) the $\delta^{18}O_W$ values of the ^{18}O-labeled water in glyphosate and AMPA degradation; (c) the $\delta^{18}O_{O2}$ values of ^{18}O-labeled dissolved O_2 in glyphosate degradation; (d) the $\delta^{18}O_{MnO2}$ values of ^{18}O-labeled birnessite minerals in glyphosate degradation.

Fractional incorporation of O (i.e., 0.21 instead of 0.25) in the released orthophosphate demands exploration of other O sources that may potentially be involved in donating an O atom, because orthophosphate impurities that may impact slope in glyphosate and AMPA stocks and birnessite minerals were very low (at

0.57±0.12 μmol L^{-1} and 0.54±0.19 μmol L^{-1}, respectively). Other potential sources of O are either dissolved oxygen or structural oxygen in the catalytic minerals. In fact, incorporation of dissolved O_2 into generated orthophosphate has been found during abiotic degradation of some organophosphorus compounds (Liang and Blake, 2006a; Liang and Blake, 2006b; Sandy et al., 2013). Glyphosate degradation experiments performed under various $\delta^{18}O_{O2}$ values of ^{18}O-labeled dissolved oxygen showed almost zero slope (-0.0009) (Figure 3.5c). This slope proved that no oxygen atoms from dissolved oxygen were incorporated into the released orthophosphate from glyphosate. Even though the measured data show up to ~4 ‰ fluctuations in the $\delta^{18}O_P$ values, this difference was negligible compared with the ~2000 ‰ difference in the $\delta^{18}O_{O2}$ values of dissolved oxygen used in these experiments. Another set of experiments performed using ^{18}O-labeled structural O in birnessite also showed an insignificant slope (-0.0080) (Figure 3.5d). This slope means that no oxygen was incorporated into released orthophosphate from the mineral that adsorbs and catalyzes glyphosate degradation. In addition, due to small fractionation of the $\delta^{18}O$ values between metal-oxide and ambient water, along with rapid isotope exchange between mineral–O and water–O under normal temperature conditions (Bao and Koch, 1999; Green and Taube, 1963), it is more likely that the $\delta^{18}O$ values of hydroxyl functional groups on the mineral surface could be fully equilibrated with ambient water. In summary, multi-oxygen isotope labeling allowed ruling out the possibility of oxygen atoms in the birnessite mineral structure or dissolved oxygen contributing to oxygen incorporated into the released orthophosphate.

The fractional incorporation of O can be discussed from interface isotope selectivity of orthophosphate. At the mineral–water interface, the $P^{16}O_4$ is

preferentially sorbed onto mineral surfaces first, leaving aqueous orthophosphate enriched with heavier isotopes (Jaisi et al., 2010; Li, 2015). Accounting for the amount of sorbed orthophosphate (Figure 3.4) and assuming ~2.5% fractionation of sorbed and aqueous orthophosphate and the fact that the isotopic composition of aqueous orthophosphate was measured in this study, this would bias the calculation towards a smaller slope (i.e., <0.25). This interpretation is supported by the data shown in Figure 3.6, where the $\delta^{18}O_P$ values of released aqueous orthophosphate over time show negative slopes for the first 5–7 h of reaction in three experiments performed in different labeled waters. This negative slope is mostly likely because maximum fractionation between these two P pools is significant only at the initial stage of sorption and, over time, efficient ion exchange between sorbed and aqueous orthophosphate erases the kinetic isotope fractionation. Therefore, the measured orthophosphate becomes relatively lighter to some extent before becoming constant at the later phase of the experiment, consistent with past studies (Jaisi et al., 2010; Li, 2015). Assuming 2.5‰ fractionation at the early stage of the experiment and noting that this difference is almost erased in > 7 h, it results in the slope difference of 0.02. These possibilities together suggest the slope between the $\delta^{18}O$ values of orthophosphate and water might be close to 0.25, representing one out of four oxygen atoms of orthophosphate derived from ambient water and not from other sources.

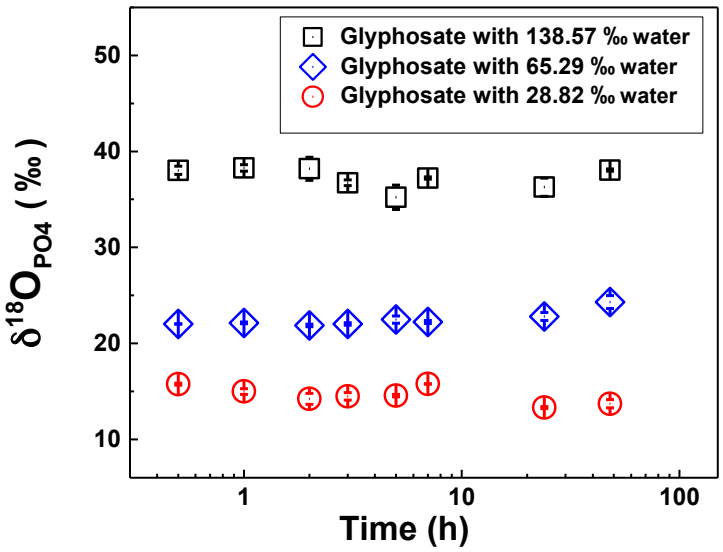

Figure 3.6. Oxygen isotopic compositions ($\delta^{18}O_P$) of released orthophosphate during glyphosate degradation in three different ^{18}O-labeled waters as a function of time.

The Y-intercept of the regression line is related to the inherited oxygen atoms from the parent substrates. Because three out of four O atoms in released orthophosphate are inherited from parental glyphosate and AMPA molecules, the similar intercepts for these two substrates (Figure 3.5) demonstrate a similar origin of phosphate oxygen sources (Jaisi et al., 2014). This similarity in the intercepts raises an interesting speculation on the origin of these synthetic phosphonate compounds. The isotopic composition of O and other elements in the glyphosate and AMPA molecules depends mainly on (i) the starting/original isotopic composition of the raw material used and (ii) the industrial production process that affects bond formation/cleavage reactions. Although there are several methods to synthesize glyphosate (Dill, 2010;

Zhou et al.), two major methods include (i) alkyl ester formation from glycine, dimethylphosphite, and paraformaldehyde and (ii) phosphonomethyl method, where phosphoric acid and formaldehyde form iminodiacetic acid hydrochloride (IDAAM-HCl), and then one of the two carboxymethyl groups in IDAAM-HCl is cleaved to form glyphosate (Dill, 2010). These results also indicate that the C−P bond cleavage in both molecules is not affected by any potential secondary isotope effect (Jaisi et al., 2014) consistent with the lowest secondary isotope effect expected for monoesters compared with that of diesters and triesters (Lassila et al., 2011). Overall, our results suggest similar sources of both glyphosate and AMPA (see below for additional insights on sources).

3.4.4 Fractionation of Oxygen between Bulk and Incorporated Water into Orthophosphate

The fractionation factor (F) of oxygen between that incorporated into orthophosphate and bulk water can be calculated following the established equation (Liang and Blake, 2006b) as:

$$F = (\delta^{18}O_P - 0.75\times\delta^{18}O_{PO}) \,/\, 0.21 - \delta^{18}O_W \quad (1)$$

As mentioned above (Figure 3.5), the slope of the regression is 0.21 for water O source. This slope means that 0.21 should be used in the calculation instead of 0.25 (one out of four Os) to calculate the fractionation factor. It is also necessary to know the isotopic signature of the 'intact' $-PO_3$ moiety (i.e., the $\delta^{18}O_{PO}$ value) in glyphosate and AMPA before degradation. Because of the existence of a carboxyl group, another O containing functional group in glyphosate, measurement of the original O isotope signature of glyphosate requires pretreatment to remove this group or replace it using other non-oxygen-containing functional groups. However, measurement of the $\delta^{18}O_{PO}$

values of AMPA is more straightforward, similar to phytate (Wu, 2015). After direct pyrolysis in TC/EA, the $\delta^{18}O_{PO}$ values of AMPA were found to be 16.43(±0.10) ‰. On the basis of the $\delta^{18}O_{PO}$ values, the $\delta^{18}O_P$ values of generated orthophosphate, and the $\delta^{18}O_W$ values of ambient water used in the experiments, O fractionation factors were calculated (Table 3.1). As shown, fractionation factors varied highly for the ranges of the $\delta^{18}O_W$ values used in the experiment with an average of -11.81 (±4.14) ‰. Negative F means that ^{16}O was preferentially incorporated into the released orthophosphate during AMPA degradation. This fractionation factor is different from those of other substrates and catalytic reagents for bond cleavage studied because the substrate-specific isotope effect is induced from structural differences among substrates and nature of enzymes (Jaisi et al., 2014; Liang and Blake, 2009).

Table 3.1. Isotope fractionation (F) of oxygen between water and incorporated into orthophosphate. The $\delta^{18}O_W$ and $\delta^{18}O_P$ values refer to oxygen isotopic composition of water and orthophosphate, respectively. The average fractionation factor (F) for all data is -11.81 ± 4.14 ‰.

Organic P compound	$\delta^{18}O_W$ (‰)	$\delta^{18}O_P$ (‰)	$\delta^{18}O_{OP}$ (‰)	F (‰)	Average F (‰)
AMPA	-7.41 ± 0.09	8.16 ± 0.17	16.43 ± 0.10	-12.15	-7.58 ± 4.79
		9.68 ± 1.10		-5.03	
		10.02 ± 0.45		-3.41	
		9.91 ± 0.30		-3.93	
		7.90 ± 0.27		-13.38	
	28.93 ± 0.04	15.74 ± 0.09		-12.87	-13.72 ± 0.94
		15.71 ± 0.31		-13.02	
		15.47 ± 0.06		-14.12	
		15.32 ± 0.17		-14.85	
	63.83 ± 0.08	22.96 ± 0.08		-13.86	-14.01 ± 0.81
		22.92 ± 0.28		-14.08	
		23.13 ± 0.23		-13.08	
		22.71 ± 0.10		-15.04	
	134.26 ± 0.11	37.24 ± 0.21		-17.16	-12.97 ± 4.05
		37.68 ± 0.22		-15.12	
		39.21 ± 0.15		-7.94	
		38.41 ± 0.62		-11.67	

3.4.5 Isotope Signatures of Commercial Glyphosate Products

Although Monsanto products dominate the herbicide market, glyphosate is manufactured and marketed worldwide under different trade names by other companies including Bayer, Dow AgroSciences, DuPont, Cenex/Land O'Lakes, Helena, Platte, Riverside/Terra and Zeneca. The $\delta^{18}O_P$ values of orthophosphate released by birnessite-catalyzed degradation of five different commercial glyphosate products (Gly-1 to Gly-5) are shown in Table 3.2. Interestingly, we found unusually light $\delta^{18}O_P$ values and distinctly different isotope signatures from each commercial glyphosate source. Although the sample size is small and these products include two

different manufacturers and three different industrial formulations for targeted applications, this range of isotopic compositions is the smallest known so far for all organophosphorus compounds studied (the $\delta^{18}O_P$ values are usually $\geqslant$14‰) (Liang and Blake, 2006b; Liang and Blake, 2009; von Sperber et al., 2014), irrespective of enzymatic or non-enzymatic pathways or mechanisms of degradation. Furthermore, the $\delta^{18}O_P$ values of individual glyphosate products are distinctly different and are isotopically separable. While more data on isotope distribution of additional glyphosate sources are needed before any generalization, our results open the new possibility of applying the $\delta^{18}O_P$ values as a proxy for differentiating glyphosate from other organophosphorus compounds as well as tracking different glyphosate sources in the environment. Another implication appears to be that the $\delta^{18}O$ values could be used to track the portion of orthophosphate in the environment derived from glyphosate degradation.

Table 3.2. Isotopic composition of released orthophosphate during birnessite-catalyzed degradation of different commercial glyphosate products. Five different glyphosate products (Gly-1 to Gly-5) were used in the experiment.

Commercial Glyphosate Products	$\delta^{18}O_P$ (‰)
Gly-1	3.92 ± 0.35
Gly-2	8.77 ± 0.36
	8.35 ± 0.42
Gly-3	6.09 ± 0.13
	5.75 ± 0.20
Gly-4	6.97 ± 0.37
	9.30 ± 0.20
Gly-5	3.91 ± 0.36

3.4.6 Implications of Tracking Glyphosate and Its Degradation Products in the Environment

Isotopic methods have long been used in biochemistry for mechanistic elucidation of organic molecule degradation. However, the application of isotopes to track sources and degradation pathways of organic contaminants in the environment is not common. There are significant challenges in method development, but compound-specific oxygen isotope composition is one of the most advanced methods to differentiate various sources and understand the role of different organic P forms in the environment (Jaisi et al., 2014). Recently, carbon isotopes (Kujawinski et al., 2013) and phosphate oxygen isotopes (Sandy et al., 2013) in glyphosate have been applied to identify reaction mechanisms. These isotope-tracking methods have raised the potential of providing source information of parent and daughter compounds.

In this study, one oxygen atom was verified to be incorporated from water into generated orthophosphate with three inherited from the original compound. The isotope effect induced by the C−P bond cleavage and corresponding isotope exchange of oxygen atoms in reagent grade glyphosate is essentially the same as that of commercial herbicides with various glyphosate compositions. Glyphosate carries a much lighter isotopic composition than most common orthophosphates studied so far (the $\delta^{18}O_P$ values vary between 16~24 ‰ VSMOW). This result might be also applicable to other mineral catalyzed redox degradations. Given that phosphate O-isotope signatures of glyphosate remain intact unless the molecule is degraded, and the isotope effect during abiotic degradation is independent of oxic/anoxic and light/dark conditions of degradation, phosphate oxygen isotope ratios offer a promising indicator for source tracking of glyphosate and its metabolites in soils and other environments. The presence of the lightest $\delta^{18}O_P$ values of inorganic P produced in glyphosate

degradation compared with all organic P compounds and inorganic P in the environment studied so far indicates that the $\delta^{18}O_P$ values could be used as a reliable tracer to track glyphosate as well as its degradation products, i.e. orthophosphate. If successfully field validated, this tool could have a profound impact on environmental forensics of glyphosate.

Acknowledgments

This research was supported by research grants from the US Department of Agriculture (NIFA awards 2012–67019–19320 and 2013–67019–21373). We would like to acknowledge the Advanced Material Characterization Lab at the University of Delaware for providing XRD, BET, and SEM analyses of birnessite minerals. We would also like to extend our gratitude to Justin Hayles (Louisiana State University) for his contribution in measuring isotope composition of birnessite minerals using the fluorination method.

REFERENCES

Bao, H. and Koch, P.L., 1999. Oxygen isotope fractionation in ferric oxide–water systems: Low temperature synthesis. Geochim. Cosmochim. Acta, 63: 599–613.

Bao, H., Koch, P.L. and Thiemens, M.H., 2000. Oxygen isotopic composition of ferric oxides from recent soil, hydrologic, and marine environments. Geochim. Cosmochim. Acta, 64: 2221–2231.

Barrett, K.A. and McBride, M.B., 2005. Oxidative degradation of glyphosate and aminomethylphosphonate by manganese oxide. Environ. Sci. Technol., 39: 9223–9228.

Battaglin, W.A., Meyer, M.T., Kuivila, K.M. and Dietze, J.E., 2014. Glyphosate and its degradation product AMPA occur frequently and widely in U.S. soils, surface water, groundwater, and precipitation. J. Am. Water Res. Assoc., 50: 275–290.

Blake, R.E., O'Neil, J.R. and Garcia, G.A., 1997. Oxygen isotope systematics of biologically mediated reactions of phosphate: I. Microbial degradation of organophosphorus compounds. Geochim. Cosmochim. Acta, 61: 4411–4422.

Cohn, M. and Urey, H.C., 1938. Oxygen exchange reactions of organic compounds and water. J. Am. Chem. Soc., 60: 679–687.

Cui, H., Li, Q., Qian, Y., Zhang, Q. and Zhai, J., 2012. Preparation and adsorption performance of MnO_2/PAC composite towards aqueous glyphosate. Environ. Technol., 33: 2049–2056.

Cygan, R.T., Post, J.E., Heaney, P.J. and Kubicki, J.D., Molecular models of birnessite and related hydrated layered minerals. Am. Mineral., 97: 1505–1514.

Dill, G.M., Sammons R.D., Feng P.C.C., Kohn F., Kretzmer K., Mehrsheikh A., Bleeke M., Honegger J.L., Farmer D., Wright D., Haupfear E.A., 2010. Glyphosate: discovery, development, applications, and properties. In: Nandula, V.K. (Editor), Glyphosate resistance in crops and weeds. John Wiley & Sons, Inc., pp 1–33.

Drits, V.A., Silvester, E., Gorshkov, A.I. and Manceau, A., 1997. Structure of synthetic monoclinic Na-rich birnessite and hexagonal birnessite: I. Results from X-ray diffraction and selected-area electron diffraction. Am. Mineral., 82: 946–961.

Foster, A.L., Brown, G.E. and Parks, G.A., 2003. X-ray absorption fine structure study of As(V) and Se(IV) sorption complexes on hydrous Mn oxides. Geochim. Cosmochim. Acta, 67: 1937–1953.

Franz, J.E., Mao, M.K. and Sikorski, J.A., 1997. Glyphosate: A unique global herbicide. American Chemical Society, Washington, D.C.

Galhardo, C.X. and Masini, J.C., 2000. Spectrophotometric determination of phosphate and silicate by sequential injection using molybdenum blue chemistry. Anal. Chim. Acta, 417: 191–200.

Ge, L., Peer, W., Robert, S., Swarup, R., Ye, S., Prigge, M., Cohen, J.D., Friml, J., Murphy, A., Tang, D. and Estelle, M., 2010. Arabidopsis ROOT UVB SENSITIVE2/WEAK AUXIN RESPONSE1 is required for polar auxin transport. Plant Cell, 22: 1749–1761.

Green, M. and Taube, H., 1963. Isotopic fractionation in the OH-H_2O exchange reaction. J. Phys. Chem., 67: 1565–1566.

Grunewald, K., Schmidt, W., Unger, C. and Hanschmann, G., 2001. Behavior of glyphosate and aminomethylphosphonic acid (AMPA) in soils and water of reservoir Radeburg II catchment (Saxony/Germany). J. Plant Nutr. Soil Sci., 164: 65–70.

Guilherme, S., Santos, M.A., Gaivao, I. and Pacheco, M., 2014. DNA and chromosomal damage induced in fish (Anguilla anguilla L.) by aminomethylphosphonic acid (AMPA)—the major environmental breakdown product of glyphosate. Environ. Sci. Pollut. Res. Int., 21: 8730–8739.

Jaisi, D.P. and Blake, R.E., 2010. Tracing sources and cycling of phosphorus in Peru Margin sediments using oxygen isotopes in authigenic and detrital phosphates. Geochim. Cosmochim. Acta, 74: 3199–3212.

Jaisi, D.P. and Blake, R.E., 2014. Advances in using oxygen isotope ratios of phosphate to understand phosphorus cycling in the environment. Adv. Agron., 125: 1–53.

Jaisi, D.P., Blake, R.E. and Kukkadapu, R.K., 2010. Fractionation of oxygen isotopes in phosphate during its interactions with iron oxides. Geochim. Cosmochim. Acta, 74: 1309–1319.

Jaisi, D.P., Blake, R.E., Liang, Y. and Chan, S.J., 2014. Investigation of compound-specific organic-inorganic phosphorus transformation using stable isotope ratios in phosphate. In Applied manure and nutrient chemistry for sustainable agriculture and environment (Eds. Z. He and H. Zhang), 267–292.

Jaisi, D.P., Dong, H.L., Plymale, A.E., Fredrickson, J.K., Zachara, J.M., Heald, S. and Liu, C.X., 2009. Reduction and long-term immobilization of technetium by Fe(II) associated with clay mineral nontronite. Chem. Geol., 264: 127–138.

Joshi, S.R., Kukkadapu, R.K., Burdige, D.J., Bowden, M.E., Sparks, D.L. and Jaisi, D.P., 2015. Organic matter remineralization predominates phosphorus cycling in the mid-bay sediments in the chesapeake bay. Environ. Sci. Technol., 49: 5887–5896.

Kujawinski, D.M., Wolbert, J.B., Zhang, L., Jochmann, M.A., Widory, D., Baran, N. and Schmidt, T.C., 2013. Carbon isotope ratio measurements of glyphosate and AMPA by liquid chromatography coupled to isotope ratio mass spectrometry. Anal. Bioanal. Chem., 405: 2869–2878.

Lassila, J.K., Zalatan, J.G. and Herschlag, D., 2011. Biological Phosphoryl-Transfer Reactions: Understanding Mechanism and Catalysis. In: R.D. Kornberg, C.R.H. Raetz, J.E. Rothman and J.W. Thorner (Editors), Annual Review of Biochemistry, Vol 80. Annual Review of Biochemistry, pp. 669–702.

Lefkowitz, J.P., Rouff, A.A. and Elzinga, E.J., 2013. Influence of pH on the reductive transformation of birnessite by aqueous Mn(II). Environ. Sci. Technol., 47: 10364–10371.

Li, H. and Jaisi, D.P., 2015. An Isotope labeling approach to investigate atom exchange during phosphate sorption and desorption. Soil Sci. Soc. Am. J., 79: 1340–1351.

Liang, Y. and Blake, R.E., 2006a. Oxygen isotope composition of phosphate in organic compounds: Isotope effects of extraction methods. Org. Geochem., 37: 1263–1277.

Liang, Y. and Blake, R.E., 2006b. Oxygen isotope signature of Pi regeneration from organic compounds by phosphomonoesterases and photooxidation. Geochim. Cosmochim. Acta, 70: 3957–3969.

Liang, Y. and Blake, R.E., 2009. Compound- and enzyme-specific phosphodiester hydrolysis mechanisms revealed by $\delta^{18}O$ of dissolved inorganic phosphate: Implications for marine P cycling. Geochim. Cosmochim. Acta, 73: 3782–3794.

Marc, J., Belle, R., Morales, J., Cormier, P. and Mulner-Lorillon, O., 2004. Formulated glyphosate activates the DNA-response checkpoint of the cell cycle leading to the prevention of G2/M transition. Toxicol. Sci., 82: 436–442.

Marcus, R.A., 1957. On the theory of oxidation-reduction reactions involving electron transfer. II. Applications to data on the rates of isotopic exchange reactions. J. Chem. Phys., 26: 867–871.

McKenzie, R.M., 1971. The influence of cobalt on the reactivity of manganese dioxide. Aust. J. Soil Res., 9: 55–58.

Meyer, M.T., Loftin, K.A., Lee, E.A., Hinshaw, G.H., Dietze, J.E. and Scribner, E.A., 2009. Determination of glyphosate, its degradation product aminomethylphosphonic acid, and glufosinate, in water by isotope dillution and online solid-phase extraction and liquid chromatography/tandem mass spectrometry. U.S. Geological Survey, Reston, Virginia.

Murphy, J. and Riley, J.P., 1962. A modified single solution method for the determination of phosphate in natural waters. Anal. Chim. Acta, 27: 31–36.

Nowack, B. and Stone, A.T., 2000. Degradation of nitrilotris(methylenephosphonic acid) and related (amino)phosphonate chelating agents in the presence of manganese and molecular oxygen. Environ. Sci. Technol., 34: 4759–4765.

Nowack, B. and Stone, A.T., 2002. Homogeneous and heterogeneous oxidation of nitrilotrismethylenephosphonic acid (NTMP) in the presence of manganese (II, III) and molecular oxygen. J. Phys. Chem. B, 106: 6227–6233.

Nowack, B. and Stone, A.T., 2006. Competitive adsorption of phosphate and phosphonates onto goethite. Water Res., 40: 2201–2209.

Paudel, P., Negusse, A. and Jaisi, D.P., 2015. Birnessite-catalyzed degradation of glyphosate: A mechanistic study aided by kinetics batch studies and NMR spectroscopy. Soil Sci. Soc. Am. J., 79: 815–825.

Peng, Y., Bao, H., Zhou, C. and Yuan, X., 2011. ^{17}O-depleted barite from two Marinoan cap dolostone sections, South China. Earth Planet. Sci. Lett., 305: 21–31.

Perez-Benito, J.F., 2002. Reduction of colloidal manganese dioxide by manganese(II). J. Colloid Interface Sci., 248: 130–135.

Post, J.E., 1999. Manganese oxide minerals: Crystal structures and economic and environmental significance. Proc. Natl. Acad. Sci. USA, 96: 3447–3454.

Remucal, C.K. and Ginder-Vogel, M., A critical review of the reactivity of manganese oxides with organic contaminants. Environ. Sci. Proc. Imp., 16: 1247–1266.

Sandy, E.H., Blake, R.E., Chang, S.J., Jun, Y. and Yu, C., 2013. Oxygen isotope signature of UV degradation of glyphosate and phosphonoacetate: Tracing sources and cycling of phosphonates. J. Hazard. Mater., 260: 947–954.

Sikorski, J.A. and Gruys, K.J., 1997. Understanding glyphosate's molecular mode of action with EPSP synthase: Evidence favoring an allosteric inhibitor model. Acc. Chem. Res., 30: 2–8.

Steinrticken, H.C. and Amrhein, N., 1980. The herbicide glyphosate is a potent inhibitor of 5-enolpyruvyl-shikimaic acid-3-phosphate synthase. Biochem. Biophys. Res. Commun., 94: 1207–1212.

Taylor, R.M., McKenzie, R.M. and Norrish, K., 1964. The mineralogy and chemistry of manganese in some Australian soils. Aust. J. Soil Res., 2: 235–248.

Thongprakaisang, S., Thiantanawat, A., Rangkadilok, N., Suriyo, T. and Satayavivad, J., 2013. Glyphosate induces human breast cancer cells growth via estrogen receptors. Food Chem. Toxicol., 59: 129–136.

United States Environmental Protection Agency, 1993. Prevention, pesticides and toxic substances (7508W). R.E.D FACTS. Glyphosate., EPA-738-F-93-011.

Villalobos, M., Bargar, J. and Sposito, G., 2005. Mechanisms of Pb(II) sorption on a biogenic manganese oxide. Environ. Sci. Technol., 39: 569–576.

Villalobos, M., Escobar-Quiroz, I.N. and Salazar-Camacho, C., 2014. The influence of particle size and structure on the sorption and oxidation behavior of birnessite: I. Adsorption of As(V) and oxidation of As(III). Geochim. Cosmochim. Acta, 125: 564–581.

von Sperber, C., Kries, H., Tamburini, F., Bernasconi, S.M. and Frossard, E., 2014. The effect of phosphomonoesterases on the oxygen isotope composition of phosphate. Geochim. Cosmochim. Acta, 125: 519–527.

Weaver, R.M., Hochella, M.F. and Ilton, E.S., 2002. Dynamic processes occurring at the Cr-aq(III)-manganite (gamma-MnOOH) interface: Simultaneous adsorption, microprecipitation, oxidation/reduction, and dissolution. Geochim. Cosmochim. Acta, 66: 4119–4132.

Wu, J., Sun, M., Paudel, P., Joshi, S.R., Stout, L.M., Greiner, R., and Jaisi, D.P., 2015. Mechanisms and pathways of phytate degradation: Evidence from $\delta^{18}O$ of phosphate, HPLC, and ^{31}P NMR spectroscopy. Soil Sci. Soc. Am. J., 79: 1615–1628.

Yin, H., Li, H., Wang, Y., Ginder-Vogel, M., Qiu, G., Feng, X.H., Zheng, L. and Liu, F., 2014. Effects of Co and Ni co-doping on the structure and reactivity of hexagonal birnessite. Chem. Geol., 381: 10–20.

Zhou, J., Li, J., An, R., Yuan, H. and Yu, F., Study on a new synthesis approach of glyphosate. J. Agric. Food Chem., 60: 6279–6285.

Chapter 4

DEGRADATION OF GLYPHOSATE BY MN-OXIDE MAY BYPASS SARCOSINE AND FORM GLYCINE DIRECTLY AFTER THE C–N BOND CLEAVAGE

Reproduced with permission from

Degradation of Glyphosate by Mn-Oxide May Bypass Sarcosine and Form Glycine Directly after C–N Bond Cleavage

Hui Li, Adam F. Wallace, Mingjing Sun, Patrick Reardon, and Deb P. Jaisi

Environ. Sci. Technol., 2018, 52(3), pp 1109–1117

DOI: 10.1021/acs.est.7b03692

https://pubs.acs.org/doi/abs/10.1021/acs.est.7b03692

4.1 Abstract

Glyphosate is the active ingredient of the common herbicide Roundup®. The increasing presence of glyphosate and its byproducts has raised concerns about its potential impact on the environment and human health. In this research, we investigated abiotic pathways of glyphosate degradation as catalyzed by birnessite under aerobic and neutral pH conditions to determine whether certain pathways have the potential to generate less harmful intermediate products. Nuclear magnetic resonance spectroscopy (NMR) and high-performance liquid chromatography (HPLC) were utilized to identify and quantify reaction products, and density functional theory (DFT) calculations were used to investigate the bond critical point (BCP) properties of the C–N bond in glyphosate and Mn(IV)-complexed glyphosate. We found that

sarcosine, the commonly recognized precursor to glycine, was not present at detectable levels in any of our experiments despite the fact that its half-life (~13.6 h) was greater than our sampling intervals. Abiotic degradation of glyphosate largely followed the glycine pathway rather than the AMPA (aminomethylphosphonic acid) pathway. Preferential cleavage of the phosphonate adjacent C–N bond to form glycine directly was also supported by our BCP analysis, which revealed that this C–N bond was disproportionately affected by the interaction of glyphosate with Mn(IV). Overall, these results provide useful insights into the potential pathways through which glyphosate may degrade via relatively benign intermediates.

4.2 Introduction

Glyphosate (N-phosphonomethyl glycine) was first introduced into the herbicidal industry by John Franz of Monsanto in the 1970s to kill broadleaf plants and grasses (Franz et al., 1997). The agricultural innovation of genetically engineered glyphosate-tolerant crops that followed dramatically enhanced the applicability of glyphosate as a non-selective, post-emergence herbicide on agricultural fields. As a result, the application rate of glyphosate skyrocketed from less than 9×10^6 Kg yr^{-1} in the U.S. in 1992 to 127×10^6 Kg yr^{-1} in 2015 with more than 70 % applied to corn and soybean crops (United States Geological Survey, 2015). The widespread usage of glyphosate in agriculture resulted in increased environmental contamination by glyphosate and its intermediate products [e.g., aminomethylphosphonic acid (AMPA)] in soils, sediments, surface water, and ground water (Battaglin et al., 2014; Kolpin et al., 2006). This alarmed the public and prompted the need for studies on the environmental and health impacts of glyphosate. Glyphosate kills plants by blocking the shikimic acid pathway, which is necessary for the synthesis of vital aromatic

amino acids in plants and some microorganisms (Haslam, 1974). Several toxicity studies suggested that the risk of adverse health effects due to glyphosate exposure were negligible in animals and humans (Kwiatkowska et al., 2016; Williams et al., 2000); however, recent studies have identified negative health effects in zebrafish, navigational honey bees (influencing navigational capabilities), and potential risks to soil nematodes (such as *Caenorhabditis elegans*), thus putting the safety of glyphosate and its widespread application under greater scrutiny (Balbuena et al., 2015; McVey et al., 2016; Roy et al., 2016). The United States Environmental Protection Agency is evaluating the potential carcinogenicity of glyphosate but has not yet reached a conclusion regarding its toxicity (Environmental Protection Agency's Office of Pesticide Programs, 2016).

The degradation of glyphosate in soils is driven by primarily biotic pathways mediated by bacteria and fungi (Rueppel et al., 1977; Sviridov et al., 2015). However, abiotic degradation may also occur in the presence of manganese oxides and/or light (photolysis) (Barrett and McBride, 2005; Li et al., 2016; Sandy et al., 2013). In each instance, glyphosate degradation occurs either through the cleavage of a C–N bond, forming AMPA and glyoxylic acid as a consequence (the AMPA pathway), or through the cleavage of a C–P bond, forming sarcosine and then glycine (the sarcosine pathway) (Franz et al., 1997; Rueppel et al., 1977; Sviridov et al., 2015). The focus of most past studies on the biotic degradation of glyphosate has been restricted to the two major degradation pathways. Biotic degradation of glyphosate in soils has been found to accumulate AMPA (Bento et al., 2016; Franz et al., 1997; Rueppel et al., 1977). Sarcosine, however, is less commonly detected as a product of biotic glyphosate degradation. For instance, the apparent formation of glycine was detected in the

absence of sarcosine during biotic degradation of ^{14}C-labeled glyphosate in soils (Rueppel et al., 1977). Glycine formation without sarcosine was also observed during the incubation of *Achromobacter* sp. MPS 12 in the presence of a sarcosine oxidase inhibitor (Sviridov et al., 2012). Similarly, sarcosine was not detected as a precursor to glycine in abiotic glyphosate degradation experiments catalyzed by either manganese oxide (Barrett and McBride, 2005), or photo-electrochemically generated hydroxyl radicals on a TiO_2 surface under alkaline conditions (Muneer and Boxall, 2008). These studies generally attributed the absence of sarcosine to its rapid degradation rate and did not consider the possibility that glycine might also form as a direct degradation product of glyphosate. However, one solid-state NMR study of *Pseudomonas* sp. cultures suggested that glycine might form directly (Jacob et al., 1985). These findings have elevated to the fore the notion that the sarcosine pathway may be circumvented by a seldom recognized direct glycine pathway. However, due to the focus of most studies on biotic pathways (using soil bacteria or microorganisms with suppressed gene expression) and the lack of unequivocal evidence substantiating the absence of sarcosine in the reaction mixture, more direct evidence of the absence of sarcosine and the presence of the glycine pathway (through direct C–N bond cleavage) is needed. In fact, glyphosate degradation may proceed through one of the two C–N bond positions; cleavage of the first C–N bond position results in the formation of AMPA, which is known to be more persistent and more toxic than glyphosate (Bento et al., 2016; Giesy et al., 2000; Li et al., 2016), while cleavage of the second may result in the direct formation of comparatively benign reaction products (e.g. glycine). Therefore, the existence of this less toxic abiotic glyphosate degradation pathway carries both scientific and environmental significance.

In our previous studies, kinetics of glyphosate degradation, two major degradation pathways (via AMPA and sarcosine intermediates), oxygen isotope effect during degradation, and the relationship of sources and products were analyzed and mechanisms during abiotic degradation had been proposed (Jaisi et al., 2016; Li et al., 2016; Paudel et al., 2015). In this chapter, my primary objective is to identify and quantify degradation products, with a special focus on sarcosine, glycine, and AMPA, that form during the degradation of glyphosate in the presence of synthetic birnessite. One- and two-dimensional (1-D and 2-D) nuclear magnetic resonance (NMR) spectroscopy, high-performance liquid chromatography (HPLC) and density functional theory (DFT) calculations were utilized in conjunction with colorimetric methods to identify and quantify products. Our results allow us to comment on the relative significance of specific degradation pathways, and the potential for further investigation into the factors that govern the preferential selection of pathways that introduce less toxic products into the environment.

4.3 Materials and Methods

4.3.1 Synthesis and Characterization of Birnessite

K^+-birnessite [$K_x(Mn^{4+}, Mn^{3+})_2O_4$; where $x<1$] was prepared by adding 45 mL of 6 mol L^{-1} HCl at a constant rate using an ISMATEC HPLC pump to a vigorously boiling solution of 300 mL of 0.667 mol L^{-1} $KMnO_4$ (Li and Jaisi, 2015; McKenzie, 1971). Synthesized mineral precipitates were washed with DI water, then freeze-dried and gently ground. Detailed characterization methods used to determine the identity, purity, specific surface area, birnessite morphology, and Mn average oxidation state (AOS) are included in the supporting information in the appendix A.

4.3.2 Glyphosate Degradation Experiments

A series of glyphosate [unlabeled glyphosate and carbon-isotope labeled (3-^{13}C counting from carboxyl group: HOOC–CH_2–NH–$^{13}CH_2$–PO_3H_2) glyphosate] (Sigma Aldrich, St Louis, MS) degradation experiments were carried out to identify the composition of intermediate products and to investigate degradation pathways. Degradation experiments were initiated by adding glyphosate stock (unlabeled glyphosate or carbon-isotope labeled glyphosate) to birnessite suspension in 10 mmol L^{-1} NaCl ionic strength (Table 4.1). Homogeneous suspensions of synthetic birnessite were kept at pH 7.00±0.05 before and after glyphosate addition, and were continuously adjusted using 1 mol L^{-1} NaOH/HNO_3. Control experiments included glyphosate under the same experimental conditions but without birnessite. Each experiment was conducted in triplicate and each reactor was continually stirred to maintain a uniform distribution of reactants at room temperature (22±1 °C). To determine the half-lives of common glyphosate-derived intermediate products, degradation experiments of AMPA, sarcosine, glycine, methylamine, and glyoxylic acid were conducted separately under similar conditions to that of glyphosate. Sample aliquots were removed from the reactor and placed into centrifuge tubes at selected time points. Aqueous and solid phases were separated by filtration [0.10 μm hydrophilic polyethersulfone (PES) filter] immediately after sampling. The solid phase was dissolved in 1 mol L^{-1} HNO_3 and 1 mol L^{-1} hydroxylamine hydrochloride to quantify adsorbed compounds. Concentrations of orthophosphate, primary amines (AMPA, glycine, and methylamine), and formaldehyde were measured using a UV/Vis spectrophotometer following the colorimetric phosphomolybdate blue method (Murphy and Riley, 1962), 2,4,6-trinitrobenzene sulfonic acid (TNBSA) method (Brown, 1968), and Nash assay (Nash, 1953), respectively.

Table 4.1. Experimental set up for glyphosate degradation by birnessite. All experiments were performed under pH 7.00±0.05 and 10 mmol L^{-1} NaCl.

Experiments label	Substrate (μmol L^{1})	Birnessite (g L^{1})
	Glyphosate	
GB3000	3000	5
GB300	300	0.5
GB150	150	0.5
	AMPA	
AB3000	3000	5
	Sarcosine	
SB3000	3000	5
	Glycine	
GCB150	150	0.5
	Methylphosphonic Acid	
MB3000	3000	5
	Glyoxylic Acid	
GAB300	300	0.5
	Methylamine	
MAB300	300	0.5

4.3.3 Analysis of Intermediate Products Using 1-D and 2-D NMR Spectroscopies

Both solution 1-D and 2-D NMR spectroscopies were utilized to identify the composition of intermediate products during birnessite-mediated degradation of glyphosate. Before analysis, aqueous subsamples collected at different time points during degradation were freeze-dried, and then re-dissolved in D_2O and mixed thoroughly. The pH was adjusted to 7.0±1.0 using 1 mol L^{-1} $NaOH/HNO_3$. Three resonance active nuclei (H, C, P) present in glyphosate and many of its products were analyzed by conventional 1-D NMR spectroscopy (^{1}H, ^{13}C, and ^{31}P NMR) in an AVIII 600 MHz Bruker spectrometer at 25 °C. The acquisition parameters were: (i) for ^{1}H

NMR 16 scans, 2 dummy scans, 10 s relaxation delay, 2.66 s acquisition time, zero-filled to the final size of 65536 points and apodized with 0.3 Hz line broadening, center frequency of 6.18 ppm, and at 600.32 MHz; (ii) for ^{13}C NMR spectra 2048 scans, 4 dummy scans, 1.1 s relaxation delay, 0.94 s acquisition time, zero-filled to final size of 65536 points and apodized with 1 Hz line broadening, center frequency of 100.0 ppm, and at 150.96 MHz; (iii) for ^{31}P NMR spectra 512 scans, 4 dummy scans, 2 s relaxation delay, 0.34 s acquisition time, zero-filled to final size of 65536 points and apodized with 1 Hz line broadening, center frequency of 0 ppm, and at 243.01 MHz. Recorded ^{1}H and ^{13}C, and ^{31}P NMR spectra were referenced to tetramethylsilane (TMS) and phosphoric acid at 0 ppm, respectively. Reference spectra of pure compounds (glyphosate, AMPA, sarcosine, glycine, methanol, methyl phosphonic acid, glyoxylic acid, methylamine, and formaldehyde) were analyzed as external standards for peak assignments of intermediate products generated during glyphosate degradation.

Two-dimensional (2-D) NMR spectroscopic analysis was performed for the assignments of unresolved peaks due to overlapping peak regions of potential compounds as well as to cross check the composition of compounds identified from 1-D NMR spectra. Heteronuclear single quantum correlation (HSQC) analysis allowed detection of correlation between ^{1}H and single bond connected heteronuclear ^{13}C, thus to provide additional confirmation on the identity of specific compounds. The HSQC spectra were collected in an AVIII 600 MHz Bruker spectrometer with the following parameters: 32768 points and 1024 points (in the ^{1}H and ^{13}C dimensions, respectively), 25 °C, 4 scans, 1.88 s relaxation delay, and acquisition time of 0.26 s.

Data were processed using MestReNova version 11. NMR peaks were assigned based on chemical shifts, peak splitting, and relative intensity.

4.3.4 Quantitation of Glyphosate and Degradation Products Using High-Performance Liquid Chromatography (HPLC)

High-performance liquid chromatography was used to quantify glyphosate and its major degradation products, including glycine and AMPA. Samples collected at selected time points were derivatized prior to the analysis, following published procedures (Ibáñez et al., 2005). Briefly, 1 mL of aqueous sample was adjusted to pH 9.0 by adding 0.12 mL of 5% borate buffer, followed by the addition of 0.12 mL of 12000 mg L^{-1} 9-fluorenylmethylchloroformate (FMOC) in acetonitrile (ACN). Derivatization was carried out at 22±1 °C for about 16 h. The reaction was then stopped by adding 0.015 mL of 6 mol L^{-1} HCl, resulting in a pH of 1.5. After 1 h, derivatized samples were filtered through 0.45 μm syringe filters. The separation and detection of products were performed on a Dionex ICS-5000 single pump, AS-AP sampler, and ICS-5000 detector/chromatography module (Thermo Scientific) using an Acclaim^{TM} 120, C18 column (2.1×250 mm) under a gradient eluent mode. The gradient used was 5 mmol L^{-1} HAc/NH_4Ac(pH 4.8)-acetonitrile, in which the percentage of acetonitrile changed with time as follows: 5–75% in 0–42 min, 100% in 42.1–45 min, and 5% in 45.1–55 min. The chromatographic separations were completed in 55 min for each sample. The separated components were detected at 210 nm by Dionex photodiode array (PDA) detector. Pure glyphosate, AMPA, glycine, and sarcosine were also derivatized and analyzed following the same methods, described above, as standards.

The linearity of the method used was evaluated by analyzing the standards in duplicate. The correlation coefficients (r^2) for the standards including glyphosate, AMPA, and glycine for the range of concentration from 5 to 1000 μmol L^{-1} were >0.99, except for sarcosine ($r^2 > 0.97$). The precision of the method used, expressed as relative standard deviation, was within 12%. The limits of detection for glyphosate, AMPA, glycine, and sarcosine in this method were 10, 5, 5 and 5 μmol L^{-1}, respectively.

4.3.5 Density Functional Theory (DFT) Electronic Structure Calculations

Electronic structure calculations were performed to quantify the influence of Mn(IV) complexation on the bond critical point (BCP) properties of the C–N bonds in glyphosate. All geometry optimizations and electron density distributions were performed or obtained with the Gaussian 09 suite of programs (Frisch et al., 2009) using the B3LYP hybrid exchange-correlation functional (Becke, 1993; Lee et al., 1988) and a standard 6-31G(d) all-electron Gaussian basis set (Ditchfield et al., 1971; Hehre et al., 1972; Rassolov et al., 1998). Given the size and composition of the theoretical system employed in this study, the B3LYP/6-31G(d) method represents a reasonable compromise between accuracy and performance. While some previous studies have utilized larger basis sets (Caetano et al., 2012; Purgel et al., 2009), a more compact basis set is warranted in the present study due to the high level of explicitly represented solvent molecules (>100 solvent atoms) included in the computations. The B3LYP functional was chosen following a survey of the literature, which showed this approach to be the main method utilized by previous computational studies of glyphosate (Ali et al., 2005; Caetano et al., 2012; Peixoto et al., 2015; Purgel et al., 2009).

The C–N bond critical point properties were obtained by analyzing the electron density distributions generated from Gaussian 09 within the theory of Atoms in Molecules (AIM) (Bader, 1985; Bader, 1991) as implemented in the AIMAll software suite (Keith, 2017). Two configurations of glyphosate were investigated in the absence of manganese; both exhibited a total charge of -2 and differed only by the placement of a proton in association with either the phosphonate or amine moieties. In a third configuration containing Mn(IV), the total system charge was +2, and because of the association of manganese with the amine, the aforementioned proton was placed on the phosphonate group. To determine the optimal spin state of Mn(IV), several preliminary geometry optimizations were performed on Mn(IV)($6H_2O$) in various electronic configurations. The lowest energy solution was taken as the optimal spin state and used in all calculations involving Mn(IV) [i.e. high spin Mn(IV) with three unpaired electrons (spin multiplicity = 4)].

4.4 Results and Discussion

4.4.1 Degradation Kinetics of Glyphosate

The XRD pattern and SEM image (Figure A.4.1) of the synthetic mineral revealed a single-phase hexagonal birnessite, composed of sheets of edge-sharing MnO_6 octahedra (Post and Veblen, 1990), with uniform flower-like morphologies, in concert with turbostratic birnessite (Yin et al., 2014). The specific surface area (SSA) of synthetic birnessite was 41.3±0.3 m^2 g^{-1}. The particle size distribution of birnessite varied within a narrow range (143.4±4.5 nm), thus the separation of aqueous media from the solid mineral phase using 0.10 μm filters was considered appropriate. Additional information about the characterization of this synthetic birnessite (i.e. the

phase identity, purity, SSA, and morphology) was presented in our previous publication (Li and Jaisi, 2015).

Glyphosate degradation was initially rapid but decreased gradually (Figure 4.1). A potential reason for this decreased rate could be the passivation of the birnessite surface, which may be attributed to the sorption of glyphosate and its degradation products (e.g. AMPA and orthophosphate) at reactive surface sites passivating the reaction. In the experiment with 3000 μmol L^{-1} glyphosate in 5 g L^{-1} birnessite (GB3000, Table 4.1), more than 80% of glyphosate degraded to form primary amines (the sum of AMPA and glycine), which were released into the aqueous solution (Figures 4.1 and 4.2) with sorbed primary amines limited to 3%. The solution chemistry results showed that ~70% of original P was transformed into orthophosphate within 24 h and the fraction of orthophosphate retained in residual solid-phase minerals was very small and limited to 7% at the conclusion of the experiments. When the concentrations of glyphosate and birnessite changed (GB300 and GB150, Table 4.1), the degradation kinetics were similar overall (Figure A.4.2) with glycine as a dominant product (Figure A.4.3). Control experiments verified that glyphosate was stable under the experimental conditions. These results indicated that the degradation of glyphosate by birnessite was highly efficient. The higher rate and extent of primary amines (sum of glycine, AMPA and methylamine) compared to that of orthophosphate production indicated either faster formation and/or slower breakdown of primary amines than orthophosphate. The higher rate of glycine production compared to AMPA (Figures 4.1 and 4.2) indicated that the glycine pathway is more dominant than the AMPA pathway. This is particularly noteworthy because the longer half-life of AMPA, ~50 h under our experimental conditions (Li et

al., 2016) and about 24 times higher than that of glyphosate (i.e., 2.1 h), should have allowed its continued accumulation over time.

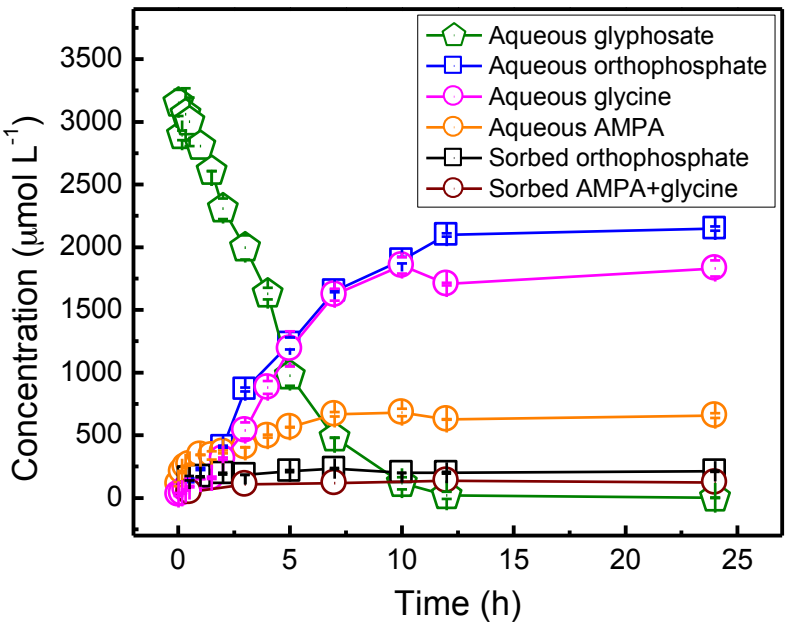

Figure 4.1. Kinetics of glyphosate (3000 μmol L^{-1}) degradation by birnessite (5 g L^{-1}). No measurable sorbed glyphosate or sarcosine were detected on the solid phase.

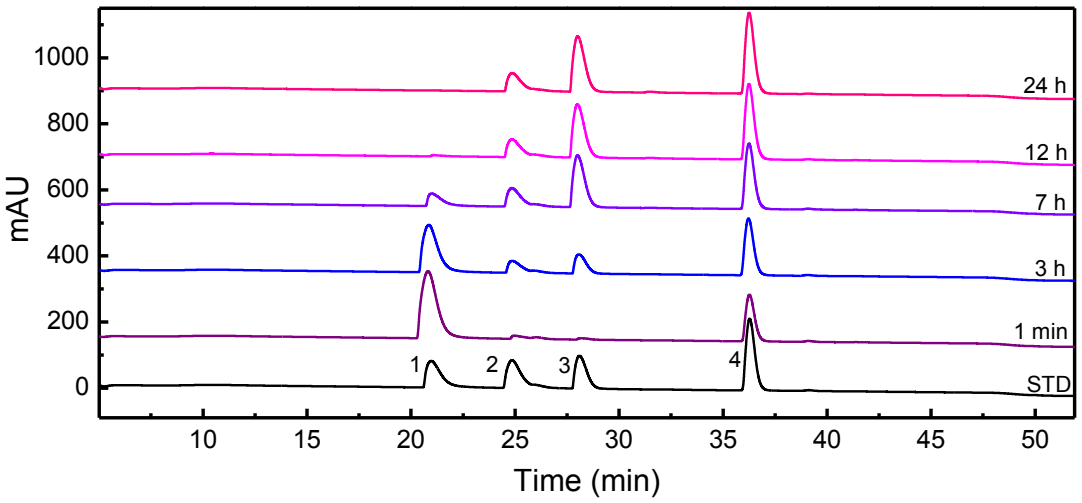

Figure 4.2. High-performance liquid chromatography (HPLC) results of aqueous degradation products of glyphosate, with glyphosate:birnessite ratio of 3000 μmol L^{-1}:5 g L^{-1}. Peaks are FMOC derivatized glyphosate (1), AMPA (2), and glycine (3). The fourth peak is for unreacted FMOC, the derivatization reagent. STD represents for mixture of standards. No sarcosine was detected in either aqueous or solid phases.

4.4.2 Identification of Glyphosate Degradation Products by Using NMR Spectroscopy

The ^{1}H, ^{13}C, and ^{31}P NMR spectra of sub-samples collected at selected time points in the GB3000 experiment demonstrated the temporal changes in compositions and concentrations of degradation products (Figure 4.3). Pure glyphosate and its common intermediate products were measured separately as reference standards under identical conditions to facilitate accurate peak assignments and product identifications. Detailed chemical shifts for these standards are provided in Table A.4.1. After 12 h of reaction, negligible glyphosate was detected in ^{1}H, ^{13}C, and ^{31}P NMR spectra indicating almost complete degradation of glyphosate. This result was also consistent

with the kinetics of glyphosate degradation (Figure 4.1). The ^{1}H and ^{13}C NMR spectra indicated that glycine, with characteristic peaks at ~3.4 (singlet) and ~41.0 (singlet) ppm, respectively, was the major product of glyphosate degradation (Figure 4.3a, b). The presence of AMPA, one of the common degradation products during biotic degradation (Franz et al., 1997; Rueppel et al., 1977), was identified by ^{1}H and ^{31}P NMR spectra with chemical shifts at ~2.8 (doublet) and ~9.0 (singlet) ppm, respectively (Figure 4.3a, c). The amount of AMPA, however, was much less than glycine based on ^{1}H and ^{13}C relative peak intensity, which was consistent with quantitation results from HPLC (Figure 4.1, 4.2). Formaldehyde (hydrated to form methylene glycol) was detected as a major product together with its oxidation product, formic acid (Figure 4.3a, b). The hydration of formaldehyde (HCHO): [$HCHO + H_2O \rightleftharpoons HOCH_2OH$] in liquid media leaves a very low concentration of the unhydrated species (Winkelman et al., 2002; Zavitsas et al., 1970). However, the chemical shifts of the hydrated formaldehyde are distinct from other products, which still validates the formation of formaldehyde. Please note that the polymerization of HCHO [$nHOCH_2OH \rightleftharpoons HO(CH_2O)_nH + (n\text{-}1)H_2O$] is only significant above 1 mol L^{-1}, much higher than the range of concentrations (μmol L^{-1}) in this study (Zavitsas et al., 1970). Therefore, the effect of HCHO polymerization during NMR analysis is not anticipated. A persistent NMR peak of hydrated formaldehyde at and after 3 h of experimentation further suggested the continued formation of formaldehyde during the mid–and–late stages of glyphosate degradation.

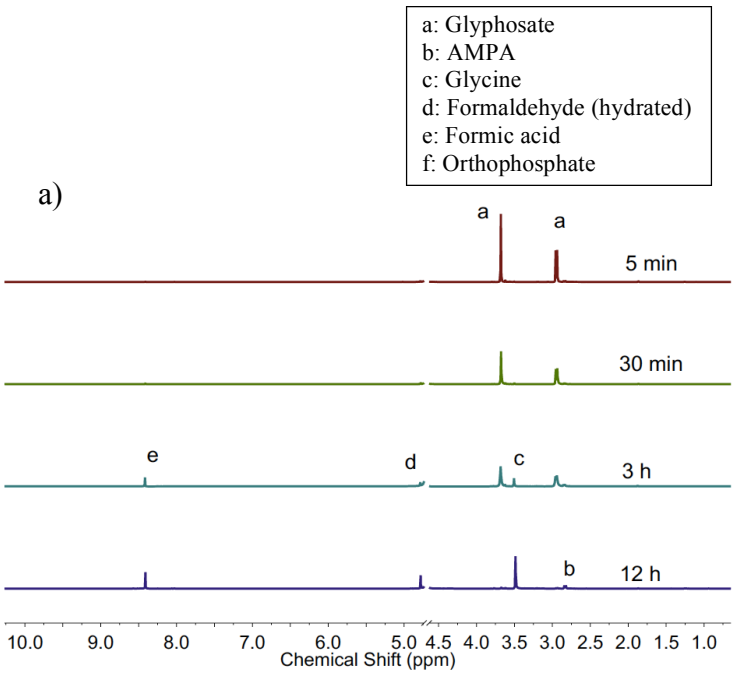
a: Glyphosate
b: AMPA
c: Glycine
d: Formaldehyde (hydrated)
e: Formic acid
f: Orthophosphate
a)
a
a
5 min
30 min
e
d
c
3 h
b
12 h
10.0 9.0 8.0 7.0 6.0 5.0 4.5 4.0 3.5 3.0 2.5 2.0 1.5 1.0
Chemical Shift (ppm)

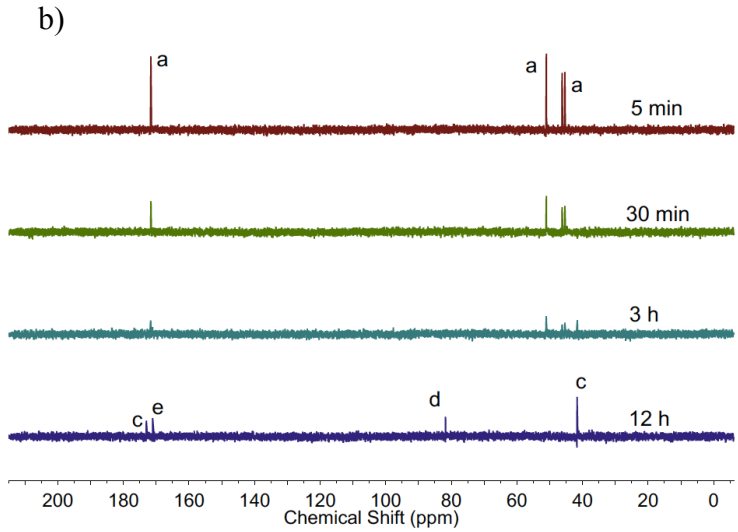
b)
a
a
a
5 min
30 min
3 h
c
d
e
c
12 h
200 180 160 140 120 100 80 60 40 20 0
Chemical Shift (ppm)

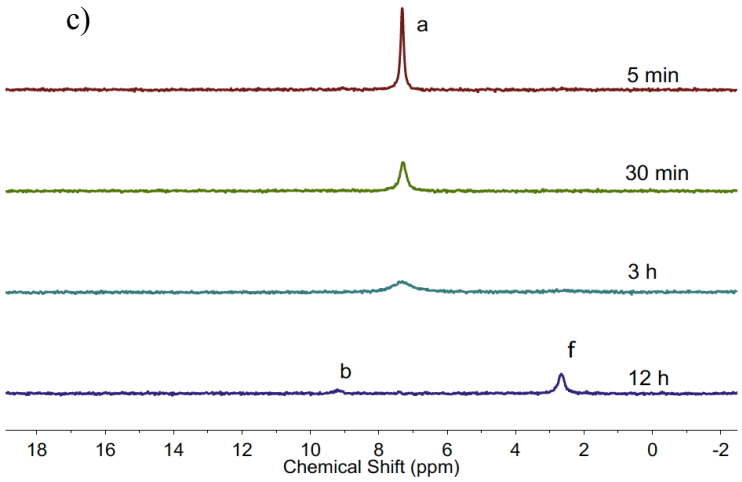

Figure 4.3. Nuclear magnetic resonance (NMR) spectra of degradation products of glyphosate: (a) ^{1}H, (b) ^{13}C, and (c) ^{31}P spectra, with glyphosate (3000 μmol L^{-1}):birnessite (5 g L^{-1}) at pH 7.00±0.05. Peak labels correspond to glyphosate (a), AMPA (b), glycine (c), formaldehyde (hydrated) (d), formic acid (e), and orthophosphate (f).

The composition of the degradation products generated under different concentrations of glyphosate or birnessite (GB300 and GB150) was generally similar, with glycine, AMPA, formic acid, and formaldehyde as major products (Figure A.4.3a, b). At the later stages of the experiment, as well as for those experiments with low initial glyphosate concentrations (GB300 and GB150), the intensity of representative doublet peaks of AMPA appeared in the ^{1}H NMR spectra, however, was too low for its presence to be confirmed reliably. Thus a positional ^{13}C-labeled glyphosate, on the third C atom counting from the carboxyl moiety in the molecule, was utilized in order to enhance the ^{13}C NMR peak intensity. The ^{13}C NMR spectra showed enhanced characteristic doublet peaks representing the third C (3-C) in glyphosate and AMPA

due to isotope labeling, thus confirming the generation of AMPA during glyphosate degradation. However, the amount of generated AMPA was still low in all cases.

To further validate the presence of other less commonly reported products such as formaldehyde, the 2-D NMR spectra for samples at the conclusion of experiments (GB3000) were collected and shown in Figure 4.4. The singlet peak at 4.71 ppm in ^{1}H NMR coupled with another singlet peak at 81.74 ppm in ^{13}C NMR indicated a direct single-bond connection between H and C. Similarly, the singlet peak at 4.86 ppm in ^{1}H NMR coupled with another singlet peak at 81.74 ppm in ^{13}C NMR in the GB300 experiment (Figure A.4.7). These results further confirmed the presence of hydrated formaldehyde in both experiments. In addition to these NMR spectra, the presence of formaldehyde was further validated using the Nash assay method. Since formaldehyde readily oxidizes into carbon dioxide in the presence of air, sunlight, or microorganisms, and should have oxidized in our aerobic experimental setup, its conspicuous persistence throughout our experiments was intriguing and most likely caused by the continuous formation of formaldehyde during the experiment.

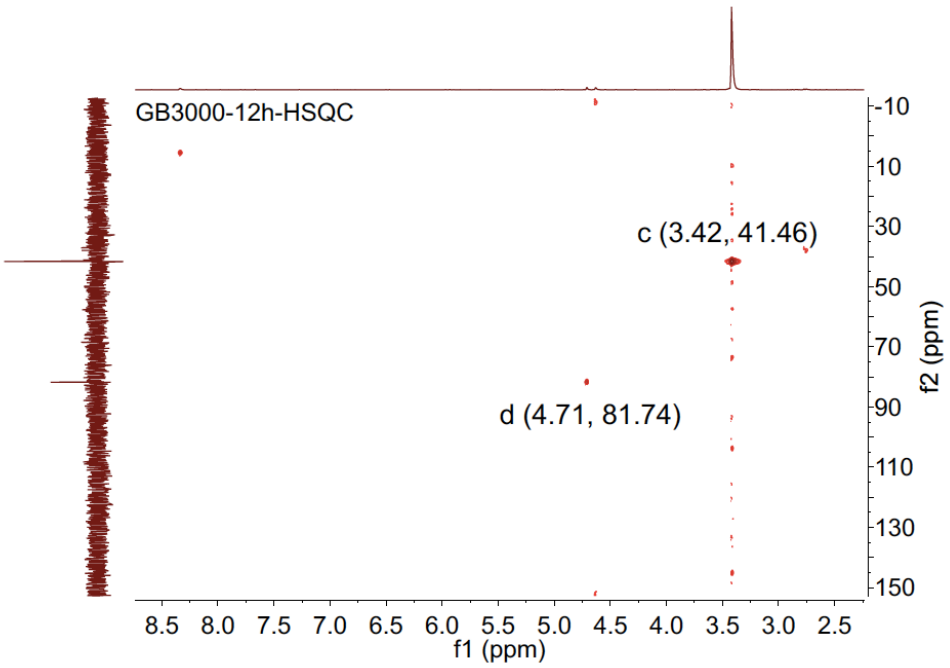

Figure 4.4. Heteronuclear single quantum correlation (HSQC) spectroscopy of degradation products of glyphosate, with glyphosate (3000 μmol L^{-1}):birnessite (5 g L^{-1}), at 12 h. Two axes in f1 and f2 represent ^{1}H and ^{13}C nuclei, respectively. Peak labels correspond to glycine (c) and formaldehyde (d).

Summarizing the NMR results from the series of degradation experiments performed, major degradation products identified included glycine, AMPA, formic acid, formaldehyde, and orthophosphate (~2.7 ppm in Figure 4.3c); these findings are consistent with a number of other studies (Barrett and McBride, 2005; Franz et al., 1997; Paudel et al., 2015; Rueppel et al., 1977; Sviridov et al., 2012). However, some other common degradation products often reported in the literature such as sarcosine, glyoxylic acid, and acetic acid were not detected. It is unclear whether these undetected products formed at levels below the detection limits or if they were otherwise rapidly oxidized after formation. Nonetheless, given that the amount of

generated AMPA was low, the formation of glyoxylic acid, a byproduct of AMPA, was also expected to be low.

4.4.3 Half-Lives of Major Intermediate Products of Glyphosate

Results from separate experiments performed to investigate the half-lives of AMPA, sarcosine, glycine, methylamine, and glyoxylic acid, major potential intermediate products of glyphosate, showed their facile degradation. For example, NMR spectral analyses demonstrated that sarcosine degraded to form glycine as the major degradation product and formic acid and methylamine as minor products (Figure A.4.6). The apparently conspicuous peak intensity of sarcosine in NMR spectra confirmed that a certain amount of sarcosine remained after 24 h of reaction, which was further validated quantitatively by HPLC results (Figures A.4.4, A.4.5). The calculated half-life of sarcosine was ~13.6 h (Figure A.4.4). Similarly, glyoxylic acid was readily degraded by birnessite (half–life < 1 h) to generate formic acid (Figure A.4.8c). AMPA has a much longer (~50 h) half-life (Li et al., 2016). The other two important primary amines, glycine and methylamine, were not degraded by birnessite within 24 h (Figure A.4.8a, b).

4.4.4 Sarcosine Is Not A Necessary Intermediate Product

Sarcosine was previously recognized as an intermediate product of glyphosate degradation; it forms as a consequence of the C–P bond dissociation, and subsequently acts as a precursor to glycine (Barrett and McBride, 2005; Sviridov et al., 2015). Intriguingly, this compound was not detected in any of the NMR spectra or HPLC chromatograms obtained from the suite of experiments performed in this study. Please note also that the presence of sarcosine was reported to be at or below detection in a

number of previous studies (Barrett and McBride, 2005; Jacob et al., 1985; Muneer and Boxall, 2008; Rueppel et al., 1977; Sviridov et al., 2012). More often, the absence of sarcosine was attributed to its presumably rapid degradation rate (Barrett and McBride, 2005). To ensure that the absence of sarcosine in our experiments is not due to its rapid oxidation, we chose to further examine the kinetics of sarcosine degradation. We found that the half-life of sarcosine under the present experimental conditions was 13.6 h (Figure A.4.4). This time is much longer than the sampling intervals employed in our experimental protocols. Consequently, if we assume that glycine is the sole degradation product of sarcosine, the amount of sarcosine in our experiments should have been much higher than that of glycine, which is inconsistent with our observations. Therefore, the absence of sarcosine in our experiments does not appear to be due to its rapid degradation rate.

In light of results discussed above, we have pursued alternative explanations for the absence of sarcosine in our experiments. One of the reasons could be the adsorption of sarcosine onto the birnessite surface, causing no or low (below detection limits) sarcosine concentrations in solution. The pKa values of sarcosine and glycine, analogous in molecular structures, are similar: 2.3 and 10.1 for sarcosine and 2.4 and 9.7 for glycine (Leussing and Hanna, 1966). Thus, at our experimental pH (7.00±0.05), both molecules should have a zwitterionic character with a positive charge on the –NH functional group and a negative charge on the –COOH moiety. Therefore, the adsorption behavior of these two compounds on birnessite is expected to be reasonably similar. Our separate sarcosine degradation experiment showed sarcosine remained almost entirely in the solution. Given that a high amount of glycine was released into the solution and hence was detected in NMR spectra, sarcosine, if formed,

should also have been present in the solution. Additional quantitation analyses using HPLC did not find any sorbed or aqueous phase sarcosine during glyphosate degradation (Figures 4.1 and 4.2).

On the basis of the series of supporting and refuting evidence listed above, it is reasonable to conclude that sarcosine did not form during the abiotic degradation of glyphosate by birnessite. This implies that the first step of glyphosate degradation does not have to involve the C–P bond cleavage or sarcosine formation. Furthermore, the preferential cleavage of the C–N bond towards the N–C–P structure and the direct formation of glycine is also supported by DFT results (see below). These lines of evidence provide a reasonable explanation for a switch-circuited sarcosine degradation pathway among the two common pathways addressed in our previous study (Jaisi et al., 2016).

4.4.5 Potential for Preferred C−N Bond Cleavage: DFT Results

At circumneutral pH, the glyphosate zwitterion oscillates between two primary states in which a proton either resides on the phosphonate group as $–PO_2OH^-$ or on the amine as $–NH_2^+$ (Figure 4.5). Therefore, we first evaluated the influence of the proton position on the BCP properties of the C–N bonds. As shown in Table 4.2, the position of the proton affected each of these bonds differently. When the proton transferred to the amine, both C–N bond lengths increased, with the phosphonate-associated bond being the most perturbed. Correspondingly, the concentration of the electron density also decreased at the bond critical points, as did the value of the Laplacian of the electron density, which indicated that the charge in the BCP region was locally depleted in the $–NH_2^+$ state relative to the $–PO_2OH$ state. As with the bond length, the

density and Laplacian values were most affected in the C–N bond adjacent to the phosphonate group.

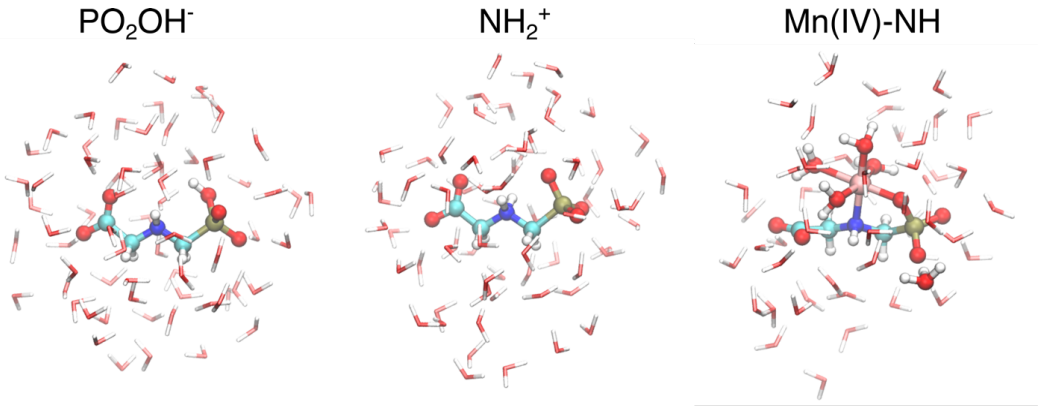

Figure 4.5. Minimum energy structures of glyphosate in two of its zwitterionic states (i.e. PO_2OH^- and NH_2^+) and in the presence of manganese (Mn(IV)–NH) as predicted by DFT. An analysis of the bond critical point properties of the C–N bonds (see Table 4.2) indicates that these bonds are similarly perturbed by the transfer of a proton from the phosphonate to the amine as by Mn(IV) complexation. In both cases the phosphonate adjacent C–N bond is the most affected. Although the effects are similar, the zwitterionic NH_2^+ state is presumably much shorter lived than the manganese complex.

To assess the influence of Mn(IV) on these bonds, a Mn(IV) atom was added adjacent to the amine group in the $–PO_2OH^-$ state, resulting in the formation of a Mn(IV)–NH bonded interaction. During the structural relaxation, the proton transferred from the phosphonate group into solution, forming an H_3O^+ ion. The influence of the bound manganese on the C–N bonds was analogous to the effect observed with the proton that was transferred from the $–PO_2OH$ state to form $–NH_2^+$. That is, the C–N bond lengths increased and the electron density and Laplacian values

at the BCP decreased, all to a greater degree on the phosphonate side of the molecule (Table 4.2).

Table 4.2. Calculated bond critical point (CBP) properties and equilibrium C–N bond distances for the configurations shown in Figure 4.5. The symbols C–N (P) and C–N (C) indicate that the bond is proximal to the phosphonate and carbonate moieties in glyphosate, respectively.

PO_2OH^-			
	$\rho\ (e/a_0^3)$	$\nabla^2(\rho)\ (e/a_0^5)$	$r_{C\text{-}N}$ (Å)
C–N (P)	0.264	-0.721	1.466
C–N (C)	0.266	-0.744	1.465
NH_2^+			
	$\rho\ (e/a_0^3)$	$\nabla^2(\rho)\ (e/a_0^5)$	$r_{C\text{-}N}$ (Å)
C–N (P)	0.234	-0.549	1.500
C–N (C)	0.248	-0.658	1.490
Mn(IV)–NH			
	$\rho\ (e/a_0^3)$	$\nabla^2(\rho)\ (e/a_0^5)$	$r_{C\text{-}N}$ (Å)
C–N (P)	0.238	-0.579	1.499
C–N (C)	0.250	-0.664	1.486

Calculations used above did not directly probe the C–N bond breaking events that would lead to the formation of glycine or AMPA. But the BCP analysis did allow us to assess which regions of the molecule were most influenced by manganese complexation. These results indicated that the C–N bond adjacent to the phosphonate group was most affected, which in light of the experimental results presented above, suggests that the presence of Mn(IV) may facilitate glycine formation directly from glyphosate. Given that the observed changes in the critical point properties of the –NH_2^+ and Mn(IV)–NH states were similar relative to the –PO_2OH state it could be assumed that the phosphonate adjacent C–N bond was equally susceptible to dissociation in either case; however, given that the lifetime of the doubly protonated

state is likely to be very short because of its zwitterionic character compared to the lifetime of a glyphosate molecule adsorbed on a manganese oxide, the potential for Mn complexation to bias the decomposition pathway towards glycine would presumably be much greater.

4.4.6 The Glycine Pathway of Glyphosate Degradation by Birnessite

The two commonly recognized degradation pathways of glyphosate are the sarcosine and AMPA pathways, which are initiated via the C–N and C–P bond cleavage, respectively (Franz et al., 1997; Szekacs and Darvas, 2012). The proportions of orthophosphate, primary amines, and other products generated in the two major pathways are distinct; however, the explicit contribution of each pathway is obscured by the various rates of formation and degradation of intermediate products. Based on the HPLC and NMR results in this study, we observed glycine as the most significant product in contrast to past studies in which AMPA was the dominant product (Barrett and McBride, 2005; Franz et al., 1997; Sviridov et al., 2015; Szekacs and Darvas, 2012). The relative ratio of glycine:AMPA, based on the peak area representing the –CH_2 moieties of glycine and AMPA in ^{1}H NMR spectra (Figure 4.3a) and concentrations in HPLC chromatograms (Figures 4.1 and 4.2), was about 3:1. The limited amount of AMPA generated in this study could be explained as a result of the suppression of the AMPA pathway of degradation. Once formed, however, AMPA could not undergo rapid degradation because of its long half-life (~50 h) under experimental conditions (Li et al., 2016). This means that the concentrations of orthophosphate derived from AMPA degradation should also be low. These lines of reasoning suggested that the majority of orthophosphate should be derived from the glycine pathway. In the glycine pathway, the C–N bond cleavage at the N–C–P

position in the glyphosate molecule also released a P containing compound, which could further be degraded to orthophosphate. The identification of this compound in our experimental data has remained elusive [see below on possible product, methylphosphonic acid (CH_3–PO_3H_2)], however, the direct release of orthophosphate following the C–P bond cleavage at the N–C–P position seems unlikely, as sarcosine and orthophosphate would both be observed as products, contrary to our experimental observations.

The formation and preference of intermediate products can be discussed from the redox properties of Mn-oxide. Birnessite consists of multi-valence Mn, varying from +2 to +4 but dominantly as +4. The measured average oxidation state of the synthetic birnessite used in this study was 3.8, suggesting its strong oxidizing capability. The C–N bond of glyphosate becomes more vulnerable, after forming a Mn–N bond (see DFT results above), due to the changes in the electron density distribution (Jaisi et al., 2016). A similar mechanism was proposed in studies on the oxidation of nitrilotrismethylene-phosphonic acid, in which the C–N bond cleavage took place at the N-centered radical, after electron transferred from N to Mn, followed by the C–P bond cleavage at the C-centered radical (Nowack and Stone, 2003). However, separate tests (MB3000, Table 4.1) performed to test the degradation of methylphosphonic acid (CH_3–PO_3H_2), a potential product formed after the C–N bond cleavage (Muneer and Boxall, 2008) by birnessite, confirmed negative results from both colorimetric and NMR analyses (Figure A.4.9). In contrast, AMPA with one more amine moiety than methylphosphonic acid, was degraded by birnessite (Li et al., 2016). AMPA is positively charged at neutral pH conditions on its NH_2– moiety, which might play a key role in binding to the negatively charged reactive surface sites

of birnessite, and thus facilitates electron transfer and bond cleavage. The lack of methylphosphonic acid degradation and high rate of orthophosphate generation conclusively suggest facile C–P bond cleavage of the unknown intermediate product. Further study on the relative dominance of this pathway in other abiotic degradation conditions is required.

4.4.7 Environmental Implications of Multi-pathway of Glyphosate Degradation

In this study, birnessite catalyzed glyphosate degradation was studied to unravel degradation pathways and their relative contributions by identifying and quantifying intermediate products using NMR spectroscopy, HPLC, and DFT calculations. The results suggested that the dominant abiotic degradation pathway initiates from the C–N bond cleavage and generates glycine, formaldehyde, and orthophosphate, bypassing the formation of sarcosine. A subordinate pathway was the C–N bond cleavage forming AMPA and glyoxylic acid that ultimately degraded to form CO_2, H_2O, NH_3, and orthophosphate. Overall, our results identified a less commonly recognized degradation pathway of glyphosate. As discussed above, the direct glycine formation was observed in one study on biotic degradation but rarely in abiotic cases; however, the glycine pathway has not been recognized.

The relative ratio of glyphosate to birnessite had a minor influence on the selection of degradation pathways. Overall, this research provided supportive evidence that glyphosate primarily degrades at the C–N bond position favoring the direct formation of glycine, which is less toxic than the major product of the other pathway. The natural abundance of Mn in soils varies within the range of 20–3000 mg Kg^{-1}. The Mn content in soil depends largely on the nature of parent materials, cycling processes, and supplemental Mn applied to crop plants and uptake by plants

(Reisenauer, 1988). Though the natural abundance of Mn is low, our results can be a reference for the fate of glyphosate sorbed to negatively charged clay minerals which are abundant in soils across the U.S. Corn Belt and for further investigations on partitioning glyphosate degradation pathways for environmentally friendly products. Potential avenues include applying Mn(IV)-oxides as supplemental Mn, an essential micronutrient to crops, as well as to degrade residual glyphosate.

Acknowledgments

This research was supported by research grants from the National Science Foundation ESPCoR 1301765 and U.S. Department of Agriculture (NIFA award 2017-05362). We would like to acknowledge Advanced Material Characterization Laboratory at the University of Delaware for providing access to XRD, BET, and SEM analyses of birnessite mineral.

REFERENCES

Ali, M.M.N., Kaliannan, P. and Venuvanalingam, P., 2005. Ab initio computational modeling of glyphosate analogs: Conformational perspective. Struct. Chem., 16: 491–506.

Bader, R.F.W., 1985. Atoms in molecules. Acc. Chem. Res., 18: 9–15.

Bader, R.F.W., 1991. A quantum theory of molecular structure and its applications. Chem. Rev., 91: 893–928.

Balbuena, M.S., Tison, L., Hahn, M.L., Greggers, U., Menzel, R. and Farina, W.M., 2015. Effects of sublethal doses of glyphosate on honeybee navigation. J. Exp. Biol., 218: 2799–2805.

Barrett, K.A. and McBride, M.B., 2005. Oxidative degradation of glyphosate and aminomethylphosphonate by manganese oxide. Environ. Sci. Technol., 39: 9223–9228.

Battaglin, W.A., Meyer, M.T., Kuivila, K.M. and Dietze, J.E., 2014. Glyphosate and its degradation product AMPA occur frequently and widely in U.S. soils, surface water, groundwater, and precipitation. J. Am. Water Res. Assoc., 50: 275–290.

Becke, A.D., 1993. Density-functional thermochemistry. 3. The role of exact exchange. J. Chem. Phys., 98: 5648–5652.

Bento, C.P., Yang, X., Gort, G., Xue, S., van Dam, R., Zomer, P., Mol, H.G., Ritsema, C.J. and Geissen, V., 2016. Persistence of glyphosate and aminomethylphosphonic acid in loess soil under different combinations of temperature, soil moisture and light/darkness. Sci. Total Environ., 572: 301–311.

Brown, H.H., 1968. A study of 2,4,6-trinitrobenzenesulfonic acid for automated amino acid chromatography. Clin. Chem., 14: 967–978.

Caetano, M.S., Ramalho, T.C., Botrel, D.F., da Cunha, E.F.F. and de Mello, W.C., 2012. Understanding the inactivation process of organophosphorus herbicides: A DFT study of glyphosate metallic complexes with Zn^{2+}, Ca^{2+}, Mg^{2+}, Cu^{2+}, Co^{3+}, Fe^{3+}, Cr^{3+}, and Al^{3+}. Int. J. Quantum Chem., 112: 2752–2762.

Ditchfield, R., Hehre, W.J. and Pople, J.A., 1971. Self-consistent molecular-orbital methods. 9. Extended Gaussian-type basis for molecular-orbital studies of organic molecules. J. Chem. Phys., 54: 724.

Environmental Protection Agency's Office of Pesticide Programs, 2016. Glyphosate issue paper: Evaluation of carcinogenic potential., EPA-HQ-OPP-2016-0385-0094.

Franz, J.E., Mao, M.K. and Sikorski, J.A., 1997. Glyphosate: A unique global herbicide. American Chemical Society, Washington, DC.

Frisch, M.J., Trucks, G.W., Schlegel, H.B., Scuseria, G.E., Robb, M.A., Cheeseman, J.R., Scalmani, G., Barone, V., Mennucci, B. and Petersson, G.A., 2009. Gaussian 09, rev. D. 01. Gaussian Inc., Wallingford, CT.

Giesy, J.P., Dobson, S. and Solomon, K., 2000. Ecotoxicological risk assessment for Roundup herbicide. Rev. Environ. Contam. Toxicol., 167: 35–120.

Haslam, E., 1974. The Shikimate Pathway. Butterworths, London.

Hehre, W.J., Ditchfield, R. and Pople, J.A., 1972. Self-consistent molecular-orbital methods. 12. Further extensions of Gaussian-type basis sets for use in molecular-orbital studies of organic-molecules. J. Chem. Phys., 56: 2257.

Ibáñez, M., Pozo, Ó.J., Sancho, J.V., López, F.J. and Hernández, F., 2005. Residue determination of glyphosate, glufosinate and aminomethylphosphonic acid in water and soil samples by liquid chromatography coupled to electrospray tandem mass spectrometry. J. Chromatogr. A, 1081: 145–155.

Jacob, G.S., Schaefer, J., Stejskal, E.O. and McKay, R.A., 1985. Solid-state NMR determination of glyphosate metabolism in a *Pseudomonas* sp. J. Biol. Chem., 260: 5899–5905.

Jaisi, D.P., Li, H., Wallace, A.F., Paudel, P., Sun, M., Balakrishna, A. and Lerch, R.N., 2016. Mechanisms of bond cleavage during manganese oxide and UV degradation of glyphosate: Results from phosphate oxygen isotopes and molecular simulations. J. Agric. Food Chem., 64: 8474–8482.

Keith, T.A., 2017. AIMAll Version 17.01.25. TK Gristmill Software, Overl. Park, KS.

Kolpin, D.W., Thurman, E.M., Lee, E.A., Meyer, M.T., Furlong, E.T. and Glassmeyer, S.T., 2006. Urban contributions of glyphosate and its degradate AMPA to streams in the United States. Sci. Total Environ., 354: 191–197.

Kwiatkowska, M., Jarosiewicz, P., Michalowicz, J., Koter-Michalak, M., Huras, B. and Bukowska, B., 2016. The impact of glyphosate, its metabolites and impurities on viability, ATP level and morphological changes in human peripheral blood mononuclear cells. PLoS One, 11: e0156946.

Lee, C.T., Yang, W.T. and Parr, R.G., 1988. Development of the colle-salvetti correlation-energy formula into a functional of the electron-density. Phys. Rev. B, 37: 785–789.

Leussing, D.L. and Hanna, E.M., 1966. Metal ion catalysis in transamination. III. Nickel (II) and Zinc (II) mixed complexes involving pyruvate and various substituted aliphatic amino acids. J. Am. Chem. Soc., 88: 693–696.

Li, H. and Jaisi, D.P., 2015. An isotope labeling technique to investigate atom exchange during phosphate sorption and desorption. Soil Sci. Soc. Am. J., 79: 1340–1351.

Li, H., Joshi, S.R. and Jaisi, D.P., 2016. Degradation and isotope source tracking of glyphosate and aminomethylphosphonic acid. J. Agric. Food Chem., 64: 529–538.

McKenzie, R.M., 1971. The influence of cobalt on the reactivity of manganese dioxide. Aust. J. Soil Res., 9: 55–58.

McVey, K.A., Snapp, I.B., Johnson, M.B., Negga, R., Pressley, A.S. and Fitsanakis, V.A., 2016. Exposure of C. elegans eggs to a glyphosate-containing herbicide leads to abnormal neuronal morphology. Neurotoxicol. Teratol., 55: 23–31.

Muneer, M. and Boxall, C., 2008. Photocatalyzed degradation of a pesticide derivative glyphosate in aqueous suspensions of titanium dioxide. Int. J. Photoenergy, 2008: 1–7.

Murphy, J. and Riley, J.P., 1962. A modified single solution method for the determination of phosphate in natural waters. Anal. Chim. Acta, 27: 31–36.

Nash, T., 1953. The colorimetric estimation of formaldehyde by means of the Hantzsch reaction. Biochem. J., 55: 416–421.

Nowack, B. and Stone, A.T., 2003. Manganese-catalyzed degradation of phosphonic acids. Environ. Chem. Lett., 1: 24–31.

Paudel, P., Negusse, A. and Jaisi, D.P., 2015. Birnessite-catalyzed degradation of glyphosate: A mechanistic study aided by kinetics batch studies and NMR spectroscopy. Soil Sci. Soc. Am. J., 79: 815–825.

Peixoto, M.M., Bauerfeldt, G.F., Herbst, M.H., Pereira, M.S. and da Silva, C.O., 2015. Study of the stepwise deprotonation reactions of glyphosate and the corresponding pKa values in aqueous solution. J. Phys. Chem. A, 119: 5241–5249.

Post, J.E. and Veblen, D.R., 1990. Crystal structure determination of synthetic sodium, magnesium, and potassium birnessite using TEM and the Rietveld method. Am. Mineral., 75: 477–489.

Purgel, M., Takács, Z., Jonsson, C.M., Nagy, L., Andersson, I., Bányai, I., Pápai, I., Persson, P., Sjöberg, S. and Tóth, I., 2009. Glyphosate complexation to aluminium(III). An equilibrium and structural study in solution using potentiometry, multinuclear NMR, ATR-FTIR, ESI-MS and DFT calculations. J. Inorg. Biochem., 103: 1426–1438.

Rassolov, V.A., Pople, J.A., Ratner, M.A. and Windus, T.L., 1998. 6-31G* basis set for atoms K through Zn. J. Chem. Phys., 109: 1223–1229.

Reisenauer, H.M., 1988. Chapter 6. Determination of plant-available soil manganese. Graham, R. D. et al., (eds.), Manganese in soils and plants., Kluwer Academic Publishers. 87–98.

Roy, N.M., Ochs, J., Zambrzycka, E. and Anderson, A., 2016. Glyphosate induces cardiovascular toxicity in Danio rerio. Environ. Toxicol. Pharmacol., 46: 292–300.

Rueppel, M.L., Brightwell, B.B., Schaefer, J. and Marvel, J.T., 1977. Metabolism and degradation of glyphosate in soil and water. J. Agric. Food Chem., 25: 517–528.

Sandy, E.H., Blake, R.E., Chang, S.J., Jun, Y. and Yu, C., 2013. Oxygen isotope signature of UV degradation of glyphosate and phosphonoacetate: Tracing sources and cycling of phosphonates. J. Hazard. Mater., 260: 947–954.

Sviridov, A.V., Shushkova, T.V., Ermakova, I.T., Ivanova, E.V., Epiktetov, D.O. and Leontievsky, A.A., 2015. Microbial degradation of glyphosate herbicides (Review). Appl. Biochem. Microbiol., 51: 188–195.

Sviridov, A.V., Shushkova, T.V., Zelenkova, N.F., Vinokurova, N.G., Morgunov, I.G., Ermakova, I.T. and Leontievsky, A.A., 2012. Distribution of glyphosate and methylphosphonate catabolism systems in soil bacteria *Ochrobactrum anthropi* and *Achromobacter* sp. Appl. Microbiol. Biotechnol., 93: 787–796.

Szekacs, A. and Darvas, B., 2012. Forty years with glyphosate, herbicides—properties, synthesis and control of weeds., Dr. Mohammed Nagib Hasaneen (Ed.), InTech.

United States Geological Survey, 2015. http://water.usgs.gov/nawqa/pnsp/usage/maps/show_map.php?year=2015&map=GLYPHOSATE&hilo=L&disp=Glyphosate. Accessed on 07/16/2018.

Williams, G.M., Kroes, R. and Munro, I.C., 2000. Safety evaluation and risk assessment of the herbicide Roundup and its active ingredient, glyphosate, for humans. Regul. Toxicol. Pharmacol., 31: 117–165.

Winkelman, J.G.M., Voorsinde, O.K., Ottens, M., Beenackers, A.A.C.M. and Janssen, L.P.B.M., 2002. Kinetics and chemical equilibrium of the hydration of formaldehyde. Chem. Eng. Sci., 57: 4067–4076.

Yin, H., Li, H., Wang, Y., Ginder-Vogel, M., Qiu, G., Feng, X.H., Zheng, L. and Liu, F., 2014. Effects of Co and Ni co-doping on the structure and reactivity of hexagonal birnessite. Chem. Geol., 381: 10–20.

Zavitsas, A.A., Coffiner, M., Wiseman, T. and Zavitsas, L.R., 1970. The reversible hydration of formaldehyde. Thermodynamic parameters. J. Phys. Chem., 74: 2746–2750.

Chapter 5

GLYPHOSATE DEGRADATION BY DELTA-MANGANESE OXIDE COATED ON FERRIHYDRITE: COMPETITION OF SORPTION AND DEGRADATION REACTIONS

5.1 Abstract

Ever since its introduction into the herbicidal industry in the 1970s, glyphosate has been a very efficient weed control herbicide and its application has steadily increased, but at the same time its toxicity has been increasingly questioned. In the present research, δ-MnO_2 coated ferrihydrite minerals were synthesized at different Mn/Fe molar ratios and competition of sorption and degradation of glyphosate was analyzed using colorimetric, nuclear magnetic resonance (NMR), and high-performance liquid chromatography (HPLC) methods. Our results showed that the degradation of glyphosate was accomplished exclusively by δ-MnO_2, while both ferrihydrite and δ-MnO_2 played important roles in the sorption processes. The difference, however, is that glyphosate sorbed onto δ-MnO_2 undergoes rapid degradation. Competition between sorption vs. degradation was controlled by the molar ratio of Mn and Fe. For example, at low Mn/Fe ratios (<0.01), the dominant mechanism of glyphosate removal from the aqueous solution was sorption by ferrihydrite, although the extent of removal was low. When the Mn/Fe ratio was higher than 0.01, the degradation reaction dominated in removing glyphosate from solution. Direct C–P bond cleavage to generate glycine was the major degradation pathway and the AMPA (aminomethylphosphonic acid) pathway was minor. Changes

in the Mn/Fe ratios incurred no detectable influence on the preference for either of the two degradation pathways. Present results highlighted the synergistic effects of the two oxides that are commonly present in soils on degradation and sorption of glyphosate and thus reducing the negative impacts of glyphosate in the environment.

5.2 Introduction

Glyphosate (N-phosphonomethyl glycine) was a milestone product developed and introduced into the herbicidal industry by John Franz in the 1970s and has attracted recognition as an effective weed control herbicide (Franz et al., 1997). As a key ingredient in top-selling weed-killer RoundUp®, glyphosate is very effective against a variety of weeds and is commercially produced and consumed in large quantities (~280 million pounds applied in the U.S. in 2015) in agriculture and horticulture (USGS, 2015). The high application rate and hence increasingly frequent occurrence of unreacted glyphosate in soils and water bodies, have led to questions over its safety (Battaglin et al., 2014; Kolpin et al., 2006). In that regard, the International Agency for Research on Cancer (IARC) initially classified glyphosate as "probably carcinogenic to humans (Group 2A)" in 2015 (IARC, 2015). This further raised public concerns about the safety of glyphosate. Thereafter, the U.S. Environmental Protection Agency (USEPA) initiated a reevaluation of the risks posed to humans from exposure to glyphosate. The initial review memorandum in 2017 suggested glyphosate classification as "not likely to be carcinogenic to humans" (USEPA, 2017). Moreover, the toxicity statement made by IARC was questionable due to a flawed and incomplete summary that the initial assessment was majorly on the basis of animal studies and several studies showing no cancer link were ignored or edited out (Kelland, 2017a,b; Tarone, 2018). Given this prevailing uncertainty on the

toxicity of glyphosate and steadily increasing application, studies on the fate of glyphosate are necessary and urgent.

Glyphosate can be strongly immobilized by soil minerals, in particular, Fe- and Al-oxides (Borggaard and Gimsing, 2008; Gimsing et al., 2007). Glyphosate contains three polar functional groups—carboxyl, amino, and phosphonate groups—and the phosphonate group provides the main linkage between glyphosate and the mineral surface (Ahmed et al., 2018; Franz et al., 1997; Sheals et al., 2002). Sorption of glyphosate is significantly influenced by the physicochemical properties of minerals (e.g., specific surface area and surface charge), pH, and competition with orthophosphate for active sorption sites (Barja and Dos Santos Afonso, 2005; Borggaard and Gimsing, 2008; Gimsing et al., 2007). Sorption of glyphosate occurs through ligand exchange or specific sorption, predominantly forming monodentate surface complexation with subordinate bidentate complexation (Sheals et al., 2002; Tribe et al., 2006). Since the major sorption mechanism of orthophosphate is bidentate inner-sphere complexation, orthophosphate should have stronger sorption than glyphosate onto soil minerals (Gimsing et al., 2007). It means glyphosate cannot outcompete orthophosphate during sorption onto mineral surfaces.

Degradation of glyphosate is predominantly accomplished by microorganisms in the environment; however, abiotic degradation by soil minerals (e.g., Mn-oxides) is expected to contribute to some extent (Jaisi et al., 2016; Li et al., 2016; Li et al., 2018; Rueppel et al., 1977; Sviridov et al., 2015). Manganese oxides are the most frequently studied minerals for the degradation of glyphosate (Barrett and McBride, 2005; Li et al., 2018). Manganese (Mn) is an essential micronutrient and one of the seventeen essential elements needed for plant growth and reproduction. The natural abundance

of Mn in soils, however, is low and varies between 0.02 to 3 g Kg^{-1}, among which only a small fraction is plant available, and hence resulting in Mn deficiency in plant growth (IPNI, 2018; Reisenauer, 1988; Shambhavi et al., 2016). Manganese frequently co-exists with iron (Fe), a more abundant element than Mn in many soils (on average by ~100 times higher), with a range of concentration from 20 to 40 g Kg^{-1} (Cornell and Schwertmann, 2003). Among various forms of primary and secondary Fe minerals, poorly ordered Fe minerals (ferrihydrite) is one of the most predominant minerals in soils because (near) neutral pH conditions in soils favor its precipitation (Colombo et al., 2014). With the positive surface charge, ferrihydrite is an ideal candidate to attract negatively charged anions (e.g., orthophosphate) and manganese oxides through electrostatic attraction (Sparks, 2002). Furthermore, Mn supplements (commonly as manganese sulfate) are added in commercial fertilizers to address Mn deficiency in plants, with an annual application rate of 1500–2500 kg Mn Km^{-2} (IPNI, 2018). The applied Mn ions may sorb onto soil minerals or precipitate into secondary minerals; in the latter case, coating onto existing minerals is anticipated.

Coatings on rocks and minerals are ubiquitously present in various environments during rock weathering and soil forming processes and could be driven or catalyzed by anthropogenic activities (Krinsley et al., 2017; Mantha et al., 2012). The first field validation of coatings was reported by Alexander von Humboldt in 1814 when describing the dark coverings by Mn-rich accretion on rocks in the Orinoco River (von Humboldt and Bonpland, 1814). Recently, research interest in organic and inorganic coatings on rocks and minerals, especially at the critical zone—the interfacial system for matter and energy exchange among the pedosphere, atmosphere, lithosphere, and hydrosphere—has increased to decipher biogeochemical processes in

the past and the present (Chorover et al., 2007). Although the mass of coating material, compared with the bulk (core) material is low, the high surface area and exposed surface of the coatings can dramatically change interfacial biogeochemical properties and thereby affect the fate and transport of nutrients and contaminants (Bertsch and Seaman, 1999; Chorover et al., 2007; D'Amore et al., 2004).

In the present research, δ-MnO_2 coated onto ferrihydrite was synthesized at various Fe/Mn molar ratios—relevant to their relative natural abundance. The objectives are to investigate the structural and morphological characteristics of the δ-MnO_2 coated ferrihydrite and to determine the competitive sorption vs. degradation of glyphosate at various Fe/Mn ratios and degradation pathways.

5.3 Materials and Methods

5.3.1 Synthesis of δ-MnO_2 Coated Ferrihydrite (Fe_2O_3/δ-MnO_2)

Ferrihydrite was synthesized by adding about 200 mL of 1 mol L^{-1} NaOH dropwise to 500 mL of 0.1 mol L^{-1} $Fe(NO_3)_3 \cdot 9H_2O$ solution at pH 7–8 under constant stirring (Cornell and Schwertmann, 2003). The precipitates were washed via repeated centrifugation and using deionized (DI) water to remove residual ions, at least five times. The resulting ferrihydrite precipitates were then suspended in NaOH and $KMn^{VII}O_4$ solution. The δ-MnO_2 coatings were prepared by dropwise addition of a selected amount of a $Mn^{II}(NO_3)_2 \cdot 4H_2O$ solution to the ferrihydrite suspension. The Mn^{II}:Mn^{VII}:OH ratio was kept constant at 3:2:4 (Morgan and Stumm, 1964). The initial molar ratio of $Mn(NO_3)_2$:Fe in ferrihydrite was varied at 0.001, 0.005, 0.01, 0.05, 0.1, and 1. Pure δ-MnO_2 mineral was synthesized in parallel for comparison. Following the synthesis, minerals were washed with DI water five times to remove

unreacted reagents and then freeze-dried and gently ground and stored in dark until further experimentation.

5.3.2 Characterization of Fe_2O_3/δ-MnO_2 Minerals

The mineralogy and crystallinity of synthetic Fe_2O_3/δ-MnO_2 minerals were characterized using the X-ray diffraction (XRD) technique on a Bruker D8 Discover Diffractometer. BET (Brunauer-Emmett-Teller) specific surface area (SSA) and Barrett-Joyner-Halenda (BJH) pore size distribution derived from the N_2 adsorption–desorption isotherms on a Micromeritics ASAP 2020 Surface Area and Porosity Analyzer (Georgia, USA). The micromorphology and elemental composition on the surface or ion-beam-cut surface of the synthetic minerals were examined using an Auriga 60 High Resolution Focused Ion Beam-Scanning Electron Microscope (FIB-SEM) equipped with Energy Dispersive Spectroscope (EDS) (Zeiss, Germany). The accelerating voltage of electron high tension (EHT) was set up to 12 kV to determine elemental compositions using the EDS technique. Each mineral was scanned at least at five different points and the average elemental composition was calculated. The average oxidation state (AOS) of Mn in δ-MnO_2 was determined using an oxalic acid-permanganate back-titration method (Lingane and Karplus, 1946).

5.3.3 Synthesis of Cobalt Oxyhydroxide

Cobalt oxyhydroxide [CoO(OH)], a strong oxidant, was synthesized following the published method (Yang et al., 2010) to examine its capability to degrade glyphosate. CoO(OH) was selected as a candidate to degrade glyphosate due to its similar standard redox potential (1.48 eV) to Mn-oxides (Sparks, 2002). In brief, $Co(OH)_2$ was first synthesized by dropwise addition of 50 mL of 0.1 mol L^{-1} NaOH to

80 mL of 0.05 mol L^{-1} $Co(NO_3)_2$ in a 45 °C water bath. The synthetic $Co(OH)_2$ was washed five times using DI water, and then suspended in 40 mL DI water followed by addition of 10 mL of 8 mol L^{-1} NaOH along with 4 mL of 30% H_2O_2 dropwise at 45 °C with continuous stirring to form CoO(OH). After 18 h, the precipitates were washed with DI water five times and dried at 65 °C for 3 d, and were then gently ground. The purity and mineralogy of the synthetic cobalt oxyhydroxide were confirmed through XRD analysis.

5.3.4 Degradation Experiments of Glyphosate

A series of glyphosate (Sigma Aldrich, St Louis, MS) degradation experiments were conducted under pH=7.00±0.05 and at room temperature (22±1 °C) to identify and quantify the intermediate products. Each reaction was performed in 250 mL glass bottle with 1 g L^{-1} of homogeneous mineral suspension (Fe_2O_3/δ-MnO_2 or pure δ-MnO_2 mineral) equilibrated in 10 mmol L^{-1} NaCl under continuous stirring. Glyphosate stock was then added to achieve an initial concentration of 2 mmol L^{-1}. The pH of the reaction was maintained at 7.00 (±0.05) by periodic adjustment using 1 mol L^{-1} NaOH or HNO_3 before and after glyphosate addition. Two sets of control experiments, under the same experimental conditions, were carried out to verify glyphosate stability. One included glyphosate without minerals and the other included glyphosate in ferrihydrite suspension. Each set of experiments was carried out in duplicate and suspension was mixed thoroughly during the experimental time. Subsamples were collected at selected time points based on the results from pilot experiments and past research experience (Li et al., 2016, 2018). Aqueous and solid phases in each aliquot were separated by filtration using 0.10 μm hydrophilic polyethersulfone (PES) filters immediately after sampling. The sorbed compounds on

the solid phase were extracted using 0.5 mol L^{-1} NaOH and adjusted to pH 7 before quantitation.

For the comparative analyses of the role of redox potential on degradation kinetics, additional metal oxides with similar or higher standard redox potential than that of MnO_2 (1.23 eV at 25 °C) were used to degrade glyphosate. These minerals included nickel peroxide (1.70 eV; Sigma Aldrich) and cobalt oxyhydroxide (1.48 eV) (Sparks, 2002). The experimental conditions were the same as that with Mn-oxides: 3 mmol L^{-1} of glyphosate in the presence of 5 g L^{-1} of homogeneous mineral suspensions in 10 mmol L^{-1} NaCl ionic strength under continuous stirring at pH of 7.00 (±0.05).

A UV/Vis spectrophotometer was used to measure the concentration of orthophosphate following the phosphomolybdate blue method (Murphy and Riley, 1962). High-performance liquid chromatography (HPLC) was used to quantify glyphosate and its major degradation products including glycine and AMPA. Before HPLC analysis, derivatization was done according to published procedures (Ibáñez et al., 2005). In brief, 1 mL of aqueous or solid extracts were derivatized by adding 0.12 mL of 12000 mg L^{-1} 9-fluorenylmethyl chloroformate (dissolved in acetonitrile) at pH 9.0 buffered (using 0.12 mL of 5% borate). After 16 h, the derivatization was stopped by adding 0.015 mL of 6 mol L^{-1} HCl and then the solution was filtered through 0.22 μm filters. The separation and detection of products were then carried out on a Dionex Ion Chromatograph (Thermo Fisher Scientific) under a gradient eluent mode. Further, nuclear magnetic resonance (NMR) spectroscopy was also utilized to identify the composition of degradation products. In brief, sub-samples were freeze-dried and then dissolved in pure D_2O. The pH was maintained at 7.0 (±1.0) by adding 1 mol L^{-1}

NaOH or HNO_3. The ^{1}H, ^{13}C, and ^{31}P NMR spectroscopies were obtained in an AVIII 600 MHz Bruker spectrometer at 25°C and data were analyzed using MestReNova software. Details on sample treatment, measurement processes, and acquisition parameters of HPLC and NMR were included in our past publication (Li et al., 2018).

5.4 Results and Discussion

5.4.1 Characterization of δ-MnO_2 Coated Ferrihydrite (Fe_2O_3/δ-MnO_2)

The XRD results of synthetic ferrihydrite, δ-MnO_2, and Fe_2O_3/δ-MnO_2 minerals are shown in Figure 5.1. Ferrihydrite and δ-MnO_2 minerals were pure, single-phase and poorly crystalline, similar to previous publications (Lafferty et al., 2010; Wang et al., 2013). No visible phase change in the crystal structure of ferrihydrite was incurred by the increasing ratios of δ-MnO_2 as the amorphous coating.

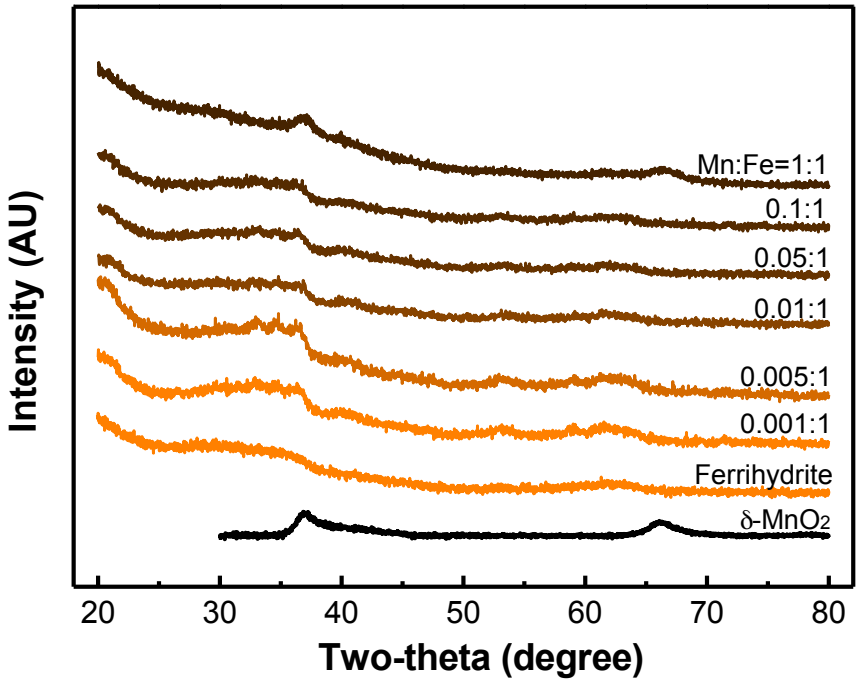

Figure 5.1. The XRD patterns of ferrihydrite, δ-MnO_2, and Fe_2O_3/δ-MnO_2.

The SEM image of synthetic minerals (Figure 5.2a) exhibited the morphology of the minerals, revealing poorly crystalline ferrihydrite particles and the coverage of flowerlike δ-MnO_2 precipitates increased as the Mn/Fe ratio increased. When the Mn/Fe ratio was increased to 1:1, a thick layer of δ-MnO_2 covered the surface of ferrihydrite particles and thereby limited the scope to the underlying structure. Given that one of the objectives of this study was to identify the role of the δ-MnO_2 shell to modify the morphology of the ferrihydrite core, FIB-SEM was utilized to sputter a chunk of aggregate and to reveal the section of the core-shell morphology. Based on the results from the EDS analysis (Figure 5.2b), the synthetic minerals, in general,

consisted of ferrihydrite core and δ-MnO_2 shell (Fe_2O_3/δ-MnO_2). However, the δ-MnO_2 coatings were not homogeneous on the ferrihydrite surface. Therefore, measurements at various particle grains were used to identify the average elemental distribution of Fe and Mn. The average Mn/Fe molar ratios calculated from elemental mapping in SEM analysis for the ranges of experiments run from 0.001 to 1 (Table 5.1) were close to the intended values set in the initial synthesis. Since the initial Mn/Fe was set as the ratio of Mn in $Mn(NO_3)_2$:Fe in ferrihydrite, reduction of $KMnO_4$ as a reactant could add up the Mn proportion and result in higher ratios after synthesis.

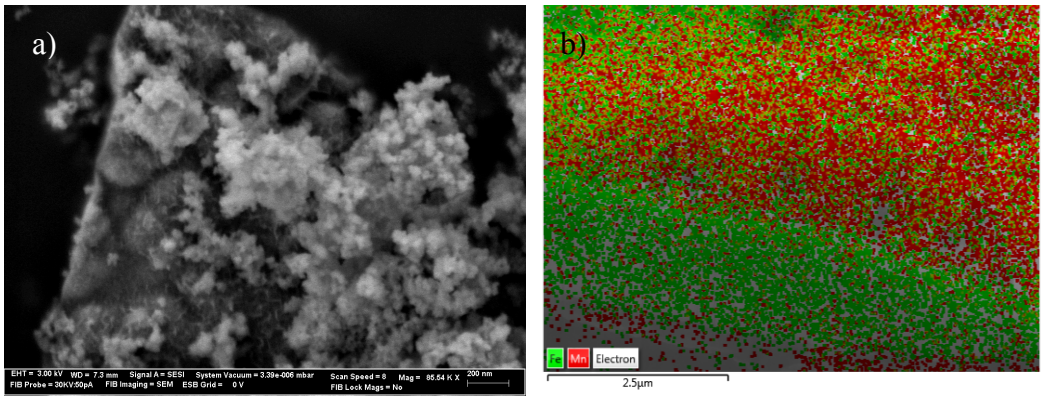

Figure 5.2. Representative SEM-EDS images of (a) Fe_2O_3/δ-MnO_2 (1:1) minerals and (b) elemental mapping after FIB sputtering. The green and red dots represent Fe and Mn elements, respectively. Figure (b) is the sectional view (after FIB sputtering) at the cross section.

The measured specific surface areas (SSA) of synthetic ferrihydrite and δ-MnO_2 were 92.8 and 99.3 m^2 g^{-1}, respectively (Table 5.1). The variable coating of δ-MnO_2 did not significantly influence SSA of ferrihydrite because SSA values varied within a small range (92.6 to 106.6 m^2 g^{-1}). According to the pore size distribution results, the synthetic Fe_2O_3/δ-MnO_2 minerals exhibited a mesoporous structure with

the pore diameter ranging between 2.5 and 4.5 nm. Overall, the large surface area and mesoporous structure of Fe_2O_3/δ-MnO_2 minerals turn them into promising candidates for the sorption and subsequent degradation of glyphosate.

Table 5.1. Characterization of synthetic ferrihydrite, Fe_2O_3/δ-MnO_2 and δ-MnO_2 minerals.

Mineral ID	Experimental Mn/Fe	BET SSA (m^2 g^{-1})	BJH Pore Diameter (nm)	Mn/Fe from SEM Results
Fe_2O_3		92.83	2.54	
Fe_2O_3/δ-MnO_2 (0.001)	0.001	96.69	2.53	0.0009±0.00
Fe_2O_3/δ-MnO_2 (0.005)	0.005	92.67	2.63	0.0072±0.02
Fe_2O_3/δ-MnO_2 (0.01)	0.01	95.96	2.62	0.0043±0.01
Fe_2O_3/δ-MnO_2 (0.05)	0.05	96.04	2.79	0.0252±0.01
Fe_2O_3/δ-MnO_2 (0.1)	0.1	98.22	2.92	0.1950±0.12
Fe_2O_3/δ-MnO_2 (1)	1	106.54	4.45	0.6572±0.30
δ-MnO_2		99.33	6.06	

5.4.2 Glyphosate Degradation by δ-MnO_2 and Fe_2O_3/δ-MnO_2 Minerals

The degradation of glyphosate (3 mmol L^{-1}) by δ-MnO_2 (5 g L^{-1}) was quite rapid with a very short half-life (< 10 min), much shorter than that catalyzed by birnessite (Li et al., 2018). The higher rate of glyphosate degradation by δ-MnO_2 than that by birnessite may be ascribed to a much larger SSA of δ-MnO_2 that facilitated rapid sorption of glyphosate onto active surface sites, which is the requisite reaction for degradation. The kinetics of the degradation reaction mainly depend on three successive and essential steps: (i) transport of glyphosate to the mineral surface; (ii) the adsorption /desorption reactions at the active surface sites (Sparks, 2002); and (iii) the electron transfer to glyphosate or hydrolysis and hence the bond cleavage. Due to the same experimental setup chosen for both experiments involving birnessite and δ-

MnO_2, for example, the same mineral/glyphosate ratio and stirring speed, the diffusion of glyphosate in the homogeneous suspension and the transport of glyphosate to the mineral surfaces and leaving of the degradation products away from them are anticipated to be similar. Therefore, the rate of degradation kinetics was independent of the transport process, and most likely was surface-controlled, means dependent on the active surface sites of the minerals. Different crystal faces of a mineral contain different bonding properties, which is dominated by the layer edge surface sites and vacancies of birnessite and δ-MnO_2 (Drits et al., 1997; Yin et al., 2012). If 60% of SSA (~100 m^2 g^{-1}) is arbitrarily assumed to pertain to the edge surface, similar to the assumption made on birnessite (Li et al., 2016), given the height of each phyllomanganate layer (~0.19 nm) and Mn–Mn distance (~0.287 nm) (Villalobos et al., 2005; Villalobos et al., 2014), we can roughly estimate the approximate active surface site density of δ-MnO_2 equals to (100×10^{18} nm^2 $g^{-1}\times5$ g $L^{-1}\times0.6$)/(0.19 nm×0.287 nm)=55×10^{20} sites L^{-1}, which is 2.5 times of that of birnessite. The initial addition of glyphosate introduced 3×10^{-3} mol $L^{-1}\times6.02\times10^{23}$ molecules $mol^{-1}=18\times10^{20}$ molecules L^{-1} of glyphosate competing and thus occupying only 33% of the total active surface sites on δ-MnO_2. Contrary to the oversaturation of glyphosate on birnessite (>80%) under the same experimental conditions (Li et al., 2016), δ-MnO_2 provided sufficient active surface sites for the sorption of glyphosate. Thus, as per the above-mentioned line of reasoning, excess available active surface sites on δ-MnO_2 accelerated the degradation.

When the concentration of the δ-MnO_2 in the suspension decreased to 1 g L^{-1}, the degradation rate was still high. The evolution of glyphosate degradation products as a function of time is presented in Figure 5.3. Due to decreased mass of the mineral,

the degradation rate was slowed. However, glyphosate still had a very short half-life (1 h) and almost 70% of glyphosate degraded in ~24 h reaction. Glycine was the major degradation product with its concentration ~2.5 times higher than AMPA in the solution at the completion of the glyphosate degradation reaction. The δ-MnO_2 mineral had a strong ability to sorb degradation products, especially AMPA and orthophosphate. For example, more than 200 μmol L^{-1} (~25%) of generated orthophosphate sorbed onto δ-MnO_2 minerals. Similarly, more than 200 μmol L^{-1} of AMPA was immobilized, which is equivalent to ~35% of total formed. Glycine remained primarily in the aqueous solution, with only 7% of 900 μmol L^{-1} of total glycine sorbed onto the δ-MnO_2 surface. The higher sorption tendency of AMPA than glycine might be attributed to the presence of the phosphonate group, a dominant functional group for glyphosate and AMPA, that facilitated sorption onto mineral surfaces via ligand exchange or specific sorption (Barrett and McBride, 2005; Sheals et al., 2002; Tribe et al., 2006).

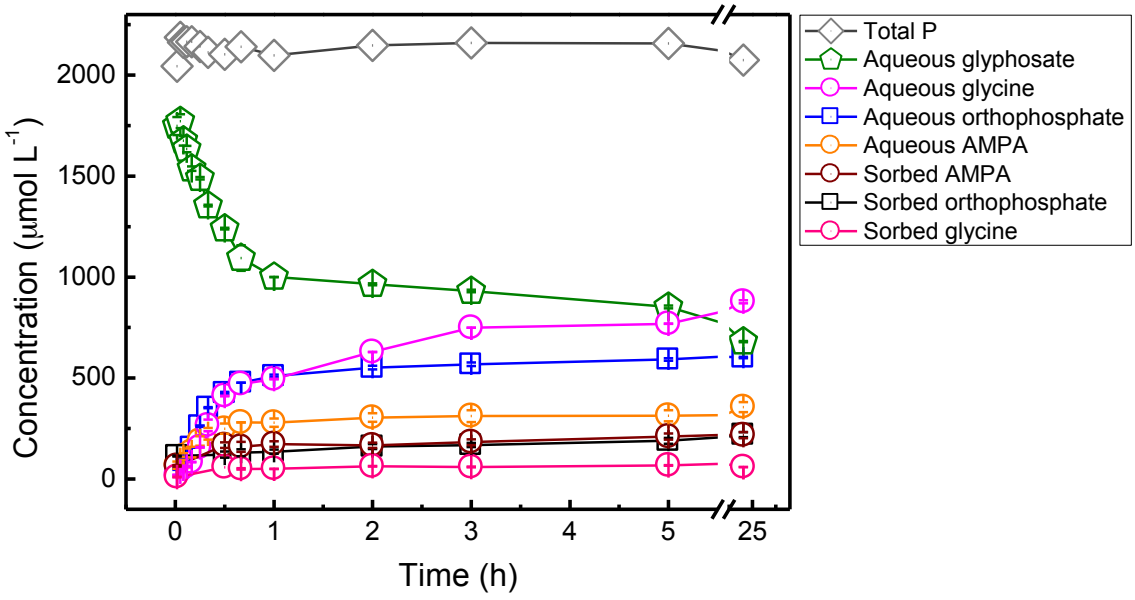

Figure 5.3. Kinetics of glyphosate (2000 μmol L^{-1}) degradation by δ-MnO_2 (1 g L^{-1}). No measurable glyphosate was detected on the solid phase. Total P was the sum of glyphosate, AMPA, and orthophosphate both in aqueous solution and sorbed onto mineral surface.

Separate control experiments run with glyphosate in pure ferrihydrite, goethite, and hematite mineral suspensions confirmed the inability of these common Fe-oxides to degrade glyphosate within the experimental time. This means that the degradation capacity of Fe_2O_3/δ-MnO_2 minerals depended entirely on the content of δ-MnO_2. Present as a coating shell, δ-MnO_2 in Fe_2O_3/δ-MnO_2 minerals was proportionally low. When the Mn/Fe molar ratio was decreased from 1.0 to 0.01, the degradation of glyphosate decreased from 65% to 5% (Figure 5.4). At still lower molar ratios (< 0.01), glyphosate degradation was negligible. However, as mentioned above, the Mn/Fe molar ratio under their natural abundance is approximately 0.01 (Cornell and

Schwertmann, 2003; Reisenauer, 1988). Thus, the results of this study point towards the possibility of limited abiotic degradation by minerals in the environment and hence corroborate some of the assumptions made in the past literature (Franz et al., 1997; Rueppel et al., 1977). The change in the Mn/Fe molar ratio did not influence the composition and relative abundance of major degradation products. In all cases, the product included about 60% glycine and 40% AMPA out of total primary amines (accounting both solution and solid phases), confirming the preferential cleavage of the C–N bond adjacent to the phosphonate group. It means that the glycine pathway is the major pathway of degradation, which is consistent with the degradation of glyphosate by birnessite (Li et al., 2018).

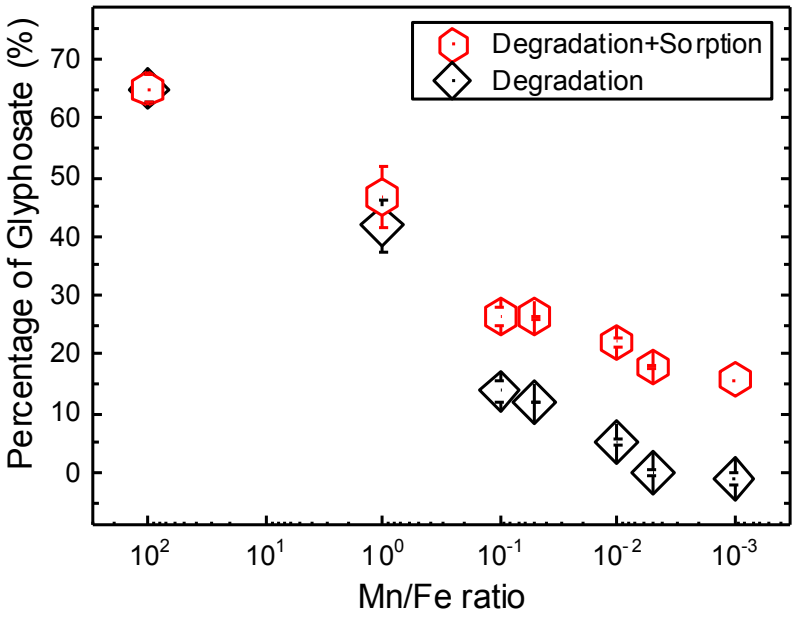

Figure 5.4. Relative roles of sorption to degradation at various Mn/Fe ratios. For the degradation reaction, sorption is the prerequisite process.

5.4.3 Identification of Glyphosate Degradation Products Using Nuclear Magnetic Resonance Method

The ^{1}H and ^{13}C NMR spectra (Figure B.5.1) demonstrated the same composition of intermediate products during glyphosate degradation by δ-MnO_2, Fe_2O_3/δ-MnO_2 minerals, and birnessite that included glycine, AMPA, formic acid, and formaldehyde as major products (Li et al., 2018). The ^{31}P NMR spectra were recorded with decoupled proton signals in order to obtain sharp singlet peaks per unique P nucleus. However, ^{31}P NMR spectra with coupled proton signals provided detailed information on the adjacent proton-coupling environment around the P nucleus. The coupling of the P signals to the protons in the products of glyphosate (3000 μmol L^{-1}) degraded by δ-MnO_2 (5g L^{-1}) is presented in Figure 5.5. The triplet peak at the chemical shift of 9 ppm resulted from the coupling of two H nuclei around the P nucleus and hence validating the structure of glyphosate (HOOC–CH_2–HN–CH_2–PO_3H_2). Similarly, the triplet peak at 12 ppm centered to a P signal is due to coupling to two H nuclei, consistent with the formula of AMPA (H_2N–CH_2–PO_3H_2). The ^{31}P-NMR spectroscopy is highly pH-dependent, which means that a small change in pH could result in more than 1.0 ppm shifts in the P NMR spectrum (Yoza et al., 1994). Thus, the about 2 ppm chemical shifts of the P peaks in this study, compared with our previous publication (Li et al., 2018), could be probably attributed to the difference in solution pH.

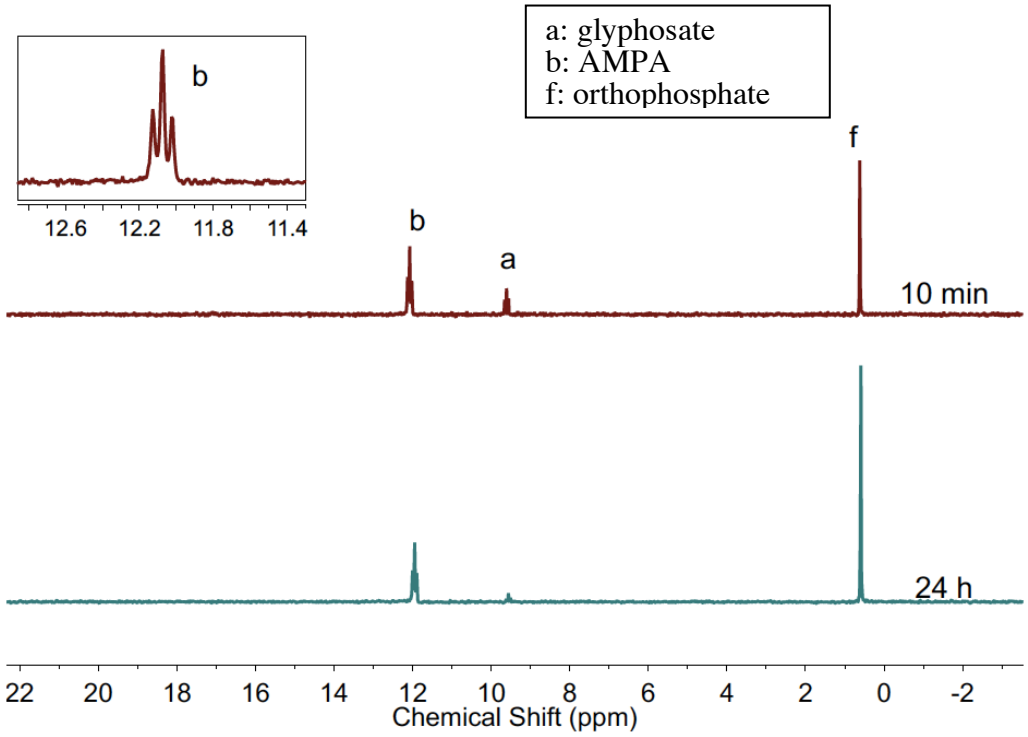

Figure 5.5. The ^{31}P NMR spectra of degradation products of glyphosate (3000 μmol L^{-1}) mediated by δ-MnO_2 mineral (5 g L^{-1}). Peak labels correspond to glyphosate (a), AMPA (b), and orthophosphate (f).

Formation of glycine after the C–N bond cleavage requires coproduction of another P-containing compound unless the simultaneous cleavage at both C–N and C–P bonds in glyphosate molecule. The absence of peaks for P species other than AMPA and orthophosphate in ^{31}P NMR spectra and colorimetric results of a high rate of orthophosphate generation conclusively suggested a facile C–P bond cleavage. However, the identity of an intermediate P bearing organic compound before its eventual breakdown into orthophosphate has remained elusive. In light of the molecular structure of glyphosate and glycine, we speculated the possible formula of the unknown intermediate product could be X–CH_2–PO_3H_2 (X represents H or OH). In

order to confirm rapid degradation as a possible reason and as a way to identify this elusive product, potential candidates including methylphosphonic acid (CH_3–PO_3H_2) and hydroxymethylphosphonic acid ($HOCH_2$–PO_3H_2) were tested for potential degradation by birnessite and δ-MnO_2. Both colorimetric and NMR results confirmed the inability of both Mn-oxides to break down methylphosphonic acid (Li et al., 2018). In contrast, hydroxymethylphosphonic acid was readily degraded by birnessite and δ-MnO_2, with a half-life of degradation of 17 h and 2 h, respectively (Figure 5.6). The half-life time was not short enough to fully consume the replenished hydroxymethylphosphonic acid because 60% of initial glyphosate broke down via the glycine pathway, and glycine and hydroxymethylphosphonic acid should have the same molar concentrations. However, the initial sorption of glyphosate through the phosphonate group could facilitate its rapid degradation by eliminating the initial sorption reaction before degradation. Moreover, the instability of the intermediate product due to electron transfer and unbalanced electron density distribution after the C–N bond cleavage could also assist its faster degradation (Nowack and Stone, 2003). In conclusion, hydroxymethylphosphonic acid could be the possible intermediate product besides glycine and might be rapidly degraded to generate orthophosphate.

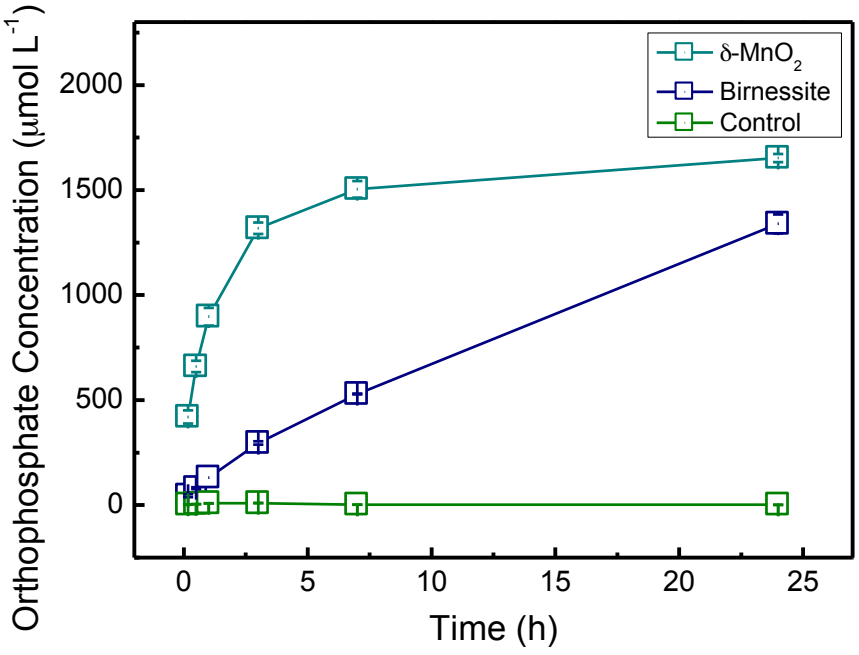

Figure 5.6. Kinetics of hydroxymethylphosphonic acid (3000 μmol L^{-1}) degradation by δ-MnO_2 and birnessite (each at 5 g L^{-1}) measured as the released orthophosphate in aqueous solution.

5.4.4 Significance of Ferrihydrite Immobilizing Glyphosate

In the Fe_2O_3/δ-MnO_2 mineral suspension, glyphosate could be removed from the aqueous solution through both degradation and sorption reactions. The higher the Mn/Fe molar ratio, the higher was the removal of glyphosate, dominantly though degradation (Figure 5.4). Thus, the contribution of ferrihydrite in enhancing the glyphosate removal could be overlooked. Though ferrihydrite was not able to degrade glyphosate (see above), it could still play a subordinate role in removing glyphosate from solution through sorption. When the Mn/Fe molar ratio gradually decreased, the contribution of ferrihydrite to remove glyphosate from solution became more and

more salient. For example, when the Mn/Fe molar ratio was below 0.01, more than 17% (~340 μmol L^{-1}) of initial glyphosate was removed via sorption. This result is within the same order of magnitude with the fitted maximum glyphosate sorption capacity of ferrihydrite (1.85 μmol m^{-2}) using the Langmuir model (Gimsing and Borggaard, 2007).

At experimental neutral pH conditions in this study, glyphosate, orthophosphate, and Mn-oxides are negatively charged; therefore, electrostatic interaction is not favored and thus ligand exchange should dominate. On the contrary, a variety of Fe-oxides are positively charged at circumneutral pH conditions, thus both electrostatic interaction and ligand exchange can synergistically contribute to the sorption of glyphosate to Fe-oxides (Franz et al., 1997; Sparks, 2002). Ferrihydrite, goethite, and hematite are the most common Fe minerals in soils and are important candidates for glyphosate and orthophosphate sorption. The nature and density of surface functional groups—especially hydroxyl group—on Fe minerals control the sorption reactions and the sorption capacity. The Langmuir model fitted sorption capacity of glyphosate has been found to increase in the order: goethite (1.75 μmol m^{-2}) <ferrihydrite (1.85 μmol m^{-2}) <hematite (2.61 μmol m^{-2}) (Gimsing and Borggaard, 2001, 2007). Thus, with larger SSA, ferrihydrate plays a dominant role in the sorption of glyphosate in soils. These Fe minerals contain different numbers of common (competitive) relative to specific (selective) active surface sites with the order as hematite <ferrihydrite <<goethite, suggesting goethite with dominant common sites for orthophosphate sorption while prevailing specific sites on hematite for glyphosate or orthophosphate coordination (Gimsing and Borggaard, 2007). Therefore, glyphosate could bind on the specific sites and compete for the common sites on

ferrihydrite surfaces, resulting in sorption capacity of about 185 μmol L^{-1} of glyphosate under certain experimental conditions (Gimsing and Borggaard, 2007).

The nature of glyphosate sorption is relevant for studying its sorption and further degradation by the minerals. Goethite has been frequently studied as a typical soil mineral for glyphosate sorption to understand the nature of sorption complexation on mineral surfaces. As mentioned above, orthophosphate has stronger sorption ability than glyphosate on common soil minerals (Gimsing et al., 2007). Once degraded, glyphosate competes with its degradation products (AMPA and orthophosphate) for sorption sites on ferrihydrite or δ-MnO_2. However, the sorption of orthophosphate outcompeted glyphosate and this might result in the desorption of some glyphosate restricting further degradation (Gimsing and Borggaard, 2007).

5.4.5 Role of Redox Potential of The Minerals on The Degradation of Glyphosate

Results form series of separate control experiments show that common Fe-oxides such as ferrihydrite, goethite, and hematite are unable to degrade glyphosate. On the contrary, Mn-oxides such as birnessite and δ-MnO_2 are highly efficient in degrading glyphosate. The measured average oxidation state (AOS) of Mn in birnessite and δ-MnO_2 minerals was close to 4 (>3.8), enabling their strong oxidizing capability (Li et al., 2018) compared to the AOS of Fe in common Fe-oxides which was 3.0. Upon degradation of glyphosate, Mn in δ-MnO_2 was reduced to Mn^{2+}. On the other hand, some C in glyphosate was oxidized to generate glycine, and formic acid as intermediate products. Meanwhile, some C in glyphosate was reduced to form AMPA and methylamine.

The rate and extent of electron transfer processes on the mineral–water interfaces depend on the band gap of the metals. Most common Mn- and Fe-oxides are semiconductors with <5 eV band gaps (and thus have potential for excitation); for example, 2.1, and 2.2 eV for birnessite and δ-MnO_2, and hematite, respectively (Shuey, 1975; Pinaud et al., 2011; Gilbert et al., 2009). A smaller band gap would facilitate the electron transfer from Mn/Fe to glyphosate. Compared with birnessite, δ-MnO_2 degraded glyphosate with a shorter half-life and relatively higher degradation capacity, likely due to a larger SSA. On the other hand, relatively higher redox potential of Mn-oxides benefited their essential oxidizing ability in redox reactions. The standard oxidation/reduction potential of Mn(IV)-oxides is 1.23 eV at 25 °C, much higher than common Fe-oxides, for example, 0.67 and 0.66 eV for goethite and hematite, respectively (Sparks, 2002), enabling strong oxidative capability of Mn-oxides.

In order to confirm the role of higher redox potential as the major factor controlling the ability to degrade glyphosate, some other metal oxides with similar or higher standard redox potential than MnO_2 were used to degrade glyphosate, including nickel peroxide (1.70 eV; Sigma Aldrich) and cobalt oxyhydroxide (1.48 eV, synthesized in the laboratory) (Sparks, 2002). Nickel peroxide is a strong oxidizer for numerous organic compounds through a free-radical pathway (George and Balachandran, 1975). Both minerals (5 g L^{-1}) were capable of degrading glyphosate (Figure 5.7), however with a much lower degradation rate than that of Mn-oxides. At 24 h of degradation reactions, only 5% of initial glyphosate was degraded by cobalt oxyhydroxide. Nickel peroxide yielded slightly higher degradation (>16%). Unexpectedly, both rates are much lower than that by birnessite and δ-MnO_2 with almost complete degradation of glyphosate under the same time and experimental

conditions. The rate of the degradation reaction is controlled by several other factors, including the transport of glyphosate to the mineral surface, the sorption/desorption or complexation at the mineral surface, and density of active surface sites (as explained above) (Sparks, 2002). One plausible reason for this incommensurate degradation ability of nickel peroxide could be its lack of hydroxyl functional groups on the surface. The prerequisite step of degradation—glyphosate sorption occurring via ligand exchange with hydroxyl groups on the mineral surface, forming strong metal–O–P bonds (Borggaard and Gimsing, 2008)—is essentially limited in this mineral. On the other hand, with a number of hydroxyl groups present on the surfaces (Post, 1999), Mn-oxides provided many active surface sites for sorption of glyphosate and therefore facilitated its further degradation. Another possible reason for the difference in degradation capacity between nickel dioxide and Mn-oxides might be ascribed to their different degradation mechanisms. Nickel peroxide is a strong oxidizer for organic compounds through a free-radical pathway (George and Balachandran, 1975). While Mn-oxides cleave the C–N bonds after sorption of glyphosate on mineral surface and electron transfer between glyphosate and minerals.

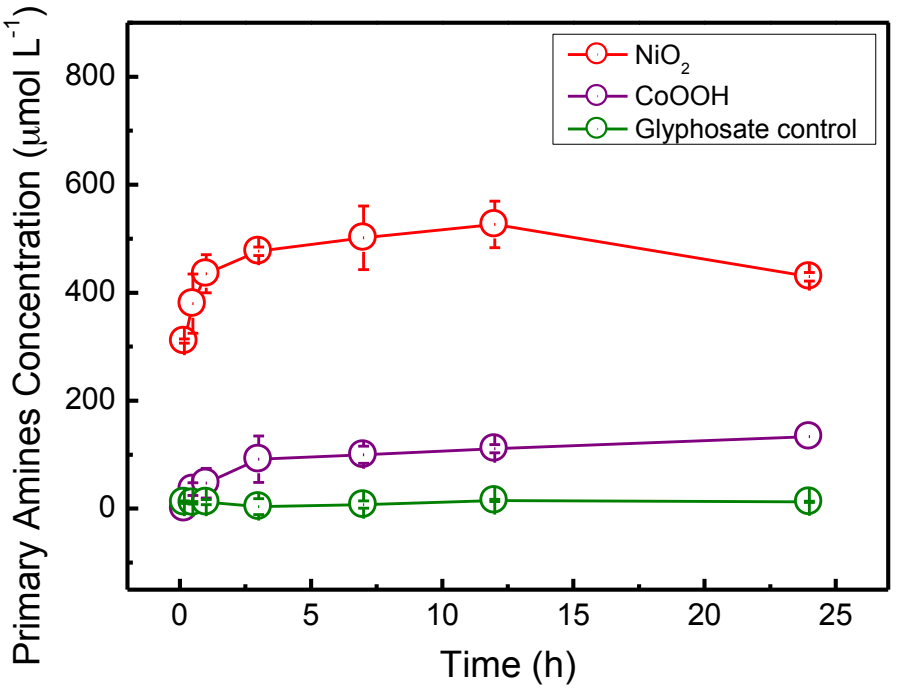

Figure 5.7. Kinetics of glyphosate (3000 μmol L^{-1}) degradation by NiO_2 and CoOOH (5 g L^{-1}) measured as the concentration of primary amines generated.

5.5 Conclusions and Implications

As the major ingredient of the most widely applied herbicides in agricultural, silvicultural and urban areas, glyphosate has attracted special research interest on its toxicity to humans and its fate in the environment. In the present research, a series of Fe_2O_3/δ-MnO_2 core-shell minerals, composed of various Mn/Fe molar ratios, were synthesized to study the glyphosate removal processes. With properties inherited from both ferrihydrite and δ-MnO_2, the synthetic minerals were capable of removing glyphosate from aqueous solutions through both degradation and sorption. The Mn/Fe molar ratio was an important factor controlling sorption vs. degradation of glyphosate

and the switchover was found at 0.01, which is the ratio at their average environmental abundance. Degradation of glyphosate could only be detected when the Mn/Fe ratio exceeds 0.01, it means δ-MnO_2 drives the reaction. It further means in natural soils, negligible abiotic degradation is expected to occur if the results could be extrapolated to the natural environment. The glycine pathway, in which the C–P bond is directly cleaved and bypass sarcosine formation, is the major pathway of degradation. Though no degradation occurred when the Mn/Fe ratio was less than 0.01, minerals sorbed a limited amount of glyphosate. As a common soil mineral, ferrihydrite is an important candidate for glyphosate sorption through electrostatic sorption or ligand exchange, thus stabilizing residual glyphosate and preventing it from leaching to adjacent water bodies. Overall, present results highlighted the synergistic effects of degradation and sorption by ferrihydrite and δ-MnO_2 coating on ferrihydrite surface.

Acknowledgments

This research was supported by a research grant from the U.S. Department of Agriculture (NIFA award 2017-05362). We would like to acknowledge the Advanced Material Characterization Laboratory at the University of Delaware for providing access to XRD, BET, and SEM analyses of synthesized minerals.

REFERENCES

Ahmed, A.A., Leinweber, P. and Kuhn, O., 2018. Unravelling the nature of glyphosate binding to goethte surfaces by ab initio molecular dynamics simulations. Phys. Chem. Chem. Phys., 20: 1531–1539.

Barja, B.C. and Dos Santos Afonso, M., 2005. Aminomethylphosphonic acid and glyphosate adsorption onto goethite: A comparative study. Environ. Sci. Technol., 39: 585–592.

Barrett, K.A. and McBride, M.B., 2005. Oxidative degradation of glyphosate and aminomethylphosphonate by manganese oxide. Environ. Sci. Technol., 39: 9223–9228.

Battaglin, W.A., Meyer, M.T., Kuivila, K.M. and Dietze, J.E., 2014. Glyphosate and its degradation product AMPA occur frequently and widely in U.S. soils, surface water, groundwater, and precipitation. J. Am. Water Res. Assoc., 50: 275–290.

Bertsch, P.M. and Seaman, J.C., 1999. Characterization of complex mineral assemblages: Implications for contaminant transport and environmental remediation. Proc. Natl. Acad. Sci. USA, 96: 3350–3357.

Borggaard, O.K. and Gimsing, A.L., 2008. Fate of glyphosate in soil and the possibility of leaching to ground and surface waters: A review. Pest Manag. Sci., 64: 441–456.

Chorover, J., Kretzschmar, R., Garcia-Pichel, F. and Sparks, D.L., 2007. Soil biogeochemical processes within the Critical Zone. Elements, 3: 321–326.

Colombo, C., Palumbo, G., He, J.Z., Pinton, R. and Cesco, S., 2014. Review on iron availability in soil: Interaction of Fe minerals, plants, and microbes. J. Soil. Sediment., 14: 538–548.

Cornell, R.M. and Schwertmann, U., 2003. The iron oxides: Structure, properties, reactions, occurrences and uses. Wiley-VCH, Weinhein, Germany.

D'Amore, D.V., Stewart, S.R. and Huddleston, J.H., 2004. Saturation, reduction, and the formation of iron–manganese concretions in the Jackson-Frazier wetland, Oregon. Soil Sci. Soc. Am. J., 68: 1012–1022.

Drits, V.A., Silvester, E., Gorshkov, A.I. and Manceau, A., 1997. Structure of synthetic monoclinic Na-rich birnessite and hexagonal birnessite: I. Results from X-ray diffraction and selected-area electron diffraction. Am. Mineral., 82: 946–961.

Franz, J.E., Mao, M.K. and Sikorski, J.A., 1997. Glyphosate: A unique global herbicide. American Chemical Society, Washington, DC.

George, M.V. and Balachandran, K.S., 1975. Nickel peroxide oxidation of organic compounds. Chem. Rev., 75: 491–519.

Gilbert, B., Frandsen, C., Maxey, E.R. and Sherman, D.M., 2009. Band-gap measurements of bulk and nanoscale hematite by soft x-ray spectroscopy. Phys. Rev. B, 79: 035108.

Gimsing, A.L. and Borggaard, O.K., 2007. Phosphate and glyphosate adsorption by hematite and ferrihydrite and comparison with other variable-charge minerals. Clays Clay Miner., 55: 108–114.

Gimsing, A.L. and Borggard, O.K., 2001. Effect of KCl and $CaCl_2$ as background electrolytes on the competitive adsorption of glyphosate and phosphate on goethite. Clays Clay Miner., 49: 270–275.

Gimsing, A.L., Szilas, C. and Borggaard, O.K., 2007. Sorption of glyphosate and phosphate by variable-charge tropical soils from Tanzania. Geoderma, 138: 127–132.

Ibáñez, M., Pozo, Ó.J., Sancho, J.V., López, F.J. and Hernández, F., 2005. Residue determination of glyphosate, glufosinate and aminomethylphosphonic acid in water and soil samples by liquid chromatography coupled to electrospray tandem mass spectrometry. J. Chromatogr. A, 1081: 145–155.

International Agency for Research on Cancer, 2015. IARC Monographs: Evaluation of five organophosphate insecticides and herbicides., 112.

International Plant Nutrition Institute, 2018. Nutri-Facts: Agronomic fact sheets on crop nutrients—Manganese. IPNI, Georgia, USA. https://www.ipni.net/publication/nutrifacts-na.nsf/0/564D810DB5510ED685257CA70074B8ED/$FILE/NutriFacts-NA-9.pdf. Accessed on 07/16/2018.

Jaisi, D.P., Li, H., Wallace, A.F., Paudel, P., Sun, M., Balakrishna, A. and Lerch, R.N., 2016. Mechanisms of bond cleavage during manganese oxide and UV degradation of glyphosate: Results from phosphate oxygen isotopes and molecular simulations. J. Agric. Food Chem., 64: 8474–8482.

Kelland, K., 2017a. Cancer agency left in the dark over glyphosate evidence. Reuters Investigates: https://www.reuters.com/investigates/special-report/glyphosate-cancer-data/. Accessed on 07/13/2018.

Kelland, K., 2017b. In glyphsate review, WHO cancer agency edited out "non-carcinogenic" findings. Reuters Investigates: https://www.reuters.com/investigates/special-report/who-iarc-glyphosate/. Accessed on 07/13/2018.

Kolpin, D.W., Thurman, E.M., Lee, E.A., Meyer, M.T., Furlong, E.T. and Glassmeyer, S.T., 2006. Urban contributions of glyphosate and its degradate AMPA to streams in the United States. Sci. Total Environ., 354: 191–197.

Krinsley, D.H., DiGregorio, B., Dorn, R.I., Razink, J. and Fisher, R., 2017. Mn-Fe-enhancing budding bacteria in century-old rock varnish, Erie Barge Canal, New York. J. Geol., 125: 317–336.

Lafferty, B.J., Ginder-Vogel, M., Zhu, M., Livi, K.J.T. and Sparks, D.L., 2010. Arsenite oxidation by a poorly crystalline manganese-oxide. 2. Results from X-ray absorption spectroscopy and X-ray diffraction. Environ. Sci. Technol., 44: 8467–8472.

Li, H., Joshi, S.R. and Jaisi, D.P., 2016. Degradation and isotope source tracking of glyphosate and aminomethylphosphonic acid. J. Agric. Food Chem., 64: 529–538.

Li, H., Wallace, A.F., Sun, M., Reardon, P. and Jaisi, D.P., 2018. Degradation of glyphosate by Mn-oxide may bypass sarcosine and form glycine directly after C–N bond cleavage. Environ. Sci. Technol., 52: 1109–1117.

Lingane, J.J. and Karplus, R., 1946. New method for determination of manganese. Ind. Eng. Chem. Anal. Ed., 18: 191–194.

Mantha, N.M., Schindler, M., Murayama, M. and Hochella, M.F., 2012. Silica- and sulfate-bearing rock coatings in smelter areas: Products of chemical weathering and atmospheric pollution. I. Formation and mineralogical composition. Geochim. Cosmochim. Acta, 85: 254–274.

Morgan, J.J. and Stumm, W., 1964. Colloid-chemical properties of manganese dioxide. J. Colloid Sci., 19: 347–359.

Murphy, J. and Riley, J.P., 1962. A modified single solution method for the determination of phosphate in natural waters. Anal. Chim. Acta, 27: 31–36.

Nowack, B. and Stone, A.T., 2003. Manganese-catalyzed degradation of phosphonic acids. Environ. Chem. Lett., 1: 24–31.

Pinaud, B.A., Chen, Z., Abram, D.N. and Jaramillo, T.F., 2011. Thin films of sodium birnessite-type MnO_2: Optical properties, electronic band structure, and solar photoelectrochemistry. J. Phys. Chem. C, 115: 11830–11838.

Post, J.E., 1999. Manganese oxide minerals: Crystal structures and economic and environmental significance. Proc. Natl. Acad. Sci. USA, 96: 3447–3454.

Reisenauer, H.M., 1988. Chapter 6. Determination of plant-available soil manganese. Graham, R. D. et al., (eds.), Manganese in soils and plants., Kluwer Academic Publishers, 87–98.

Rueppel, M.L., Brightwell, B.B., Schaefer, J. and Marvel, J.T., 1977. Metabolism and degradation of glyphosate in soil and water. J. Agric. Food Chem., 25: 517–528.

Shambhavi, S., Padbhushan, R., Beura, K., Sharma, S.P. and Sharma, S.K., 2016. Fractions of manganese in soil under long-term experiment and their contribution to manganese availability and uptake by maize–wheat cropping sequence. Commun. Soil Sci. Plant Anal., 47: 470–486.

Sheals, J., Sjoberg, S. and Persson, P., 2002. Adsorption of glyphosate on goethite: Molecular characterization of surface complexes. Environ. Sci. Technol., 36: 3090–3095.

Shuey, R.T., 1975. Semiconducting ore minerals. Elsevier, Amsterdam.

Sparks, D.L., 2002. Environmental soil chemistry. 2nd Edition. Elsevier. Academic Press, San Diego, CA.

Sviridov, A.V., Shushkova, T.V., Ermakova, I.T., Ivanova, E.V., Epiktetov, D.O. and Leontievsky, A.A., 2015. Microbial degradation of glyphosate herbicides (Review). Appl. Biochem. Microbiol., 51: 188–195.

Tarone, R.E., 2018. On the international agency for research on cancer classification of glyphosate as a probable human carcinogen. Eur. J. Cancer Prev., 27: 82–87.

Tribe, L., Kwon, K.D., Trout, C.C. and Kubicki, J.D., 2006. Molecular orbital theory study on surface complex structures of glyphosate on goethite: Calculation of vibrational frequencies. Environ. Sci. Technol., 40: 3836–3841.

United States Environmental Protection Agency, 2017. Glyphosate. Draft human health risk assessment in support of registration review. Washington, DC, 20460.

United States Geological Survey, 2015. http://water.usgs.gov/nawqa/pnsp/usage/maps/show_map.php?year=2015&map=GLYPHOSATE&hilo=L&disp=Glyphosate. Accessed on 07/16/2018.

Villalobos, M., Bargar, J. and Sposito, G., 2005. Mechanisms of Pb(II) sorption on a biogenic manganese oxide. Environ. Sci. Technol., 39: 569–576.

Villalobos, M., Escobar-Quiroz, I.N. and Salazar-Camacho, C., 2014. The influence of particle size and structure on the sorption and oxidation behavior of birnessite: I. Adsorption of As(V) and oxidation of As(III). Geochim. Cosmochim. Acta, 125: 564–581.

von Humboldt, A. and Bonpland, A., 1814. Personal narrative of travels to the equnoctial regions of the new continent during the years 1799–1804. Longman, Hurst, Rees, Orme and Brown, London. 521 pp.

Wang, X., Liu, F., Tan, W.F., Li, W., Feng, X.H. and Sparks, D.L., 2013. Characteristics of phosphate adsorption-desorption onto ferrihydrite. Soil Sci., 178: 1–11.

Yang, J., Liu, H., Martens, W.N. and Frost, R.L., 2010. Synthesis and characterization of cobalt hydroxide, cobalt oxyhydroxide, and cobalt oxide nanodiscs. J. Phys. Chem. C, 114: 111–119.

Yin, H., Tan, W., Zheng, L., Cui, H., Qiu, G., Liu, F. and Feng, X., 2012. Characterization of Ni-rich hexagonal birnessite and its geochemical effects on aqueous Pb^{2+}/Zn^{2+} and As(III). Geochim. Cosmochim. Acta, 93: 47–62.

Yoza, N., Ueda, N. and Nakashima, S., 1994. pH-dependence of ^{31}P-NMR spectroscopic parameters of monofluorophosphate, phosphate, hypophosphate, phosphonate, phosphinate and their dimers and trimers. Fresenius J. Anal. Chem., 348: 633–638.

Chapter 6

CONCLUSIONS

6.1 Summary

Glyphosate is the reactive component in Roundup® and other herbicides and has wide application in more than 160 countries and for more than 100 crops (Monsanto, 1996). As a consequence, glyphosate and its main metabolite, AMPA, have been frequently reported to be present in soils and other environments (Battaglin et al., 2014; Kolpin et al., 2006). The degradation of glyphosate by soil microorganisms and minerals has received increasing interest proportional to the increase in public concerns on the potential carcinogenicity of glyphosate. In this dissertation research, two common Mn-oxide minerals—birnessite and δ-MnO_2—were studied for their ability to degrade glyphosate. Both minerals rapidly degraded glyphosate with short half-lives, which are ascribed to their high standard redox potential (1.23 eV) due to high Mn average oxidation states (~4). However, the natural abundance of Mn in soils is low, varying within 20–3000 mg Kg^{-1} (Reisenauer, 1988), hence the possibility of Mn-oxides playing a significant role in glyphosate degradation in the environment is very slim. On the other hand, ferrihydrite and other common Fe-(hydro)oxides (e.g., goethite and hematite) were not able to degrade glyphosate. Since Mn-oxides normally coexist with Fe-oxides as coatings, the role of δ-MnO_2 coated ferrihydrite on degradation was further studied. Interestingly, the average Mn/Fe molar ratio in soils (~0.01) (Cornell and Schwertmann, 2003; Reisenauer, 1988) was found to be an important boundary where the switchover of two important reactions

removing glyphosate from solution occurs: at the ratios less than 0.01, negligible glyphosate degradation occurred, but ferrihydrite removed glyphosate from aqueous solution through sorption. When Mn/Fe was greater than 0.01, δ-MnO_2 degraded glyphosate. These results point towards the possibility of limited abiotic degradation of glyphosate by minerals in the environment and hence corroborate some of the speculation made in the literature (Franz et al., 1997; Rueppel et al., 1977). Overall, synergistic effects of Fe- and Mn-oxides that are commonly present in soils are anticipated to play some limited roles in the degradation and sorption of glyphosate. Both processes reduce the amount of dissolved glyphosate and thereby reduce the potential loss to open waters. But the sorption reaction restricts the degradation and increases the half-life of glyphosate causing local increase in the adverse impact.

The biotic degradation of glyphosate mediated by soil microorganisms has been subject to many studies, little is known about the abiotic degradation pathways of glyphosate. In this study, degradation pathways were identified by analyzing the degradation products. In the majority of cases, glyphosate degradation occurred through the glycine pathway, generating glycine, formaldehyde, and orthophosphate. To a minor extent, glyphosate also degraded through the AMPA pathway forming AMPA and glyoxylic acid. These intermediate products ultimately degraded to form CO_2, H_2O, NH_3, and orthophosphate. Interestingly, sarcosine, the commonly recognized precursor to glycine, was not detected in any of the experiments. This result was surprising considering the fact that its half-life (~13.6 h) was greater than the sampling intervals. Moreover, the existence of preferential cleavage of the C–N bond adjacent to the phosphonate group to form glycine directly was also supported by the BCP analysis that this C–N bond was disproportionately affected by the interaction

of glyphosate with Mn(IV). However, AMPA is frequently detected together with glyphosate in the environment (Battaglin et al., 2014), which could mean the AMPA pathway is significant during biotic degradation in soils. In that case, the negative effects of glyphosate are aggravated because AMPA is more toxic and persistent than glyphosate. The outcome of this research suggested that the glycine pathway is the major pathway during abiotic degradation, generating relatively less toxic products and thus being more environmentally friendly. Moreover, Mn-oxides are also capable of efficiently degrading intermediate degradation products (e.g., AMPA, sarcosine, and glyoxylic acid) into inorganic products, further reducing the negative effects of glyphosate. Thus, if the role of Mn-oxides in glyphosate degradation could be enhanced in the natural environment, these findings suggested a potential shift towards more environmentally friendly products.

Developing proxies for source tracking glyphosate and phosphonate compounds requires an accurate understanding of how isotope fractionation is affected by sorption–desorption processes. The results of such studies on four common Fe- and Mn-oxides including goethite, hematite, hausmannite, and birnessite revealed the bond cleavage occurs at the Fe–O(OH) or Mn–O(OH), not at the P–O(OH) bond during sorption and desorption reactions, consistent with past findings on ferrihydrite (Jaisi et al., 2010). This means that the oxygen isotope ratios ($\delta^{18}O_P$) of orthophosphate are preserved by these reactions on soil minerals, enabling the tracking of original phosphorus sources. When glyphosate or AMPA molecules are degraded, however, the regenerated orthophosphate incorporates one external oxygen atom from ambient water and the other three oxygen atoms are inherited from the parent molecules. The $\delta^{18}O_P$ values of orthophosphate derived from all commercial glyphosate products

analyzed were found to be lighter (3.91–9.30 ‰ VSMOW) than most other known sources of orthophosphate (16–24 ‰ VSMOW). Moreover, the isotope fractionation factor, which is essential to connect sources and products, is similar for glyphosate and AMPA. These findings provide a new and unsurpassed tool to track glyphosate and its degradation products in the environment by using naturally abundant isotopes in these compounds.

6.2 Future Research

6.2.1 Isotope Fractionation during Biotic Degradation of Glyphosate

Glyphosate is degraded predominantly by soil microorganisms (Rueppel et al., 1977). A number of bacterial species that have been studied such as *Pseudomonas* sp*., Sinorhizobium meliloti, Ochrobactrum anthropi, and Agrobacterium radiobacter* are found to utilize glyphosate as a source of phosphorus, indicating that they possess C–P lyase to break the C–P bond (Hove-Jensen et al., 2014; Kishore and Jacob, 1987; Parker et al., 1999; Shinabarger and Braymer, 1986; Wackett et al., 1987). However, several attempts at *in vitro* studies of C–P lyase were unsuccessful due to irreversible inactivation after cell disintegration. Only recently, successful *in vitro* activation of C–P lyase was accomplished (Kamat et al., 2011; Zhang and van der Donk, 2012). Therefore, the future research on the mechanism of glyphosate degradation via the C–P bond cleavage pathway is needed to determine degradation products, pathways and more importantly, the isotope fractionation of this enzyme.

The C–P bond cleavage during biotic degradation also requires an external O to be incorporated into each orthophosphate. However, the source of this O atom during biotic degradation and isotope fractionation is not known. In the limited studies

of abiotic reactions, the oxygen isotope fractionation factor is around -11.81(±4.14) ‰. Given recent successful *in vitro* activation of C–P lyase, future studies on isotope fractionation during enzymatic degradation are promising. Research on fractionation during degradation reactions mediated by various enzymes provides a major piece of information. In the event that glyphosate degradation under biotic vs. abiotic routes shows distinct trends of $\delta^{18}O_P$ evolution or fractionation factors, this would be useful for approximating the relative extent as well as contribution of biotic and abiotic cycling.

6.2.2 Development of Multi-Isotope Tool to Track Glyphosate and Its Degradation Products in The Environment

Stable isotope ratios of nutrients, including nitrogen ($\delta^{15}N$), carbon ($\delta^{13}C$) and oxygen ($\delta^{18}O$) in N, C and P compounds have been routinely used as a means to track nutrient sources and cycling (Bohlke and Denver, 1995; Kendall, 1998; Wang et al., 1998). In this present study, uncommonly light $\delta^{18}O_P$ values (3.91–9.30 ‰) found in orthophosphate generated from several commercial glyphosate products indicate that $\delta^{18}O_P$ values can serve as a powerful proxy to distinguish glyphosate-derived orthophosphates from other organophosphorus compounds. A broad range of $\delta^{13}C$ values, varying from -24 to -34‰, has been reported for several commercial glyphosate sources (Kujawinski et al., 2013). The $\delta^{15}N$ values of nitrogen, however, have not been reported in the literature. Accurate measurement of isotopic compositions of each product will require the development of methods on separation and purification of products using HPLC or other methods, which may introduce other challenges. Future studies obtaining a combination of the natural abundance of triple isotopes $\delta^{13}C$, $\delta^{15}N$, and $\delta^{18}O_P$ in glyphosate and its degradation products will allow

further scrutiny of the variation within glyphosate (commercial) sources and discriminate glyphosate-derived products, in the case that the single isotope method is insufficient or analytically challenging.

6.2.3 Site-Specific ^{13}C Analysis of Glyphosate and Intermediate Products Using Isotopic ^{13}C NMR Spectrometry

The compound-specific ^{13}C isotope measurement analyzes the bulk isotopic composition of the whole molecule (if separation of the compound is possible); however, the ^{13}C distribution in glyphosate and its degradation products may not be uniform (Diomande et al., 2015). Therefore, site-specific isotope analysis could be a highly innovative method to investigate the substrate-product relationships by directly measuring the isotope values of target C of specific molecules without the need for prior separation. Site-specific isotopic fractionation studies have been carried out in protons (by analyzing ^{2}H) but less commonly on ^{13}C due to the narrow range of ^{13}C natural isotopic variation, which is about 100 ‰ (Martin et al., 2006). Thus, the site-specific analysis on ^{13}C requires signal-to-noise ratio higher than 500 in order to obtain sufficient analytical precision for quantitative measurement (Diomande et al., 2015). With improved analytical precision of a new generation of instruments, positional isotope analyses of some compounds such as xanthines, caffeine, aspirin, and paracetamol, and the alkaloids nicotine and tropine, have been feasible using ^{13}C NMR methods (Diomande et al., 2015; Romek et al., 2016; Silvestre et al., 2009). This suggests that the site-specific ^{13}C isotope on glyphosate is quite feasible. If successful, this method could provide another powerful proxy to identify and source track glyphosate and its products in the environment.

REFERENCES

Barrett, K.A. and McBride, M.B., 2005. Oxidative degradation of glyphosate and aminomethylphosphonate by manganese oxide. Environ. Sci. Technol., 39: 9223–9228.

Battaglin, W.A., Meyer, M.T., Kuivila, K.M. and Dietze, J.E., 2014. Glyphosate and its degradation product AMPA occur frequently and widely in U.S. soils, surface water, groundwater, and precipitation. J. Am. Water Res. Assoc., 50: 275–290.

Bohlke, J.K. and Denver, J.M., 1995. Combined use of groundwater dating, chemical and isotopic analyses to resolve the history and fate of nitrate contamination in two agricultural watersheds, Atlantic coastal plain, Maryland. Water Resour. Res., 31: 2319–2339.

Cornell, R.M. and Schwertmann, U., 2003. The iron oxides: Structure, properties, reactions, occurrences and uses. Wiley-VCH, Weinhein, Germany.

Diomande, D.G., Martineau, E., Gilbert, A., Nun, P., Murata, A., Yamada, K., Watanabe, N., Tea, I., Robins, R.J., Yoshida, N. and Remaud, G.S., 2015. Position-specific isotope analysis of xanthines: A (13)C nuclear magnetic resonance method to determine the (13)C intramolecular composition at natural abundance. Anal. Chem., 87: 6600–6606.

Franz, J.E., Mao, M.K. and Sikorski, J.A., 1997. Glyphosate: A unique global herbicide. American Chemical Society, Washington, DC.

Hove-Jensen, B., Zechel, D.L. and Jochimsen, B., 2014. Utilization of glyphosate as phosphate source: Biochemistry and genetics of bacterial carbon-phosphorus lyase. Microbiol. Mol. Biol. Rev., 78: 176–197.

Jaisi, D.P., Blake, R.E. and Kukkadapu, R.K., 2010. Fractionation of oxygen isotopes in phosphate during its interactions with iron oxides. Geochim. Cosmochim. Acta, 74: 1309–1319.

Kamat, S.S., Williams, H.J. and Raushel, F.M., 2011. Intermediates in the transformation of phosphonates to phosphate by bacteria. Nature, 480: 570–573.

Kendall, C., 1998. Tracing nitrogen sources and cycles in catchments. In C. Kendall and J. J. McDonnell ed. Isotope tracers in catchment hydrology. Elsevier Science: 519–576.

Kishore, G.M. and Jacob, G.S., 1987. Degradation of glyphosate by *Pseudomonas* sp. PG 2982 via a sarcosine intermediate. J. Biol. Chem., 262: 12164–12168.

Kolpin, D.W., Thurman, E.M., Lee, E.A., Meyer, M.T., Furlong, E.T. and Glassmeyer, S.T., 2006. Urban contributions of glyphosate and its degradate AMPA to streams in the United States. Sci. Total Environ., 354: 191–197.

Kujawinski, D.M., Wolbert, J.B., Zhang, L., Jochmann, M.A., Widory, D., Baran, N. and Schmidt, T.C., 2013. Carbon isotope ratio measurements of glyphosate and AMPA by liquid chromatography coupled to isotope ratio mass spectrometry. Anal. Bioanal. Chem., 405: 2869–2878.

Li, H., Wallace, A.F., Sun, M., Reardon, P. and Jaisi, D.P., 2018. Degradation of glyphosate by Mn-oxide may bypass sarcosine and form glycine directly after C–N bond cleavage. Environ. Sci. Technol., 52: 1109–1117.

Martin, G.J., Martin, M. and Remaud, G.S., 2006. Modern magnetic resonance. Webb, G. A., Ed.; Springer, Berlin. 1647–1658.

Parker, G.F., Higgins, T.P., Hawkes, T. and Robson, R.L., 1999. Rhizobium (Sinorhizobium) meliloti phn genes: Characterization and identification of their protein products. J. Bacteriol., 181: 389–395.

Reisenauer, H.M., 1988. Chapter 6. Determination of plant-available soil manganese. Graham, R. D. et al., (eds.), Manganese in soils and plants, Kluwer Academic Publishers. 87–98.

Romek, K.M., Remaud, G.S., Silvestre, V., Paneth, P. and Robins, R.J., 2016. Non-statistical ^{13}C fractionation distinguishes co-incident and divergent steps in the biosynthesis of the alkaloids nicotine and tropine. J. Biol. Chem., 291: 16620–16629.

Rueppel, M.L., Brightwell, B.B., Schaefer, J. and Marvel, J.T., 1977. Metabolism and degradation of glyphosate in soil and water. J. Agric. Food Chem., 25: 517–528.

Shinabarger, D.L. and Braymer, H.D., 1986. Glyphosate catabolism by *Pseudomonas* sp. Strain PG 2982. J. Bacteriol., 168: 702–707.

Silvestre, V., Maroga Mboula, V., Jouitteau, C., Akoka, S., Robins, R.J. and Remaud, G.S., 2009. Isotopic ^{13}C NMR spectrometry to assess counterfeiting of active pharmaceutical ingredients: Site-specific ^{13}C content of aspirin and paracetamol. J. Pharm. Biomed. Anal., 50: 336–341.

Wackett, L.P., Shames, S.L., Venditti, C.P. and Walsh, C.T., 1987. Bacterial carbon–phosphorus lyase: Products, rates, and regulation of phosphonic and phosphinic acid metabolism. J. Bacteriol., 169: 710–717.

Wang, Z., Fingas, M., Landriault, M., Sigouin, L., Castle, B., Hostetter, D., Zhang, D. and Spencer, B., 1998. Identification and linkage of tarballs from the coasts of Vancouver island and Northern California using GC/MS and isotopic techniquess. J. High Resol. Chromatogr., 21: 383–395.

Zhang, Q. and van der Donk, W.A., 2012. Answers to the carbon–phosphorus lyase conundrum. Chembiochem., 13: 627–629.

Appendix A

ADDITIONAL TABLES AND FIGURES OF CHAPTER 4

A.1 Materials and Methods

A.1.1 Characterization of Birnessite

The mineralogy, crystallinity and micromorphology, BET (Brunauer-Emmett-Teller) specific surface area (SSA), and particle size distribution of synthesized birnessite were characterized using X-ray diffraction (XRD), field emission capable scanning electron microscope (JSM-7400F, JEOL Japan), Micromeritics ASAP 2020 Surface Area and Porosity Analyzer (Georgia, USA), and Wyatt Mobius Dynamic Light Scattering (DLS; Santa Barbara, California), respectively. The SSA of birnessite was determined by the physical adsorption of nitrogen gas on the surface of birnessite at cryogenic (liquid nitrogen) temperature. With information on birnessite mass and density, and the amount of adsorbed nitrogen gas measured, SSA was calculated based on the assumption that a monomolecular layer of nitrogen adsorption formed on birnessite. For measuring particle size distribution, birnessite suspension of 1 mg L^{-1} in DI water was prepared and transformed in a quartz cuvette immediately after sonication for 10 min. The particle size distribution was calculated with results of 10 measurements. The Mn average oxidation state (AOS) was determined using the potentiometric titration method (Lingane and Karplus, 1946).

REFERENCES

Lingane, J. J.; Karplus, R. New method for determination of manganese. Ind. Eng. Chem. Anal. Ed., 1946, 18: 191–194.

Table A.1. The ^{1}H and ^{13}C NMR chemical shifts of glyphosate and its major potential degradation products obtained from pure chemicals (pH was maintained at 7.0±1.0).

	Chemical shifts ^{1}H NMR (ppm)	^{13}C NMR (ppm)
Glyphosate	3.76 (singlet); 3.12, 3.15 (doublet)	171.43 (singlet); 50.75 (singlet); 46.08, 45.23 (doublet)
AMPA	2.95, 2.99 (doublet)	37.75, 36.89 (doublet)
Glyoxylic Acid	5.06 (singlet)	87.35 (singlet); 179.50 (singlet)
Sarcosine	3.44 (singlet); 2.57 (singlet)	171.43 (singlet); 50.75 (singlet); 32.49 (singlet)
Glycine	3.44 (singlet)	172.30 (singlet); 41.33 (singlet)
Formaldehyde (hydrated)	4.83 (singlet)	81.73 (singlet)
Formic Acid	8.41 (singlet)	166.31 (singlet)
Methylamine	2.25 (singlet)	26.68 (singlet)
Methylphosphonic Acid	1.39, 1.42 (doublet)	12.30, 11.43 (doublet)
Methanol	3.33 (singlet)	48.73 (singlet)

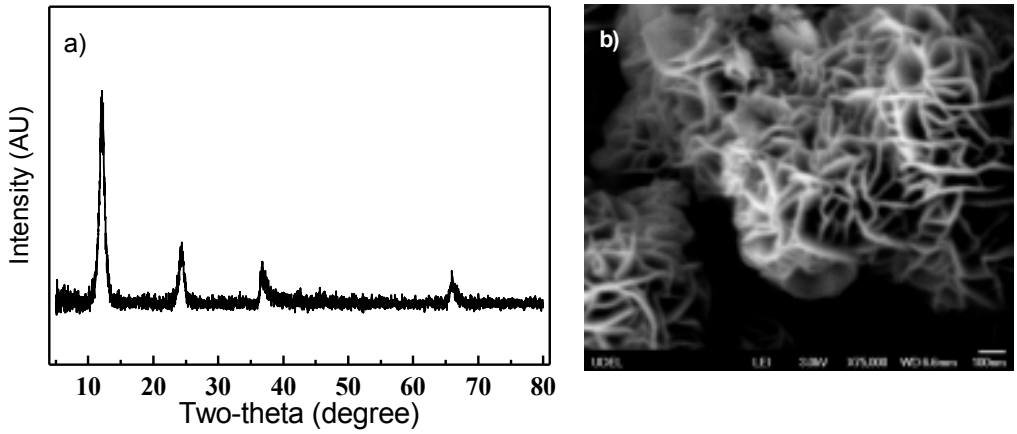

Figure A.1. X-ray diffraction patterns (a) and scanning electron microscope (SEM) images (b) of synthetic birnessite.

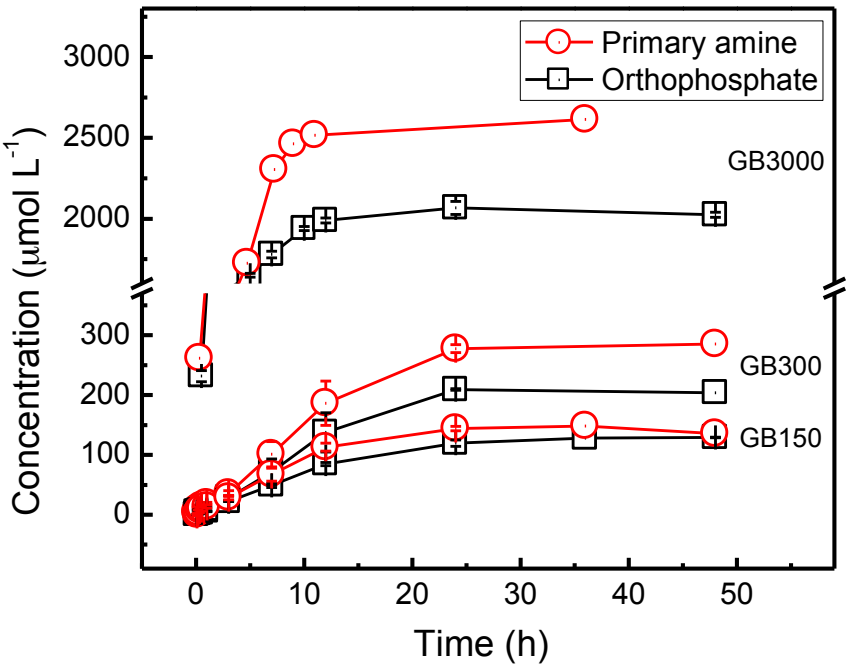

Figure A.2. Degradation kinetics of glyphosate. Open squares and circles represent concentrations of orthophosphate and primary amines, respectively. GB3000, GB300, and GB150 represent experiments performed at glyphosate:birnessite ratio of 3000 μmol L^{-1}:5 g L^{-1}, 300 μmol L^{-1}:0.5 g L^{-1}, and 150 μmol L^{-1}:0.5 g L^{-1}, respectively.

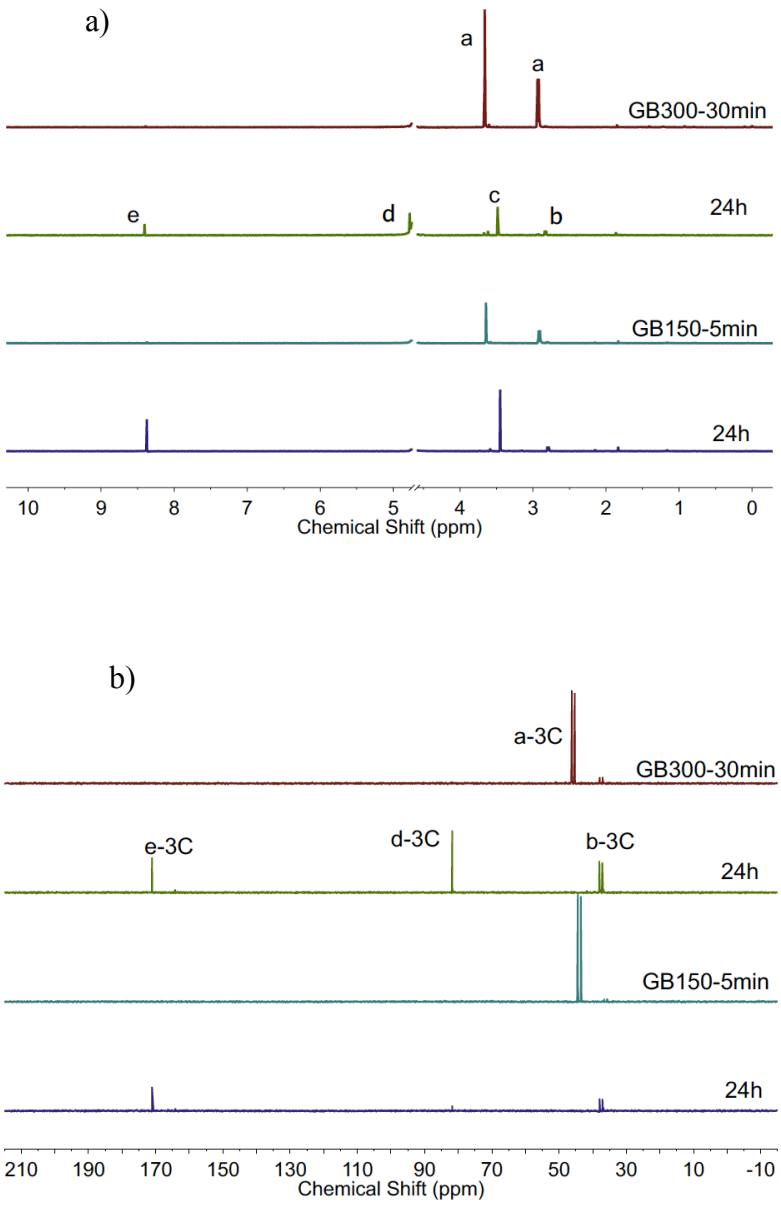

Figure A.3. NMR spectra of degradation products of glyphosate: a) ^{1}H and b) ^{13}C NMR spectra for experiments performed with glyphosate (300 or 150 μmol L^{-1}):birnessite (0.5 g L^{-1}). Glyphosate was ^{13}C labeled on 3-^{13}C counting form carboxyl group ($HOOC–CH_2–NH–^{13}CH_2–PO_3H_2$), labeled as 3C in the spectra. Peak labels correspond to glyphosate (a), AMPA (b), glycine (c), formaldehyde (hydrated) (d), and formic acid (e).

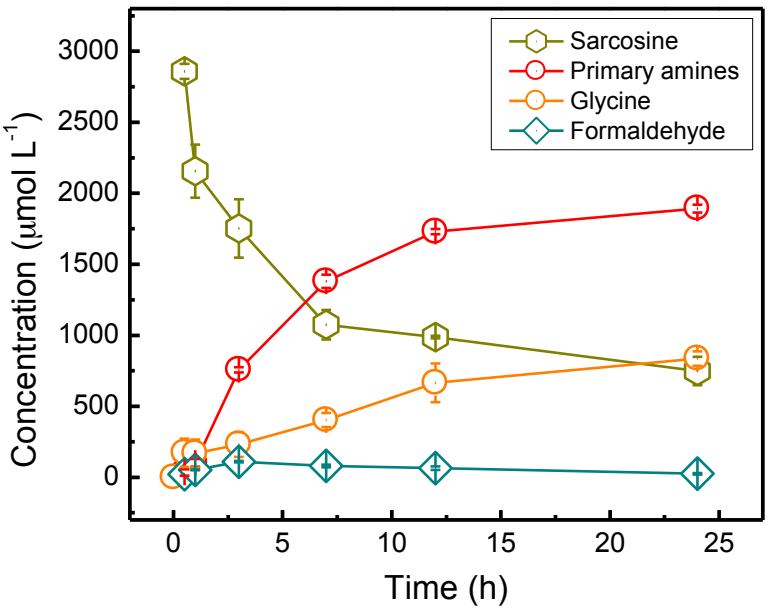

Figure A.4. Kinetics of sarcosine (3000 μmol L^{-1}) degradation by birnessite (5 g L^{-1}).

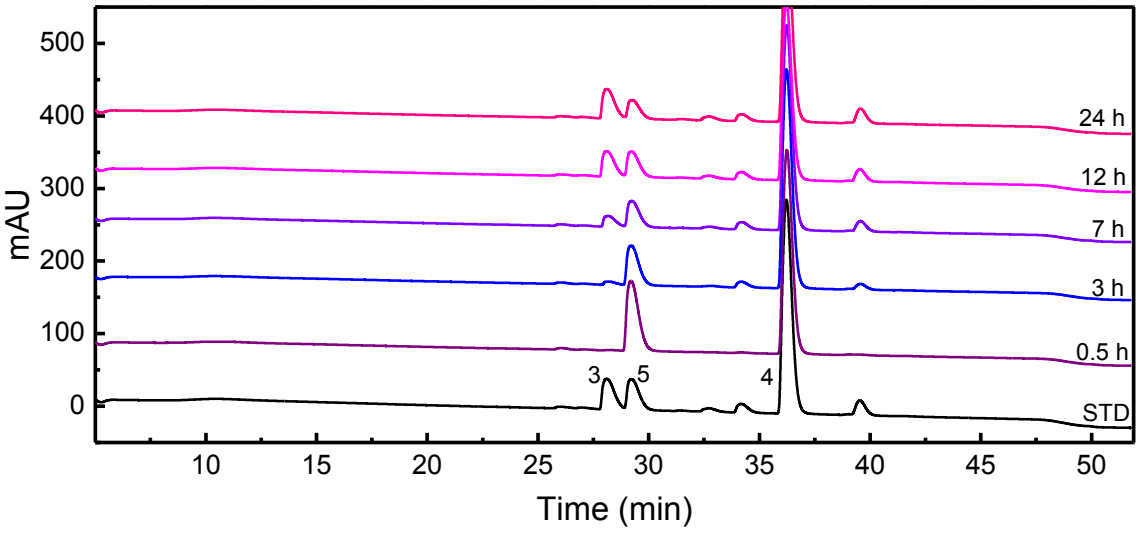

Figure A.5. Representative HPLC chromatograms of aqueous degradation products of sarcosine, in the experiment performed at sarcosine:birnessite ratio of 3000 μmol L^{-1}:5 g L^{-1}. Peaks: 3) glycine; 4) FMOC; 5) sarcosine. STD represents for mixture of standards.

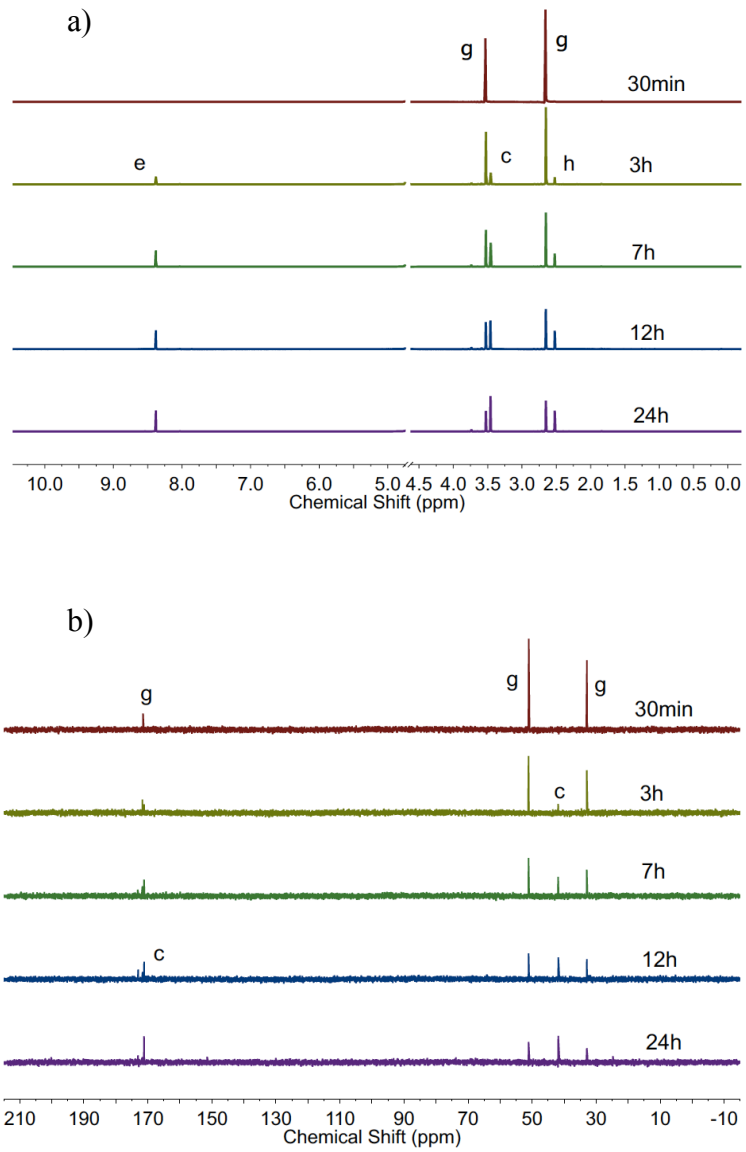

Figure A.6. NMR spectra of degradation products of sarcosine: a) ^{1}H and b) ^{13}C NMR spectra, with sarcosine (3000 μmol L^{-1}):birnessite(5 g L^{-1}) in pH range of 7±0.05 and 10 mmol L^{-1} NaCl as ionic medium. Peak labels correspond to glycine (c), formic acid (e), sarcosine (g), and methylamine (h).

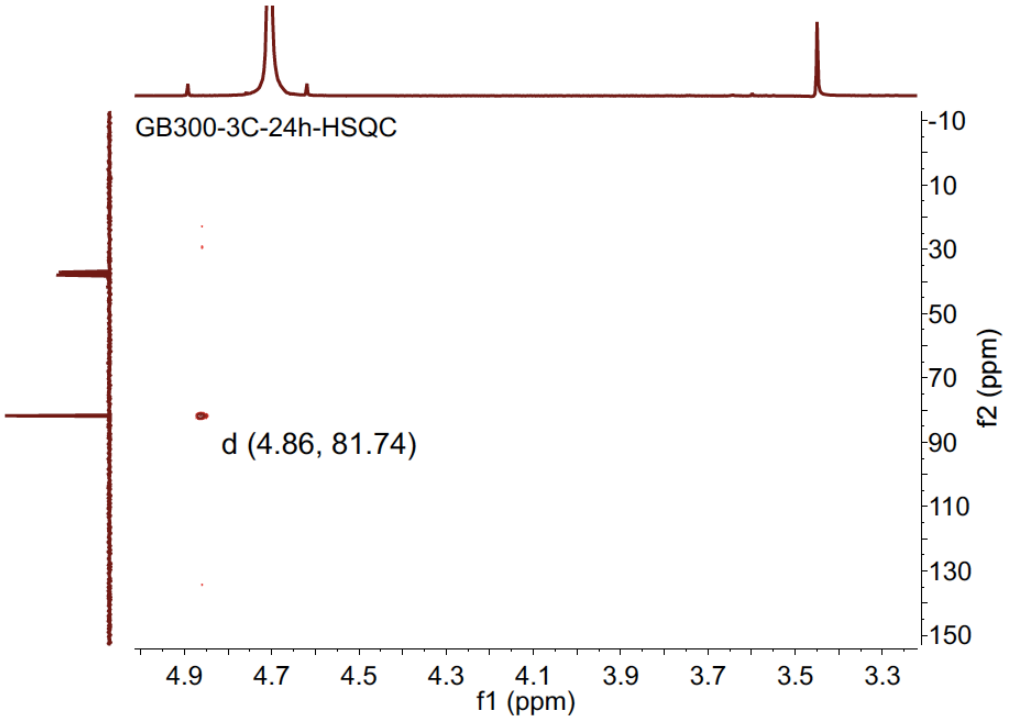

Figure A.7. Heteronuclear single quantum correlation (HSQC) spectroscopy of glyphosate degradation products, with glyphosate (300 μmol L^{-1}):birnessite (0.5 g L^{-1}) at 24 h. Two axes include f1 and f2 represent ^{1}H nuclei and ^{13}C nuclei, respectively. Peak labels correspond to formaldehyde (hydrated) (d).

a)

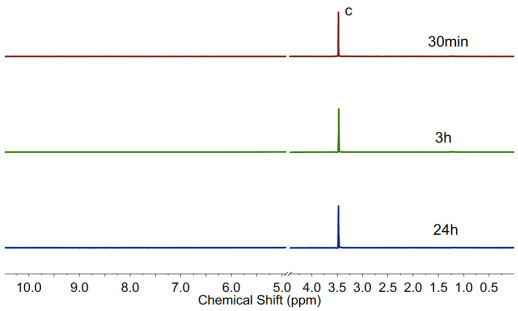
c
30min
3h
24h
10.0 9.0 8.0 7.0 6.0 5.0 4.0 3.5 3.0 2.5 2.0 1.5 1.0 0.5
Chemical Shift (ppm)

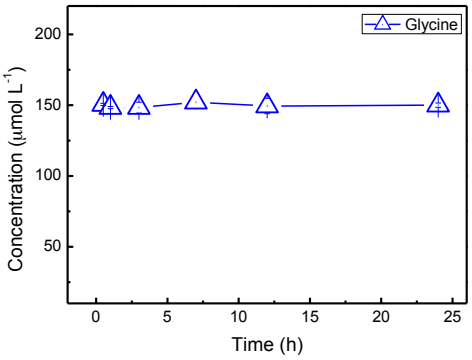
Glycine
Concentration (μmol L-1)
200
150
100
50
0 5 10 15 20 25
Time (h)

b)

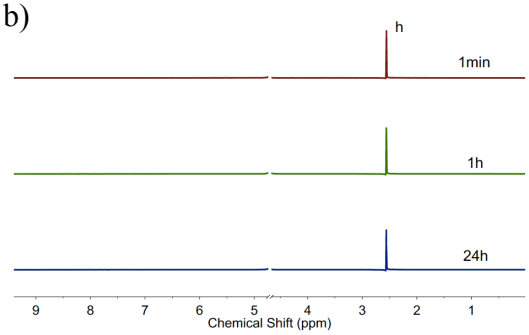
h
1min
1h
24h
9 8 7 6 5 4 3 2 1
Chemical Shift (ppm)

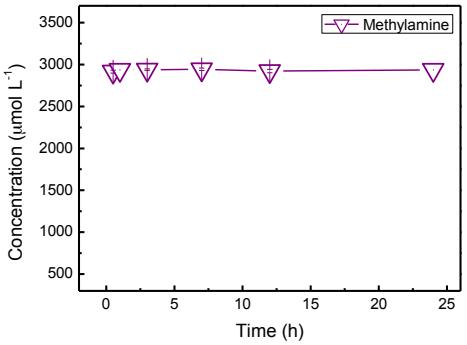
Methylamine
Concentration (μmol L-1)
3500
3000
2500
2000
1500
1000
500
0 5 10 15 20 25
Time (h)

c)

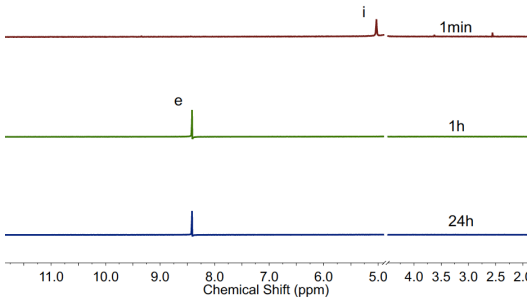
i
1min
e
1h
24h
11.0 10.0 9.0 8.0 7.0 6.0 5.0 4.0 3.5 3.0 2.5
Chemical Shift (ppm)

Figure A.8. The ^{1}H NMR spectra of degradation products of: a) glycine; b) methylamine; c) glyoxylic acid. Peak labels correspond to glycine (c), formic acid (e), methylamine (h), glyoxylic acid (i). Concentrations of glycine and methylamine were measured using the 2,4,6-trinitrobenzene sulfonic acid colorimetric method.

a)

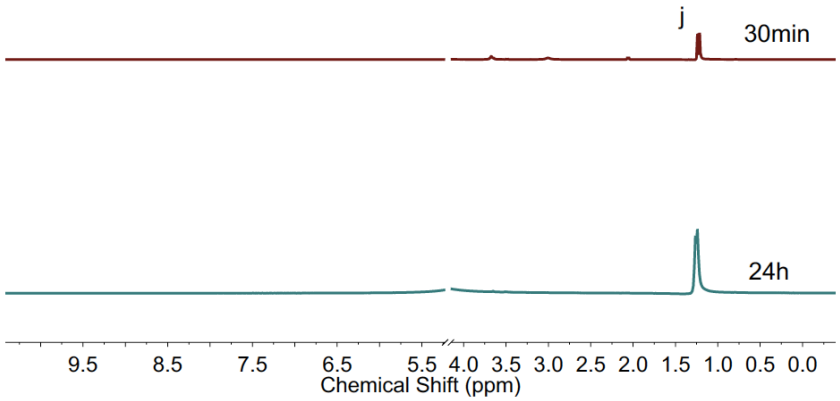
j
30min
24h
9.5
8.5
7.5
6.5
5.5
4.0
3.5
3.0
2.5
2.0
1.5
1.0
0.5
0.0
Chemical Shift (ppm)

b)

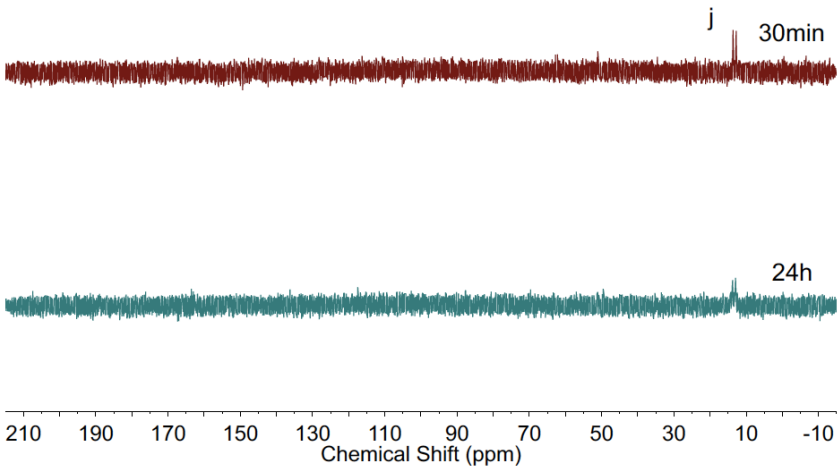
j
30min
24h
210
190
170
150
130
110
90
70
50
30
10
-10
Chemical Shift (ppm)

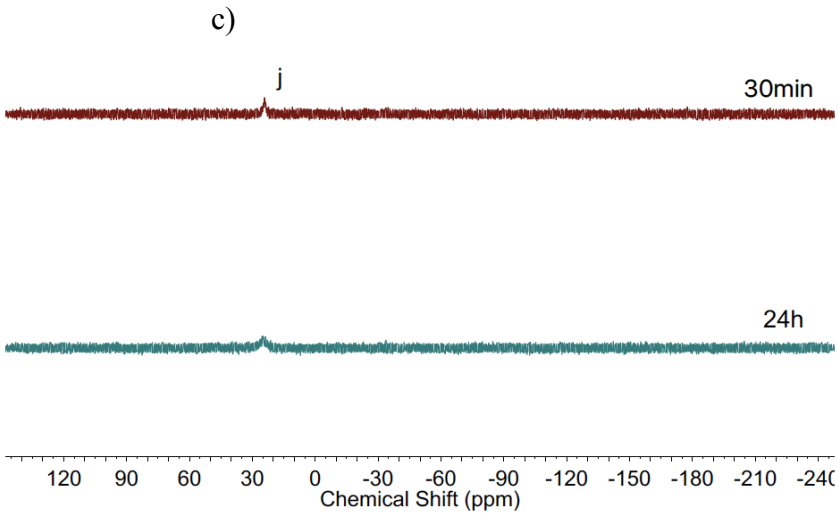

Figure A.9. The ^{1}H (a), ^{13}C (b), and ^{31}P (c) NMR spectra of degradation products of methylphosphonic acid, in the experiment with methylphosphonic acid (3000 μmol L^{-1}):birnessite (5 g L^{-1}). Peak label corresponds to methylphosphonic acid (j).

Appendix B

ADDITIONAL TABLES AND FIGURES OF CHAPTER 5

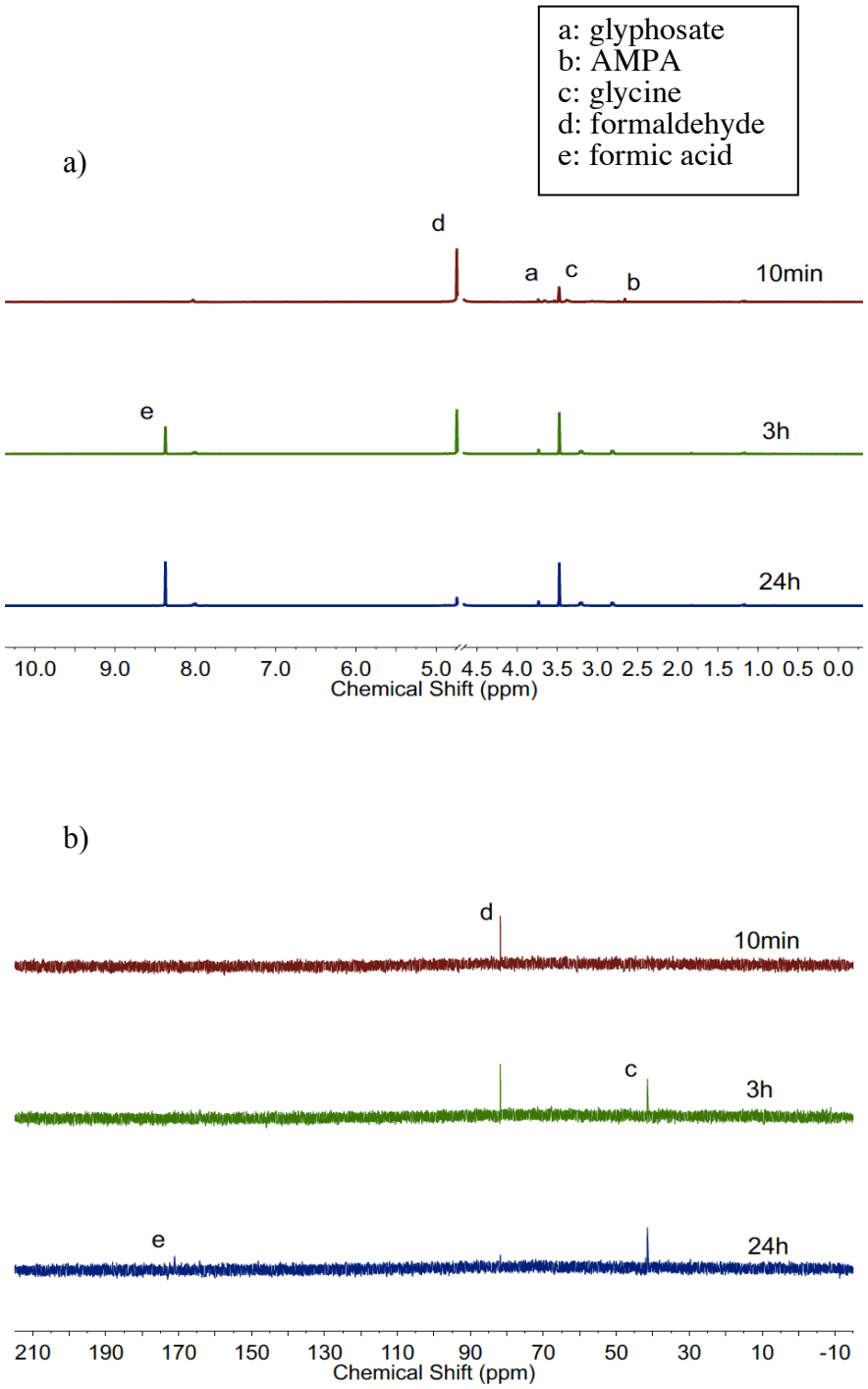

Figure B.1. Nuclear magnetic resonance (NMR) spectra of degradation products of glyphosate in aqueous solutions: (a) ^{1}H and (b) ^{13}C spectra with glyphosate (3000 μmol L^{-1}): δ-MnO_2 (5 g L^{-1}) at pH 7.00±0.05.

Appendix C

PERMISSIONS

Soil Science Society of America LICENSE TERMS AND CONDITIONS

Jul 16, 2018

This is a License Agreement between Hui Li ("You") and Soil Science Society of America ("Soil Science Society of America") provided by Copyright Clearance Center ("CCC"). The license consists of your order details, the terms and conditions provided by Soil Science Society of America, and the payment terms and conditions.

All payments must be made in full to CCC. For payment instructions, please see information listed at the bottom of this form.

License Number	4370921454980
License date	Jun 14, 2018
Licensed content publisher	Soil Science Society of America
Licensed content title	Soil Science Society of America journal
Licensed content date	Jan 1, 1976
Type of Use	Thesis/Dissertation
Requestor type	Author of requested content
Format	Print, Electronic
Portion	chapter/article
The requesting person/organization is:	Hui Li/ University of Delaware
Title or numeric reference of the portion(s)	An isotope labeling technique to investigate atom exchange during phosphate sorption and desorption
Title of the article or chapter the portion is from	An isotope labeling technique to investigate atom exchange during phosphate sorption and desorption
Editor of portion(s)	N/A
Author of portion(s)	Hui Li and Deb Jaisi
Volume of serial or monograph.	N/A
Page range of the portion	
Publication date of portion	2015
Rights for	Main product
Duration of use	Life of current edition
Creation of copies for the disabled	no
With minor editing privileges	yes
For distribution to	Worldwide
In the following language(s)	Original language of publication
With incidental promotional use	no

The lifetime unit quantity of new product	Up to 499
Title	An isotope labeling technique to investigate atom exchange during phosphate sorption and desorption
Instructor name	Deb Jaisi
Institution name	University of Delaware
Expected presentation date	Jun 2018
Billing Type	Invoice
Billing Address	Hui Li 531 S college ave Newark, DE 19713 United States Attn: Hui Li
Total (may include CCC user fee)	0.00 USD

Terms and Conditions

TERMS AND CONDITIONS
The following terms are individual to this publisher:

None

Other Terms and Conditions:
STANDARD TERMS AND CONDITIONS

1. Description of Service; Defined Terms. This Republication License enables the User to obtain licenses for republication of one or more copyrighted works as described in detail on the relevant Order Confirmation (the "Work(s)"). Copyright Clearance Center, Inc. ("CCC") grants licenses through the Service on behalf of the rightsholder identified on the Order Confirmation (the "Rightsholder"). "Republication", as used herein, generally means the inclusion of a Work, in whole or in part, in a new work or works, also as described on the Order Confirmation. "User", as used herein, means the person or entity making such republication.

2. The terms set forth in the relevant Order Confirmation, and any terms set by the Rightsholder with respect to a particular Work, govern the terms of use of Works in connection with the Service. By using the Service, the person transacting for a republication license on behalf of the User represents and warrants that he/she/it (a) has been duly authorized by the User to accept, and hereby does accept, all such terms and conditions on behalf of User, and (b) shall inform User of all such terms and conditions. In the event such person is a "freelancer" or other third party independent of User and CCC, such party shall be deemed jointly a "User" for purposes of these terms and conditions. In any event, User shall be deemed to have accepted and agreed to all such terms and conditions if User republishes the Work in any fashion.

3. Scope of License; Limitations and Obligations.

3.1 All Works and all rights therein, including copyright rights, remain the sole and exclusive property of the Rightsholder. The license created by the exchange of an Order Confirmation (and/or any invoice) and payment by User of the full amount set forth on that document includes only those rights expressly set forth in the Order Confirmation and in these terms and conditions, and conveys no other rights in the Work(s) to User. All rights not expressly granted are hereby reserved.

3.2 General Payment Terms: You may pay by credit card or through an account with us

payable at the end of the month. If you and we agree that you may establish a standing account with CCC, then the following terms apply: Remit Payment to: Copyright Clearance Center, 29118 Network Place, Chicago, IL 60673-1291. Payments Due: Invoices are payable upon their delivery to you (or upon our notice to you that they are available to you for downloading). After 30 days, outstanding amounts will be subject to a service charge of 1-1/2% per month or, if less, the maximum rate allowed by applicable law. Unless otherwise specifically set forth in the Order Confirmation or in a separate written agreement signed by CCC, invoices are due and payable on "net 30" terms. While User may exercise the rights licensed immediately upon issuance of the Order Confirmation, the license is automatically revoked and is null and void, as if it had never been issued, if complete payment for the license is not received on a timely basis either from User directly or through a payment agent, such as a credit card company.

3.3 Unless otherwise provided in the Order Confirmation, any grant of rights to User (i) is "one-time" (including the editions and product family specified in the license), (ii) is non-exclusive and non-transferable and (iii) is subject to any and all limitations and restrictions (such as, but not limited to, limitations on duration of use or circulation) included in the Order Confirmation or invoice and/or in these terms and conditions. Upon completion of the licensed use, User shall either secure a new permission for further use of the Work(s) or immediately cease any new use of the Work(s) and shall render inaccessible (such as by deleting or by removing or severing links or other locators) any further copies of the Work (except for copies printed on paper in accordance with this license and still in User's stock at the end of such period).

3.4 In the event that the material for which a republication license is sought includes third party materials (such as photographs, illustrations, graphs, inserts and similar materials) which are identified in such material as having been used by permission, User is responsible for identifying, and seeking separate licenses (under this Service or otherwise) for, any of such third party materials; without a separate license, such third party materials may not be used.

3.5 Use of proper copyright notice for a Work is required as a condition of any license granted under the Service. Unless otherwise provided in the Order Confirmation, a proper copyright notice will read substantially as follows: "Republished with permission of [Rightsholder's name], from [Work's title, author, volume, edition number and year of copyright]; permission conveyed through Copyright Clearance Center, Inc. " Such notice must be provided in a reasonably legible font size and must be placed either immediately adjacent to the Work as used (for example, as part of a by-line or footnote but not as a separate electronic link) or in the place where substantially all other credits or notices for the new work containing the republished Work are located. Failure to include the required notice results in loss to the Rightsholder and CCC, and the User shall be liable to pay liquidated damages for each such failure equal to twice the use fee specified in the Order Confirmation, in addition to the use fee itself and any other fees and charges specified.

3.6 User may only make alterations to the Work if and as expressly set forth in the Order Confirmation. No Work may be used in any way that is defamatory, violates the rights of third parties (including such third parties' rights of copyright, privacy, publicity, or other tangible or intangible property), or is otherwise illegal, sexually explicit or obscene. In addition, User may not conjoin a Work with any other material that may result in damage to the reputation of the Rightsholder. User agrees to inform CCC if it becomes aware of any infringement of any rights in a Work and to cooperate with any reasonable request of CCC or the Rightsholder in connection therewith.

4. Indemnity. User hereby indemnifies and agrees to defend the Rightsholder and CCC, and their respective employees and directors, against all claims, liability, damages, costs and

and conditions or any rights granted hereunder; provided, however, that User may assign such license in its entirety on written notice to CCC in the event of a transfer of all or substantially all of User's rights in the new material which includes the Work(s) licensed under this Service.
8.4 No amendment or waiver of any terms is binding unless set forth in writing and signed by the parties. The Rightsholder and CCC hereby object to any terms contained in any writing prepared by the User or its principals, employees, agents or affiliates and purporting to govern or otherwise relate to the licensing transaction described in the Order Confirmation, which terms are in any way inconsistent with any terms set forth in the Order Confirmation and/or in these terms and conditions or CCC's standard operating procedures, whether such writing is prepared prior to, simultaneously with or subsequent to the Order Confirmation, and whether such writing appears on a copy of the Order Confirmation or in a separate instrument.
8.5 The licensing transaction described in the Order Confirmation document shall be governed by and construed under the law of the State of New York, USA, without regard to the principles thereof of conflicts of law. Any case, controversy, suit, action, or proceeding arising out of, in connection with, or related to such licensing transaction shall be brought, at CCC's sole discretion, in any federal or state court located in the County of New York, State of New York, USA, or in any federal or state court whose geographical jurisdiction covers the location of the Rightsholder set forth in the Order Confirmation. The parties expressly submit to the personal jurisdiction and venue of each such federal or state court.If you have any comments or questions about the Service or Copyright Clearance Center, please contact us at 978-750-8400 or send an e-mail to info@copyright.com.
v 1.1